



UNIL | Université de Lausanne

Unicentre

CH-1015 Lausanne

<http://serval.unil.ch>

Year : 2017

DYNAMIC SINGLE CELL MEASUREMENTS OF SIGNALLING CASCADE ACTIVITY

Durandau Eric

Durandau Eric, 2017, DYNAMIC SINGLE CELL MEASUREMENTS OF SIGNALLING CASCADE ACTIVITY

Originally published at : Thesis, University of Lausanne

Posted at the University of Lausanne Open Archive <http://serval.unil.ch>

Document URN : urn:nbn:ch:serval-BIB_BD5011C1A48E6

Droits d'auteur

L'Université de Lausanne attire expressément l'attention des utilisateurs sur le fait que tous les documents publiés dans l'Archive SERVAL sont protégés par le droit d'auteur, conformément à la loi fédérale sur le droit d'auteur et les droits voisins (LDA). A ce titre, il est indispensable d'obtenir le consentement préalable de l'auteur et/ou de l'éditeur avant toute utilisation d'une oeuvre ou d'une partie d'une oeuvre ne relevant pas d'une utilisation à des fins personnelles au sens de la LDA (art. 19, al. 1 lettre a). A défaut, tout contrevenant s'expose aux sanctions prévues par cette loi. Nous déclinons toute responsabilité en la matière.

Copyright

The University of Lausanne expressly draws the attention of users to the fact that all documents published in the SERVAL Archive are protected by copyright in accordance with federal law on copyright and similar rights (LDA). Accordingly it is indispensable to obtain prior consent from the author and/or publisher before any use of a work or part of a work for purposes other than personal use within the meaning of LDA (art. 19, para. 1 letter a). Failure to do so will expose offenders to the sanctions laid down by this law. We accept no liability in this respect.



UNIL | Université de Lausanne

Unicentre

CH-1015 Lausanne

<http://serval.unil.ch>

Year : 2017

DYNAMIC SINGLE CELL MEASUREMENTS OF SIGNALLING CASCADE ACTIVITY

Durandau Eric

Durandau Eric, 2017, DYNAMIC SINGLE CELL MEASUREMENTS OF SIGNALLING CASCADE ACTIVITY

Originally published at : Thesis, University of Lausanne

Posted at the University of Lausanne Open Archive <http://serval.unil.ch>

Document URN : urn:nbn:ch:serval-BIB_BD5011C1A48E6

Droits d'auteur

L'Université de Lausanne attire expressément l'attention des utilisateurs sur le fait que tous les documents publiés dans l'Archive SERVAL sont protégés par le droit d'auteur, conformément à la loi fédérale sur le droit d'auteur et les droits voisins (LDA). A ce titre, il est indispensable d'obtenir le consentement préalable de l'auteur et/ou de l'éditeur avant toute utilisation d'une oeuvre ou d'une partie d'une oeuvre ne relevant pas d'une utilisation à des fins personnelles au sens de la LDA (art. 19, al. 1 lettre a). A défaut, tout contrevenant s'expose aux sanctions prévues par cette loi. Nous déclinons toute responsabilité en la matière.

Copyright

The University of Lausanne expressly draws the attention of users to the fact that all documents published in the SERVAL Archive are protected by copyright in accordance with federal law on copyright and similar rights (LDA). Accordingly it is indispensable to obtain prior consent from the author and/or publisher before any use of a work or part of a work for purposes other than personal use within the meaning of LDA (art. 19, para. 1 letter a). Failure to do so will expose offenders to the sanctions laid down by this law. We accept no liability in this respect.



UNIL | Université de Lausanne

Faculté de biologie
et de médecine

Département de Microbiologie Fondamentale

**DYNAMIC SINGLE CELL MEASUREMENTS OF SIGNALLING CASCADE
ACTIVITY**

Thèse de doctorat sciences de la vie (PhD)

présentée à la

Faculté de biologie et de médecine
de l'Université de Lausanne

par

Éric DURANDAU

Master Immunologie, Microbiologie, Infectiologie (IMI)
de l'Université de Grenoble Alpes

Jury

Prof. François SPERTINI, Président
Dr. Serge PELET, Directeur de thèse
Prof. Sophie MARTIN, Co-directrice
Prof. Robbie LOEWITH, expert
Prof. Andreas MAYER, expert

Lausanne 2017

Imprimatur

Vu le rapport présenté par le jury d'examen, composé de

Président· e	Monsieur Prof. François Spertini
Directeur· rice de thèse	Monsieur Dr Serge Pelet
Co-directeur· rice	Madame Prof. Sophie Martin
Experts· es	Monsieur Prof. Robbie Joseph Loewith Monsieur Prof. Andreas Mayer

le Conseil de Faculté autorise l'impression de la thèse de

Monsieur Eric Durandau

Master biologie de l' Université Joseph Fourier de Grenoble, France

intitulée

**DYNAMIC SINGLE CELL MEASUREMENT
OF SIGNALLING CASCADE ACTIVITY**

Lausanne, le 6 octobre 2017

pour le Doyen
de la Faculté de biologie et de médecine

Prof. 
François Spertini

*”Le travail finit toujours par payer, un jour ou
l’autre...”*

Joël Durandau

Acknowledgements

The end of this thesis constitutes the culmination point of long years of works. I always desired to reach the PhD level since I started the university. Achieving this objective has implied a lot of sacrifices either for me and the peoples that surrounding me. For this reason, I would like to thank my entire family, and especially my parents. My mother, Cécile, always did trust me blindly for all choices I did without judgement and she did some sacrifices to let me pursue my path. My father, Joël, was always a good support during difficult times although he does not really trust the academic training. He was always there to remind me everything I accomplished, to support me and push me to continue. I have a little thought for my grandmother who left us last year. She was one of the first women being chemical engineer. I hope that, from where she is now, she is proud of me. I do not forget all of my close friends, from here, but also from Grenoble. Those last friends really contribute to the person I am now and I am very proud to know them and to count them as friends.

A thesis cannot be achieved without the support of colleagues. I would like first to thank all the DMF. I was warmly welcomed and the scientific level is impressive and this led to very interesting scientific discussions. I would like to thank the group of Sophie Martin. We are making the lab meeting together with our group and during the times I presented I really get good suggestions about my project. They also helped me to watch my project from a different point of view which helped me a lot during the breaking phases. I would like to thank my chief Serge Pelet for trusted me. When we met, I was far from being the best recruit he would have had. However, we worked hard together to correct my weaknesses. I would like to tell him that

Acknowledgements

I did only one application after my Master degree. It was for the position in his group. When I read the project, I immediately knew that this is what I wanted to do and this with him as a supervisor. I was not wrong. I would like to thank all the other members of the lab, past and present, Clemence, Min, Nadim, Victoria and trainees who pass through. I would like to thank Delphine and especially Marta who helped me to write and correct this manuscript. Without her everything would not be possible because she was also a good support during the last moment of the writing, like a second mother.

To finish, I would like to thank the person that I love the most, my daily life partner, my friend, my love, Clémence. She daily contributes to make me better, and learn me many good aspects of the life that I did not suspect before I met her. I am convinced that I would not produce a work of this quality if she were not beside me.

Abstract

All organisms are composed of a multitude of cell types, having each a specific task to accomplish. This cell-to-cell heterogeneity results from a complex process of differentiation initiated by the interpretation of intra and extracellular cues by signalling cascades. Therefore, it becomes fundamental to study the signal processing driven by signalling cascades, in order to understand how cells organise during development, but also to comprehend how and why signals are sometimes misinterpreted and lead to diseases such as cancer. MAPK pathways belong to a very well-conserved family of signalling cascades, known to be mostly implicated in the adaptation to environmental stimuli and to regulate various key physiological processes. The various components of the MAPK pathways are well defined. However, we still need to understand how signalling cascades cross-communicate with each other and how this leads to different cell-fate decision making. The limitation is mostly technical, as such investigation would require to dynamically and simultaneously investigate the activity state of MAPK components in live single cells. The aim of this thesis was to build a new kind of assay, enabling to extract these information. Here, I described the design of the synthetic protein SKARS, that relocates from the nucleus to the cytoplasm following specific phosphorylation. This synthetic protein is composed of a docking site (DS), that enables a specific interaction with a MAP kinase, a nuclear localisation sequence (NLS), that promotes an active nuclear importation, and a fluorescent protein (FP), that allows to determine its sub-cellular localisation. Once the cell activates the MAPK, the NLS gets inhibited by phosphorylation, which leads to the cytoplasmic accumulation of the fluorescent protein. This nucleus-to-cytoplasm shuttling is used as a proxy for MAPK activity. In

Abstract

order to demonstrate this, we applied this technology in the mating pathway study of the model organism *Saccharomyces cerevisiae*. By combining time-lapse fluorescent microscopy with computational analysis, we extracted the dynamic MAPK activity in hundreds of cells, and observed that when cells are exposed to exogenous pheromone, the MAPK is differentially activated from one cell to another. Using the Whi5 transcription factor as a sensor for the cell cycle progression, we showed that these different signal patterns are specific to the cell-cycle stage of the cell. The MAPK is fully activated in G1, inhibited in S, G2 and M and transiently activated during the transition between G1 and S. Moreover, single cell analysis of mutants let us conclude that the model describing how the cell cycle regulates the mating pathway is incomplete. To conclude, we showed that the parallel measurement of multiple signalling cascades is a valuable strategy enlighten very subtle pathway cross-regulation events. Thanks to the straightforward structure of the SKARS, crosstalk mechanisms between signalling cascades can be assessed, by combining multiple sensors in the same cell. We are currently applying this technology to mammalian cells, and strongly believe that this technique can be an advantage in fields such as development or cancer research.

Résumé scientifique

Tous les organismes sont composés d'une multitude de cellules ayant chacune une tâche spécifique à accomplir. Cette hétérogénéité résulte d'un processus complexe de différenciation initié par l'analyse de signaux intracellulaires et extracellulaires par des cascades de signalisation. Par conséquent, il devient fondamental d'étudier le traitement du signal par les voies de signalisation pour comprendre comment les cellules s'organisent pendant le développement, mais aussi pour comprendre comment et pourquoi ces signaux peuvent parfois être mal interprétés et entraîner l'apparition de maladies telles que le cancer. Les voies impliquant les MAP Kinases (MAPK) appartiennent à une famille très bien conservée de cascades de signalisation connues pour leurs rôles dans l'adaptation aux stimuli environnementaux et dans la régulation de divers processus physiologiques clés. Les différents composants des voies impliquant les MAPK commencent à être bien connus. Cependant, nous ne comprenons toujours pas comment les cascades de signalisation s'autorégulent et comment cela conduit à divers comportements cellulaires. La limitation est principalement technique, car une telle recherche nécessiterait de sonder l'état d'activité des composants des cascades de MAPK, dynamiquement et simultanément dans chaque cellule vivante. L'objectif de cette thèse fut de construire un nouveau type de senseur permettant d'extraire ces informations. Dans ce manuscrit, nous décrivons le design, ainsi qu'une application de la protéine synthétique SKARS (Synthetic Kinase Activity Relocation Sensor). Elle a été conçue pour se déplacer du noyau vers le cytoplasme après avoir été spécifiquement phosphorylée par la kinase d'intérêt. La protéine est composée d'un domaine de docking (DS), qui permet une interaction spécifique avec une MAPK, un signal de localisation nucléaire (NLS), qui favorise

Résumé scientifique

une importation active dans le noyau et une protéine fluorescente pour observer sa position dans les compartiments cellulaires. Une fois que la cellule active la MAPK, le NLS est inhibé après phosphorylation ce qui conduit à l'accumulation de la protéine fluorescente dans le cytoplasme. Le passage du noyau au cytoplasme est utilisé comme mesure de l'activité MAPK. Comme preuve de concept, nous avons appliqué cette technologie dans l'étude de la voie d'accouplement chez l'organisme modèle *Saccharomyces cerevisiae*. En combinant la microscopie à fluorescence en temps réel avec une analyse informatique, nous avons extrait l'activité dynamique de la MAPK dans des centaines de cellules et avons observé que lorsque les cellules sont exposées à de la phéromone exogène, la MAPK s'active de manière différente d'une cellule à l'autre. En utilisant le facteur de transcription Whi5 comme senseur de la progression du cycle cellulaire, nous avons montré que ces différents types de trace d'activité de MAPK sont spécifiques à chaque phase du cycle cellulaire dans laquelle se trouve la cellule. La MAPK est entièrement activée en G1, inhibée en S, G2 et M et activée de manière transitoire à l'interaction entre G1 et S. De plus, l'analyse de cellule mutantes individuellement nous a permis de conclure que le modèle décrivant le mécanisme de régulation de la voie d'accouplement par le cycle cellulaire est incomplet. Pour conclure, la mesure en parallèle de plusieurs cascades de signalisation est une stratégie intéressante pour détecter de fins événements de régulation entre les voies de signalisation. Grâce à sa structure modulable, plusieurs SKARS peuvent être construits et combinés dans le but d'étudier les mécanismes de régulation croisés entre les cascades de signalisation. Nous appliquons actuellement cette technologie aux cellules mammifères et nous sommes fermement convaincus que cette technique pourrait bénéficier à divers domaines tels que la recherche sur le développement ou la recherche sur le cancer.

Résumé

La cellule est l'unité biologique structurelle et fonctionnelle fondamentale de tous les êtres vivants. Chez l'homme, les cellules s'assemblent pour former des structures complexes telles que des organes, des muscles ou des os. Bien que la plupart des cellules qui composent notre corps possèdent exactement le même code génétique, chacune d'entre elles se différencie, entre autres, par sa fonction. Cette diversité émerge d'une interprétation différente des changements environnementaux. L'analyse de ces signaux se fait à l'intérieur de la cellule par un grand réseau de protéines. Ce réseau s'apparente à un circuit électrique, où chaque interrupteur est relié à un ou plusieurs autres interrupteurs. Au niveau cellulaire, à chaque interrupteur correspond une protéine faisant circuler le signal dans une branche précise du réseau en contrôlant son état "ON/OFF". Suivant le type de chemin parcouru, le signal induira un type de réponse ou un autre. Ce processus est communément appelé transduction du signal. Si la transduction du signal d'une cellule était mesurée, sa voie de différenciation cellulaire serait anticipée. Cette thèse présente une technique permettant de mesurer la transduction du signal dans des cellules vivantes et en temps réel. La technique se base sur une protéine synthétique appelée SKARS qui va agir comme une sonde pour l'activité d'un nœud du circuit de signalisation. Lorsque le nœud n'est pas actif, la protéine est dans le noyau de la cellule et lorsque le nœud s'active, la protéine s'accumule en dehors. Afin de visualiser ce processus, la sonde a été marquée avec une protéine fluorescente. En utilisant un microscope à fluorescence, nous pouvons suivre la position de la sonde au cours du temps et en déduire le degré d'activation du nœud mesuré. Nous avons appliqué cette méthode dans l'étude du processus d'accouplement chez la levure *Saccharomyces cerevisiae*. Deux sondes

Résumé

ont été utilisées pour mesurer en parallèle l'activité du nœud de l'accouplement et du nœud impliqué dans le déclenchement de la division cellulaire. Nos résultats montrent que la voie de l'accouplement ne peut être activée qu'à condition que les cellules sentent de la phéromone et que la voie de la division cellulaire soit éteinte. Par conséquent, la cellule ne peut choisir que l'une de ces deux voies de différenciation. Grâce à cette méthode, nous avons aussi démontré que le modèle décrivant le mécanisme d'inhibition croisé de ces deux voies était incomplet. En conclusion, la sonde SKARS est outil extrêmement utile pour définir comment la cellule interprète les signaux de l'environnement et ainsi comprendre pourquoi certaines voies de différenciation sont choisies plus que d'autres. Cette sonde a été utilisée chez un organisme très simplifié, mais nous sommes convaincus que cette technique permettra de répondre à d'importantes questions dans les domaines de recherche sur le développement et sur le cancer.

Contents

Acknowledgements	5
Abstract	7
Résumé scientifique	9
Résumé	11
1. Introduction	21
2. Dynamic single cell measurements of MAPK activity	29
2.1. Background	30
2.2. Results	32
2.2.1. Sensor design	32
2.2.2. Inferring MAPK activity	37
2.2.3. Single cell measurements	40
2.2.4. Combination of sensors	46
2.2.5. Cell wall integrity pathway	51
2.2.6. Single cell response to cell wall damage	54
2.3. Discussion	57
2.4. Conclusion	60

Contents

3. Mating and cell-cycle cross-inhibition mechanism.	63
3.1. Background	64
3.2. Result	68
3.2.1. SKARS and Whi5 as proxies for MAPK and CDK activity.	68
3.2.2. Single cell analysis of the MAPK activity signal	75
3.2.3. The mating pathway regulates the cell cycle in a pheromone dose-dependent manner.	82
3.2.4. Far1 and CDK activities are both required for the mating and the cell cycle cross-inhibition mechanism	88
3.2.5. CDK Inhibition of the mating pathway	93
3.2.6. Molecular mechanism of mating inhibition in S-G2-M.	95
3.3. Discussion	103
3.4. Conclusion	106
4. General discussion	109
5. Material and methods	117
A. Strains and plasmids	141
B. Mathematical Model	149
C. Clustering and synchronisation	157

List of Figures

1.1. MAPK pathways in <i>S. cerevisiae</i>	24
2.1. MAPK pathways in <i>S. cerevisiae</i>	31
2.2. Schematic of the three domains of the SKARS sensor	33
2.3. Microscopy images of cells before and after stimulation with α -factor.	33
2.4. Image segmentation process.	34
2.5. Dynamic response of the sensor in different background.	35
2.6. Inhibition of the MAPK Fus3 prevents the relocation of the sensor.	36
2.7. Effect of the sensor on polarisation and pheromone dependent cell cycle arrest.	37
2.8. Effect of the sensor on the pheromone dependent gene expression.	38
2.9. Scheme of the reaction implemented by the model.	39
2.10. Simulated nuclear to cytoplasm ratio from MAPK activity.	40
2.11. Simulated MAPK activity at various pheromone concentrations and prior and after Fus3-as inhibition.	41
2.12. Variability of the basal ratio N/C from cell-to-cell	42
2.13. Initial and final response define the dynamic relocation of the sensor at the single cell level.	43
2.14. Single cell analysis of MAPK activity upon pheromone stimulation	44
2.15. Quantification of single cell response.	45
2.16. Subcellular localization of the Whi5 and Yox1 cell cycle marker.	46
2.17. Cell cycle dependent dynamics of signalling in the mating pathway.	47

List of Figures

2.18. Slow responding cell in G2/M cell cycle stage.	48
2.19. Combination in the same cell of two equivalent sensors.	49
2.20. A. Fus3-specific sensor.	50
2.21. Engineering of a Cell Wall Integrity MAPK activity sensor.	51
2.22. Optimisation of the Cell Wall Integrity MAPK activity sensor.	52
2.23. Mpk1 activity dynamics upon zymolyase stress.	53
2.24. Mpk1 activity dynamics upon hypo-osmotic stress.	54
2.25. Single cell responses upon zymolyase-induced cell wall damage: Whi5 marker . . .	55
2.26. Single cell responses upon zymolyase-induced cell wall damage: Yox1 marker . . .	56
2.27. Single cell analysis of Mpk1 activation by zymolyase in low glucose concentration	58
3.1. Schematic representation of the <i>Saccharomyces cerevisiae</i> mating pathway.	65
3.2. Scheme of the CDK and MAPK sensors.	68
3.3. Subcellular localisation of Whi5 and quantification of the CDK activity.	69
3.4. Synchronisation of CDK activity traces relative to the G1-entry	71
3.5. Optimization of the MAPK activity quantification.	72
3.6. Dynamic MAPK activity in unstimulated conditions.	73
3.7. SKARS sub-cellular localisation and MAPK activity quantification.	74
3.8. Pheromone induced MAPK activation of cells in G1 or S-G2-M phases.	76
3.9. CDK and MAPK activities relative to G1-entry	77
3.10. MAPK activity of cells in transition between cell-cycle phases.	78
3.11. Contribution of cluster signals to the average of MAPK activity.	80
3.12. MAPK signal degradation induced by Bar1.	82
3.13. Pheromone dose-dependent MAPK activation.	84
3.14. Pheromone dose-dependent cell distribution in the various clusters.	85
3.15. Dynamic Cdk activity of cells entering in S-phase.	86
3.16. Maximum CDK activity required to commit to cell cycle	87

3.17. Pheromone dose-dependent activation of the MAPK in <i>WT</i> and <i>far1Δ</i>	89
3.18. Cell cycle arrest in G1 in <i>WT</i> and <i>far1Δ</i> background.	90
3.19. Dynamic CDK and MAPK activities after Cdc28-as inhibition.	91
3.20. Final MAPK activity at various concentrations of CDK inhibitors.	93
3.21. Dynamic MAPK activity estimation from CDK activity.	94
3.22. The current model of the mating and cell-cycle cross-inhibition mechanism	96
3.23. MAPK activity response in mutants expressing non-phosphorylatable Ste5. . . .	97
3.24. MAPK activation after CDK inhibition in the Ste5_{ND} mutant.	98
3.25. Potential inhibition of the MAPK through Ste7	100
3.26. Inhibition of the MAPK through Ste20.	101
C.1. Schematic representation of a histogram of the whole Whi5 _{N/C}	158

List of Tables

A.1. Table of strains	142
A.2. Table of plasmids.	147
B.1. Reactions implemented in the model.	150
B.2. Kinetic parameters and starting concentrations	154
B.3. Parameters describing the MAPK activity dynamics.	154
B.4. Equation parameters.	155

1. Introduction

1. Introduction

Cell-Cell heterogeneity The cell is the smallest living entity which composes every organism. Although cells from a pluri-cellular individual contain the same genetic code, they differ according to several properties, which provide them various physiological functions. This led scientists to classify cells in various cell types such as neuronal cells, blood cells, fibroblasts and other. Interestingly, heterogeneity is also found among one particular cell-type. This can be an advantage, as for the B-lymphocytes that produce different types of antibodies, or a disadvantage, as for cancer cell lines expressing different markers not necessarily targeted by drugs [1, 118].

Heterogeneity among a clonal cell population can be triggered by stochastic events. For example, the DNA is known to be subjected to random modifications such as:

- single-nucleotide polymorphism (SNP) [63, 118]
- noisy gene expression [33, 98].

Those random modifications contribute to the evolution of species

Heterogeneity among a clonal cell population can also be triggered by deterministic events. . . Indeed, the cell probe and analyse changes occurring in the environment to adapt its physiology state. The interpretation of extracellular cues can vary among a population leading to cell-to-cell variability. Deterministic-related variability can be associated with the physical and chemical properties of the environment (cell-cell contacts, growth factors) and influences many cell physiological processes, such as proliferation, sensitivity to apoptosis, metabolic activity, cell shape and motility [114, 2, 36]. Intra-cellular cues, such as the cell cycle position, also contribute to the emergence of heterogeneity. Studies in the budding yeast *Saccharomyces cerevisiae* have shown that activation of the mating process is only allowed in G1. Thus, the response to pheromone will vary from one cell to another depending on their cell cycle position [81, 129].

To summarise, stochastic and deterministic events influence the behaviour of each individual among a population. The fate chosen by a cell is defined by they interpret intra- and extracellular cues.

MAPK pathways. Cell-to-cell heterogeneity emerges because each individual cell interprets intra-/extracellular cues in a different way. Cue interpretation is carried on by a complex network of proteins communicating with each other through post-translational modifications. This is what is commonly called the signal transduction. The network composition and the relationship between the nodes start to be well known for organisms commonly studied . However, it is still challenging to correlate signal transduction with a particular cell fate, as it would mean to get access to the activity state of all components of the signalling network simultaneously [114, 1]. Assays enabling to get such information can only acquired the physiological state of a whole population and in one condition [78, 103]. Single cell analysis is thus required to analyse the signal transduction and to correlate signalling activity patterns with a given cell-fate.

Since current dynamic single cell strategy does not enable to report the activity of the entire signalling network, the solution consists on focusing on particular nodes with important regulatory function [2, 62]. Mitogen activated protein kinases (MAPK) pathways are very well conserved signalling cascades. In mammals, the three most studied MAPK are ERK, JNK and p38, and regulate cell physiological processes, such as morphology, adaptation to stresses or cell cycle progression. They are extensively studied for their implication into development, immune response or cancer [89].

Such cascades transduces a signal coming from a receptor that senses environmental changes. The information is then transmitted to the core of the signalling cascades composed of three kinases, the mitogen activated protein kinase kinase kinase (MAP3K), the mitogen activated protein kinase kinase (MAP2K) and the mitogen activated protein kinase (MAPK), which phosphorylate each other. Once the MAPK gets activated, this kinase up/down-regulates various proteins to trigger a specific adaptation program [24, 89, 6, 96]. Some studies focusing on ERK, p38 or JNK observed that these MAPKs exhibit numerous dynamic activity patterns that are signatures of particular cell fate choices [95, 36, 2, 105]. For example, in normal rat epithelial cells, ERK was shown to exhibit pulse activity that promotes entry into cell cycle. These pulses disappear as cells touch each other and leads to the induction of a quiescent state [2].

1. Introduction

MAPK pathways in Budding Yeast *Saccharomyces cerevisiae* is a prototypical eukaryote for the study of signalling cascades. The four well-studied MAPK pathways of *S.cerevisiae* haploid strains are the Cell Wall Integrity (CWI), the Hyper-Osmotic Glycerol (HOG), the Filamentous Growth (FG) and the Pheromone Response (PR) or mating pathway (figure 1.1) [6, 16, 108, 107, 109] and are extremely well conserved among eukaryotes [130]. The CWI is homologous to

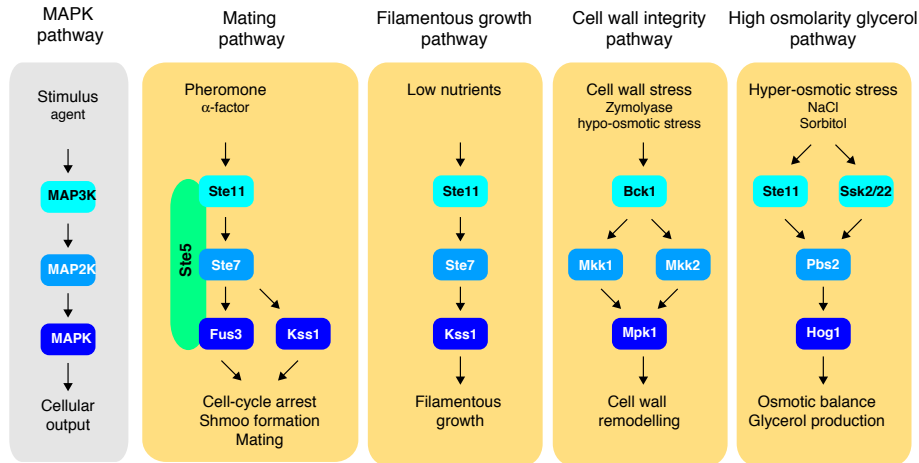


Figure 1.1.: MAPK pathways in *S. cerevisiae* General scheme depicting the four MAPK pathways active in haploid budding yeast cells: the mating pathway, the filamentous growth pathway, the Cell Wall Integrity (CWI) pathway and the High Osmolarity Glycerol (HOG) pathway.

the JNK/P38 pathways. It is activated by cell-wall degradation, hypo-osmotic shocks or DNA damages. It is composed of the Bck1 (MAP3K), Mkk1/2 (MAP2Ks) and the Mpk1 (MAPK), which drive the adaptation through the regulation of cell wall synthesis [6, 16, 108, 107, 109]. The HOG pathway is also close to the p38 pathway and is induced upon hyper-osmotic shock. It can be activated through two possible MAP3K branches, either the Ste11 or the Ssk2/22. Both tracks lead to the activation of the MAP2K Pbs2, which then activates the MAPK Hog1 by phosphorylation [6, 16, 108, 107, 109]. The filamentous growth pathway is probably the less understood MAPK signalling cascade. It shares homology with the mammalian ERK pathway and gets activated by nutrient deprivation. It is composed of the MAP3K Ste11 that activates the MAP2K Ste7, that subsequently activates the MAPK Kss1. Once active, Kss1 triggers cell

filamentation and promotes invasive growth [6, 16, 108, 107, 109] . The last, but not least, MAPK signalling cascade is the mating pathway. It shares homology with the ERK pathway and controls the mating process between two haploid cells of opposite mating types. Activation of this cascade starts from the sensing of exogenous pheromones, which leads to the recruitment at the plasma membrane of a protein complex formed by the scaffold protein Ste5, the MAP3K Ste11, the MAP2K Ste7 and the MAPK Fus3. A phosphorylation cascade occurs and leads to the activation of the MAPKs Fus3 and Kss1 and induce the cell cycle arrest in G1. MAPKs trigger also a transcriptional program and regulate proteins implicated in cell polarisation, cell fusion and karyogamy [20, 44, 104, 7].

To sum up, MAPK pathways of *S.cerevisiae* are very well conserved and close to those of the mammals [130]. Thus, this organism is a very good model to investigate signalling cascades cross-regulation mechanisms.

The HOG pathway induces an homogeneous adaptation to stress. In budding yeast, most of the MAPK pathways are implicated into the adaptation to stresses. . Hyper-osmotic shock induces a rapid decrease of the cell volume. The process of adaptation starts by the activation of the HOG pathway through the Ssk2/1 and the Ste11 tracks. Once the signal reaches Hog1, the MAPK activates enzymes implicated in the glycerol production. Interestingly, phosphorylated Hog1 is strongly imported into the nucleus to trigger a transcriptional program. The MAPK then returns into the cytoplasm as cells recover their original size [37, 86, 74, 75].

The cell size recovery happens to be impressively homogeneous in the population. How can this adaptation be so robust? First, the HOG pathway is identically activated in all cells. This can be achieved by avoiding improper crosstalks with other signalling cascades through: specific protein-protein interactions between components of the HOG pathway [41, 101, 108], the use of scaffold proteins to recruit the required pool of signalling cascade components at the right place [108, 6], direct inhibition of pathways that may interfere with osmotic shock response [108, 112, 107, 82, 45]. Second, the HOG pathway blocks many dynamic processes, such as the

1. Introduction

cell cycle, that could be corrupted by the stress [18, 42]. Consequently, the HOG pathway exhibits a uniform dynamic activity pattern, and triggers a homogeneous cell adaptation to stress.

The pheromone response is heterogeneous In contrast to the adaptation to hyper-osmotic shock, cells respond differentially to the pheromone. Indeed, various cell shapes can be observed when cells are exposed to intermediate concentrations of pheromone [4, 83]. Moreover, it was reported that the pheromone response genes are induced with a dynamic that varies depending on the cell cycle [129, 81]. This heterogeneity was described to be associated with a cross-inhibition mechanism between the mating pathway and regulators of the cell cycle progression. The mating regulates the cell cycle through the Fus3-dependent activation of the Far1. This cyclin kinase inhibitor (CKI) inhibits the cyclin-dependent kinase Cdc28 by outcompeting with the cyclins Cln1/2. This results in inhibition of the CDK and arrest of the cell cycle progression [91, 87].

On the other hand, it was reported that pheromone-response gene expression, such as *FUS1*, occurs in G1 and not in S-phase. This suggests that the cell cycle regulates the mating. [81]. This inhibition mechanism driven by the cell-cycle requires the expression of the S-phase cyclins Cln1, Cln2 and Cln3 (CLN) and occurs through the regulation of the Far1 CKI and the Ste5 scaffold protein. When CLN start to be expressed at the interplay between G1- and S-phase, Far1 is thought to be degraded avoiding mating-induced cell-cycle arrest [72, 80]. In parallel, CLN induce the detachment of the Ste5 from membrane by promoting the phosphorylation of a membrane binding domain of the scaffold protein by Cdc28 and leading to reduced signalling through the mating pathway [93, 116].

To sum up, cells are not permissive to mating in all phases of the cell cycle. This explains why the response to pheromone is heterogeneous. This heterogeneous pheromone response imposes some technical limitations in the study of the cell cycle and mating cross-inhibition. The current strategies used to counteract these problems are either to synchronise cells in a particular cell cycle phase using chemicals (or thermosensitive mutants[80, 53]), or to overexpress one regulator of the cell cycle, usually cyclins (CLN) [129, 116]. These are very artificial conditions that illus-

trate the requirement of new live single cell-based techniques that report on signalling cascades activity without affecting the cell fitness.

Dynamic kinase activity measurements at the single cell level Variability in the cell behaviour is often associated with specific dynamic signalling cascade activity patterns. Such patterns emphasise the processing of the signalling cascade inputs. For example, pulsed activation of the mammalian MAPK Erk induces proliferation while sustained activity is thought to promote cell differentiation [95, 2]. Thus, to comprehend how a cell undergoes a given fate, the signalling cascade activity must be dynamically visualised in living single cells. In addition, to confirm the relevancy of an observed pattern, these measurements must be performed on hundreds of cells.

Some groups succeeded in observing the dynamic activity of MAPKs using Western Blot. However, they only extract whole population information and therefore cannot judge whether the observed activity pattern corresponds to the dynamic kinase activity of the single cells [54, 43, 77, 136]. This can be solved using fluorescent protein-based transcriptional or translational reporters [84, 102, 83]. Although transcriptional reporters are good in steady state conditions, the dynamic of the output signal does not necessarily reflect the dynamic activation of the upstream signalling cascade. This is mostly because transcription is a slow process compared to signal transduction and because fluorescent proteins require a maturation time [3, 86, 103].

Kinase activity can, in some cases, be translated in a subcellular localisation change. Some proteins, such as the NF κ B transcription factor in mammals or the MAPK Hog1 and the transcription factor Whi5 in yeast, enter or exit the nucleus after being phosphorylated [37, 86, 74, 75, 21, 29, 28]. This is an interesting property, as the relocation from/to the nucleus occurs with a rate closer to signal transduction than transcription. Unfortunately, not all kinases or their substrates exhibit such a behaviour. This limits us in the capacity to report the activity of a specific node in the signalling cascade network [133].

10 years ago, brand new synthetic biology techniques appeared. The most relevant example is a technique which combines a synthetic fluorescence resonance energy transfer (FRET)-based

1. Introduction

kinase sensor with time lapse fluorescent microscopy and automated image analysis [124, 51, 39, 38, 2]. This system showed its potential in the context of the study of the ERK dynamic activation [2] but also in studies focusing on Fus3 and Kss1 [19]. However, this FRET sensor limits the capacity to report on various pathway activity states at the same time, because multiple fluorescent channels are used by one reporter. Moreover, multiple rounds of optimisation are often required to reach the best signal-to-noise ratio for one particular target [124, 62, 19].

To sum up, various cell fates are observed among a population, because cells adjust their adaptation process to environmental changes with their current physiological state. Intra- and extraellular cues are processed by signalling cascades that cross-regulate each others. In order to define the cross-regulation mechanisms between signalling pathways, the activity state of multiple signalling cascades must be analysed in live single cells. However, current methods do not enable to perform such measurements.

The first chapter of this thesis describes a new approach combining synthetic biology, fluorescent microscopy and automated image analysis. The system we engineered enables kinase activity measurement, dynamically and in hundreds of living cells [85, 30]. We also show that our technique is very specific to the target, can be easily adapted to report the activity of various kinases and is compatible with other fluorescent based techniques. The second chapter of this thesis describes how we applied this technique in the context of the study of the cross-inhibition mechanism between the mating pathway and the cell cycle in *S.cerevisiae*.

2. Dynamic single cell measurements of yeast MAPK activity by synthetic kinase activity relocation sensor.¹

¹All the Data presented in this chapter were published in 2015 in the BMC biology journal (See Durandau *et al.* [30]). The article is in open access <http://www.biomedcentral.com/1741-7007/13/55>

2.1. Background

Signal transduction is an essential part of cellular life. Cells perceive changes in their environment and integrate these extra-cellular signals with intra-cellular cues to mount an appropriate response. This is achieved by signal transduction cascades, where receptors at the plasma membrane sense the surrounding medium and transmit this information to intracellular enzymes that modulate the activity of other proteins to induce a specific response via post-translational modifications .

The Mitogen Activated Protein Kinase (MAPK) pathways are a conserved family of signalling cascades which respond to a wide range of signals, such as growth hormones, nutrient status or stresses [96]. These pathways are activated by surface sensors (often G-protein coupled receptors), which transduce their information via membrane-associated proteins to the highest member of the MAPK cascade, the MAP kinase kinase kinase (MAP3K). In turn, the MAP3K phosphorylates the MAP kinase kinase (MAP2K), which finally doubly phosphorylates the MAPK to activate it. MAPKs have a large range of substrates both in the cytoplasm and in the nucleus where they actively promote the transcription of new genes. Although these pathways are often viewed as linear signalling routes where a given output elicits a specific response, they actually are part of a complex signalling network where cross-activation and cross-inhibition mechanisms are readily found.

In the model organism *Saccharomyces cerevisiae*, four MAPK pathways are active in haploid cells: the mating pathway, the filamentous growth pathway, the High Osmolarity Glycerol (HOG) pathway and the Cell Wall Integrity (CWI) pathway [107] (figure 2.1). The mating pathway is activated in haploid cells in response to pheromones (α - or α -factor). In MAT α cells, α -factor is sensed by the G-protein coupled receptor Ste2. The binding of the ligand results in the dissociation of the trimeric G-protein. Free G $_{\beta\gamma}$ recruits the scaffold protein Ste5 to the plasma membrane, which promotes the activation of the MAP3K Ste11, which in turn activates the MAP2K Ste7. This kinase further activates two MAPKs Fus3 and Kss1 which both contribute

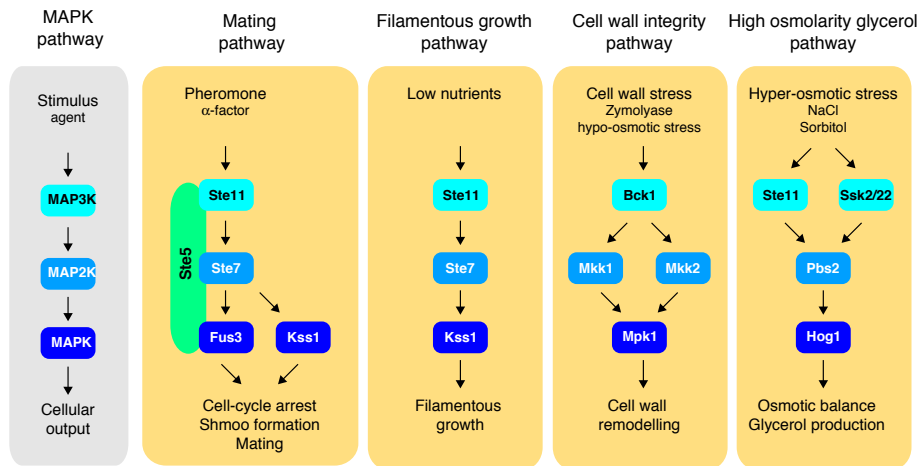


Figure 2.1.: MAPK pathways in *S. cerevisiae* General scheme depicting the four MAPK pathways active in haploid budding yeast cells: the mating pathway, the filamentous growth pathway, the Cell Wall Integrity (CWI) pathway and the High Osmolarity Glycerol (HOG) pathway.

to the mating response [68, 7].

While this pathway is a prototypical example of a growth response pathway, the CWI is more akin to a stress response cascade. Cell wall remodeling is constantly taking place during growth of the yeast. In addition, the CWI pathway is also acutely activated by environmental stresses such as heat, hypo-osmotic stress, or cell wall damaging agents [68]. The sensing mechanism of these stresses is not fully understood, it is nevertheless clear that they act via MAP3K Bck1, which activates the MAP2Ks Mkk1 and Mkk2, both of which phosphorylate the MAPK Mpk1 (Slt2). Mid2 and Wsc1 have been identified as the most important sensors for this pathway and transduce their status via Rho1 and Pkc1 to the MAPK cascade [68]; however, other stimuli take alternative routes. As an example, zymolyase (which consists of a cocktail of enzymes degrading the cell wall) activates the HOG pathway and, subsequently, its MAPK Hog1 activates Pkc1 via an unknown mechanism[10].

Despite its apparent simplicity, the budding yeast MAPK network shares multiple common features with its counterparts in higher eukaryotes, such as MAP3K or MAP2K, which can activate multiple downstream MAPKs depending on the stimulus. Extensive experimental evidence

2. Dynamic single cell measurements of MAPK activity

has demonstrated that these [108, 5]. Thus, they can regulate cell cycle progression, metabolism, or stress response, or in other instances be regulated by these same processes. The integration of these signals can lead to a variability in the response of individual cells to a given stimulus because the physiological state of each individual cells can vary [36, 83, 124, 94]. Thus, dynamic and quantitative single cell measurements are required to untangle the complex regulatory network that controls the activity of MAPKs in a cell.

Therefore, we set out to design synthetic substrates for MAPKs that would relocate between the cytoplasm and the nucleus upon phosphorylation. These synthetic kinase activity relocation sensors (SKARS) were designed with a modular architecture based on three parts: a docking site offering specificity for the kinase of interest, a nuclear localization sequence that is inactivated by phosphorylation, and a fluorescent protein that reports on the nuclear-to-cytoplasm shuttling of the sensor. Herein, we demonstrate the modularity of this strategy by engineering sensors for the mating pathway MAPKs Fus3 and Kss1 as well as for the CWI MAPK Mpk1. These sensors allowed measurement of the dynamics of MAPK activation in single cells. We could identify a heterogeneity in the response of the cells upon α -factor or zymolyase treatments which demonstrates the ability of the MAPK signalling pathways to integrate intra-cellular cues to tune the response delivered by the MAPK.

2.2. Results

2.2.1. Sensor design

Nuclear localization sequences (NLSs) consist of a stretch of positively charged residues associated with importin, which will subsequently shuttle its cargo into the nucleus [56]. Harreman *et al.* [49] demonstrated that additional negative charges around the NLS compromise its binding to importin and thereby decrease the enrichment of the cargo in the nucleus. Further, they observed that the NLS for the Swi6 transcription cofactor was led by a serine, which is a potential phosphorylation target. Indeed, mutation of this residue to an alanine resulted in a constitutively

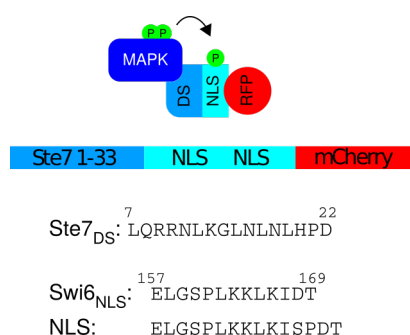


Figure 2.2.: Schematic of the three domains of the SKARS sensor. The docking site (DS), the nuclear localization signal (NLS), and the fluorescent protein (FP). The Ste7_{DS}-NLS-RFP SKARS is composed of the Ste7 docking site (Ste7_{DS}, amino-acids 1-33), a double NLS, and the mCherry protein

nuclear Swi6 protein. Based on these findings, we used the Swi6 NLS as a phosphorylation target for our sensor, with the idea that phosphorylation would lead to an exit of the sensor from the nucleus. To increase the efficiency of relocation, we added a second phosphorylation site after the positive stretch of amino-acids and combined two such NLSs in our sensor (figure 2.2).

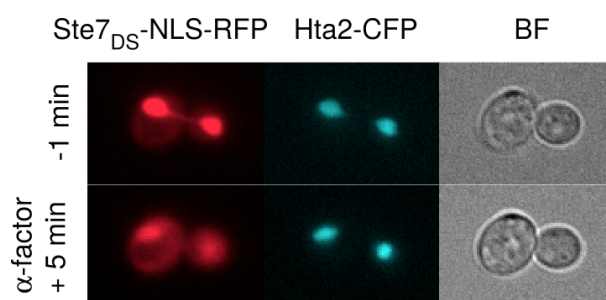


Figure 2.3.: Microscopy images of cells before and after stimulation with α -factor. In the red channel, one can observe the nuclear exit of the sensor after stimulus while the CFP-histone tag signal remains stable.

All MAPKs share the same consensus phosphorylation motif SP or TP. Specificity is achieved via an interaction surface in the kinase called the docking groove. This motif associates with a docking site (DS) with the consensus motif (R/K) 1-2-X4-6-LXL, which has been identified on MAPK substrates as well as on MAPK phosphatases and up-stream activators (MAP2K) [120, 121]. These interaction motifs are present throughout eukaryotes from yeast to mammals.

2. Dynamic single cell measurements of MAPK activity

Exchange of this DS has been shown to dictate specificity towards a substrate or, in the case of a MAP2K, control the specificity of the activated MAPK [135, 101]. The group of Wendell

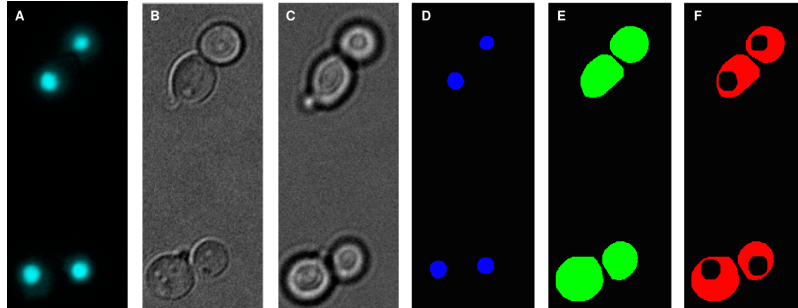


Figure 2.4.: Image segmentation process. A, B and C. Three pictures are used for image segmentation: CFP: Hta2-CFP nuclear tag (A), BF0: in-focus brightfield image (B), BF1: slightly out of focus brightfield image (C). D, E and F. Based on these pictures, three objects are defined in the image. First, the Nucleus object is segmented based on the CFP intensity (D, blue). Then, using the two brightfield images, the contour of the cell is defined allowing to identify the Cell object (E, green). Finally, by subtracting the Nucleus object enlarged by 2 pixels from the Cell object, we define the Cytoplasm object (F, red).

Lim has characterized various DSs that interact with Fus3 and Kss1 [101]. We used the first 33 amino acids of Ste7, which contains the DS with the strongest affinity towards Fus3 and Kss1. The Ste7_{DS} and double-NLS construct was fused to mCherry (figure 2.2). As shown in figure 2.3, the sensor is enriched in the nucleus under vegetative growth conditions. Upon stimulation of the cells with α -factor, the fluorescent protein quickly relocates to the cytoplasm. Automated segmentation of the images allows the identification of the nucleus and cytoplasm for each cell (figure 2.4) [85]. The ratio of the average intensities in the nucleus and in the cytoplasm is calculated as a function of time for each cell. The median, 25-, and 75-percentiles of the population are plotted for cells treated with 1 μ M α -factor or unstimulated cells (figure 2.5.A). At the onset of the experiment, the ratio is high, denoting an enrichment of the sensor in the nucleus. Upon α -factor addition, this ratio drops within a few minutes. This result suggests that the sensor is phosphorylated by Fus3 and/or Kss1 in response to α -factor treatment, leading to its relocation from the nucleus to the cytoplasm.

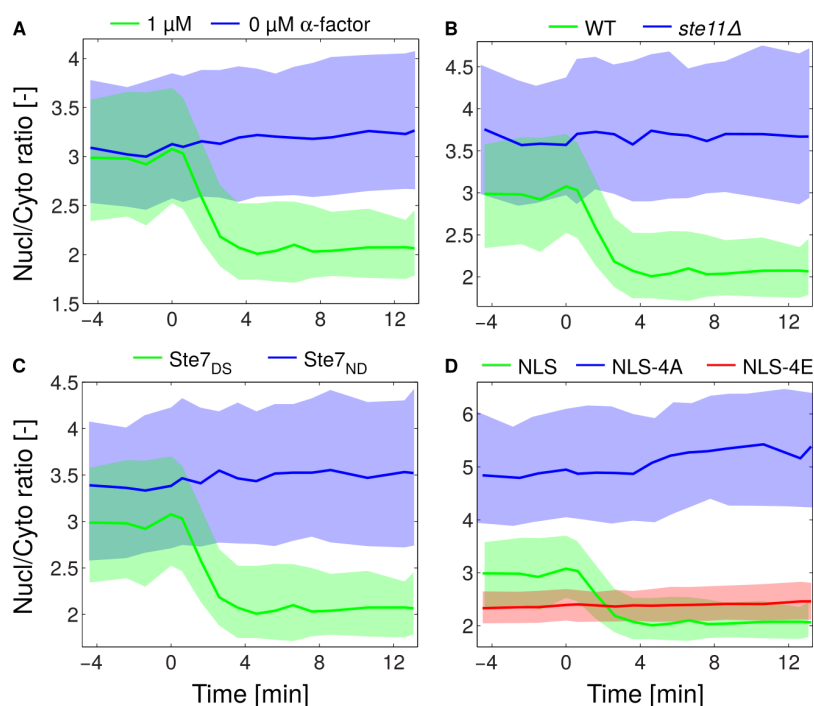


Figure 2.5.: Response of cells bearing the functional sensor and stimulated with $1 \mu\text{M}$ α -factor ($N_c = 170$) is compared to cells deficient for signal transduction ($ste11\Delta$, $N_c = 360$, A), cells bearing a non-docking variant of the sensor (Ste7 ND, $N_c = 300$, B), or a non-phosphorylatable (NLS-4A, $N_c = 360$, C) or phospho-mimicking variant of the sensor (NLS-4E, $N_c = 750$, D). Unitless measurements, such as the Nucl/Cyto ratio, are denoted by the symbol [-] in the axis legend. For all similar graphs and unless stated otherwise, the solid lines represent the median of the cell population and the shaded area the 25 and 75 percentile of the population. N_c represents the number of single cells measured

To demonstrate the specificity of this response, we repeated this experiment in cells deficient for MAPK activation ($ste11\Delta$), in which the sensor remained enriched in the nucleus upon stimulation (figure 2.5.B). We can further demonstrate that this response depends on an intact DS. Indeed, mutation of the DS of Ste7 abolishes the response (figure 2.5.C). Moreover, mutation of the four serines in the two NLSs to phospho-mimicking residues (glutamic acid:NLS-4E) or to non-phosphorylatable residues (alanine: NLS-4A) alters the localization of the fluorescent protein in the cell, but neither of these constructs display a change in nuclear-to-cytoplasmic partitioning upon pheromone stimulation (figure 2.5.D).

2. Dynamic single cell measurements of MAPK activity

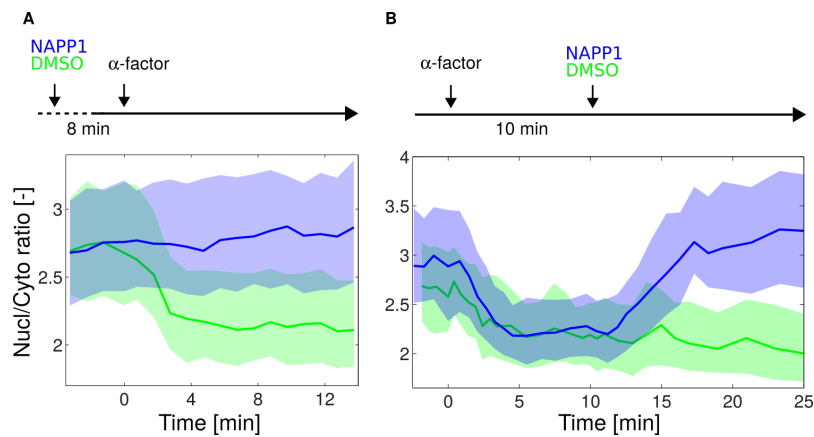


Figure 2.6.: Inhibition of the MAPK Fus3 prevents the relocation of the sensor. *fus3Δkss1Δ* cells bearing the Ste7_{DS}-NLS-RFP SKARS and an integrated *fus3-as* were stimulated with pheromone in presence or absence of the inhibitor NAPP1. A. NAPP1 or DMSO were added 8 minutes prior to the addition of α -factor. The median nuclear-to-cytoplasmic ratio is plotted as function of time (NAPP1: Nc = 343, DMSO: Nc = 230). B. Ten minutes after α -factor stimulation, cells were treated with NAPP1 or DMSO. Note that, upon inhibition of Fus3-as, the sensor returns within 7 minutes to its basal nuclear enrichment level (NAPP1: Nc = 177, DMSO: Nc = 123)

Finally, we also verified that the direct inhibition of the MAPK using an analog-sensitive allele blocked the phosphorylation and hence the relocation of the SKARS (*fus3-as* in *fus3Δkss1Δ*, figure 2.6.A) [15]. Interestingly, addition of the inhibitor after the activation of the pathway leads to a rapid return of the sensor to its basal nuclear enrichment level, underlying the dynamic nature of the bio-sensor phosphorylation (figure 2.6.B). Taken together, these results clearly demonstrate that we have generated a specific sensor for mating MAPK activity.. The relocation is dependent on an active kinase that binds to the sensor via the specific DS and phosphorylates the serines in the NLSs. This modification is reversible, allowing for a dynamic measurement of the MAPK activity.

To assess if the presence of the SKARS perturbs the mating response of the cells, we confirmed that cells could arrest their cell cycle and form mating projections (figure 2.7.A and B). These qualitative tests revealed no difference between cells bearing docking or non-docking versions of the sensor. However, we noted a minor difference in the transcriptional response of cells due

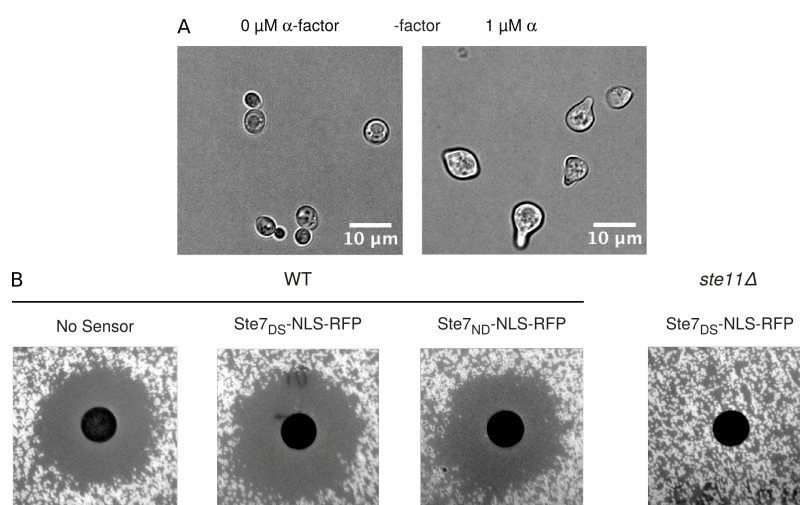


Figure 2.7.: Effect of the sensor on polarisation and pheromone dependent cell cycle arrest. A. Cells bearing the Ste7_{DS}-NLS-RFP sensor are able to form a mating projection upon α -factor stimulation. B. The ability of cell to arrest their cell cycle upon pheromone treatment was observed by halo assay. WT, Ste7_{DS}-NLS-RFP, Ste7_{ND}-NLS-RFP and Ste7_{DS}-NLS-RFP in *ste11* Δ cells were plated on rich medium. Cells were sowed with beads on a plate and 10 μl of α -factor 1mg/ml was added on a filter disk. The absence of cell growth around the filter is indicative of the cell cycle arrest. The comparable size of the halo between cells bearing a functional sensor, a non-functional sensor or no sensor indicates an equivalent sensitivity to pheromone.

to the presence of the sensor by quantifying by flow cytometry the expression of the P_{FIG1}-quadrupleVenus expression reporter [86] (figure 2.8). This slight increase in expression could potentially be explained by a minor enrichment of the MAPKs in the nucleus induced by the presence of the sensor.

2.2.2. Inferring MAPK activity

To extract MAPK activity from sensor relocation measurements, we have developed a simple mathematical model describing the relationship between the relative concentration of the sensor in the nucleus and in the cytoplasm and the activity of the MAPK (See Appendix B for description of reactions and parameters). Figure 2.9 is a scheme of the various reactions included in the model. A MAPK and a phosphatase regulate the level of phosphorylation of the sensor. The

2. Dynamic single cell measurements of MAPK activity

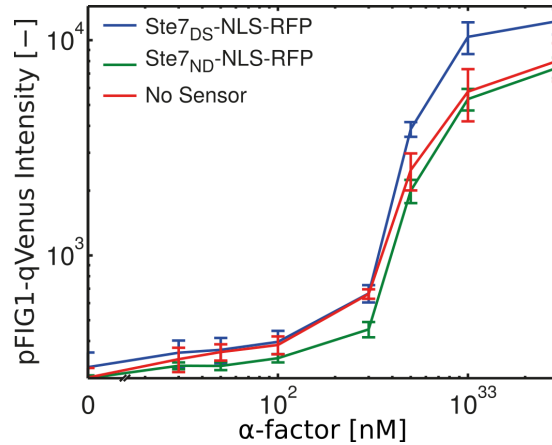


Figure 2.8.: Cells bearing an expression reporter pFIG1-qVenus were transformed with a functional ($Ste7_{DS}$ -NLS-RFP) or non-functional ($Ste7_{ND}$ -NLS-RFP) sensor. Cells were stimulated with a range of α -factor concentrations. 1.5 hours after stimulation they were treated with cycloheximide (0.1 mg/ml) and 1.5 hour later measured by flow cytometry. A minor increase in fluorescence level in cells bearing the functional sensor indicates a slight increase in expression ability of these cells.

action of the phosphatase is constitutive. The concentration of MAPK in the cell is constant; however, the ratio of active MAPK (MAPK activity defined as the fraction of the total MAPK pool in the active state) changes as a function of time. For simplicity, we consider that these reactions occur with similar rate constants in the nucleus and in the cytoplasm. The sensor can freely diffuse between the nucleus and the cytoplasm (k_{Diff}), but only the unphosphorylated SKARS is actively imported in the nucleus (k_{Imp}). The model can be forward-simulated by generating a specific time-course of MAPK activity (figure 2.10.A) and calculating the resulting nuclear-to-cytoplasmic partitioning of the sensor (figure 2.10.B). At steady-state, there is a close to linear relationship between the MAPK activity and the nuclear-to-cytoplasmic ratio of the sensor (figure 2.10.C).

We can also use the model to estimate MAPK activity based on a measured nuclear-to-cytoplasmic ratio. We quantified the steady-state nuclear enrichment of the sensor in a population of cells 15 minutes after induction with various concentrations of α -factor (figure 2.11.A). Based on these data, we can obtain the dose-response curve of MAPK activity, which extends

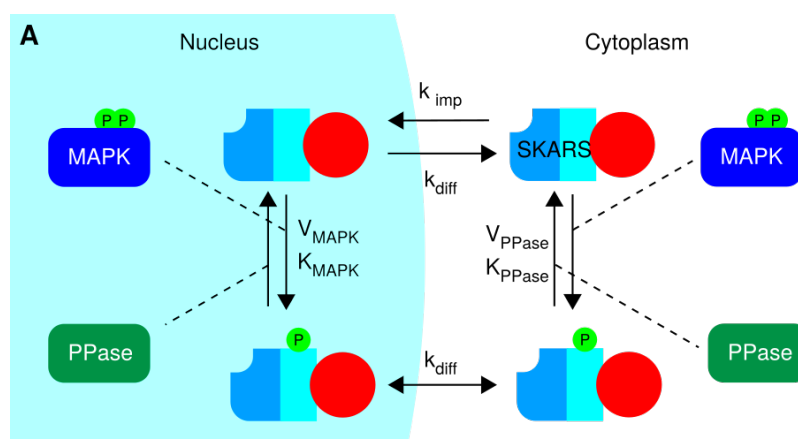


Figure 2.9.: Scheme of the reaction implemented by the model. Schematic of the reactions implemented in the model. The SKARS is phosphorylated in the nucleus and in the cytoplasm by MAPK and dephosphorylated by phosphatase. The exchange of SKARS between the cytoplasm and the nucleus can occur through passive diffusion, while only the unphosphorylated SKARS is actively imported in the nucleus.

from 0.2 for an unstimulated sample to 1 for saturating levels of pheromone ($1 \mu\text{M}$). A MAPK activity of 1 implies that both Fus3 and Kss1 are completely phosphorylated in saturating levels of pheromone. While this level might seem high, a recent study on the HOG pathway suggests that close to 100 % of MAPK Hog1 is phosphorylated upon hyper-osmotic shock [34]. A non-docking mutant is used as reference and displays no MAPK activity. It has been shown that HOG and the mating pathways have some basal level of MAPK activity under normal growth conditions [71]. The exact level of this basal signal is difficult to estimate, but we consistently observe an increase in nuclear enrichment of the sensor in signalling dead cells as well as in non-docking versions of the sensor (figure 2.5.B and .C).

Using a similar strategy, the dynamics of MAPK activity can be estimated from time-course measurements of sensor relocation. As a proof of concept, we use the activation and inhibition of the pathway by α -factor and subsequent inhibitor addition presented in figure 2.6.B. Before stimulus, the MAPK activity was low. Upon α -factor addition, it reached 0.8 in less than 3 minutes after stimulus. Upon inhibition, MAPK activity dropped at a much slower rate. This decay is controlled by multiple factors such as the time of entry of the drug in the cell,

2. Dynamic single cell measurements of MAPK activity

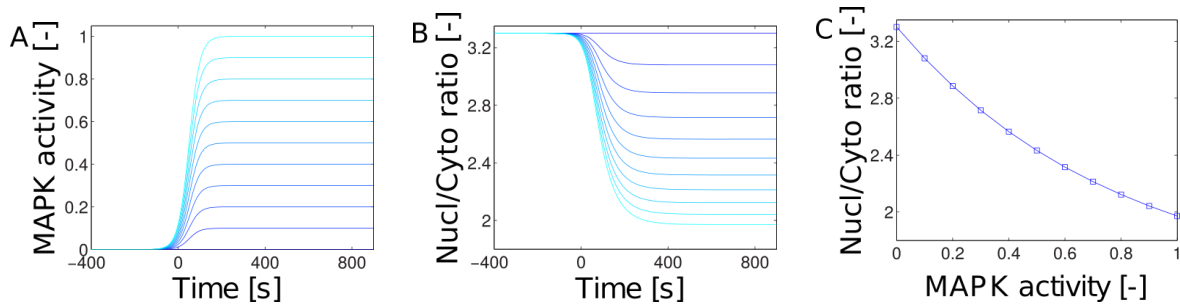


Figure 2.10.: Simulated nuclear to cytoplasm ratio from MAPK activity. A. Time-course of MAPK activity is calculated for different final levels of MAPK activity and used as inputs into the model. B. The resulting nuclear- to-cytoplasmic partitioning of the sensor for these different MAPK activity traces are obtained as output. C. Correlation between MAPK activity and the nuclear-to-cytoplasmic ratio at the end of the simulation.

the dephosphorylation of the bio-sensor, and its exit by diffusion out of the nucleus. This mathematical model demonstrates that there is a tight relationship between SKARS localization and MAPK activity and that, using a few simple assumptions, it is possible to extract the mean MAPK activity of the population from the experimental measurements.

2.2.3. Single cell measurements

While a clear exit of the sensor out of the nucleus can be measured at the population level, we next wanted to verify whether we could also obtain kinase activity measurements at the single cell level. We noticed that there is a large variability in the nuclear enrichment of the sensor between individual cells prior to induction (figure 2.12.A). This large difference could arise from varying basal activity of the pathway [71] or from an intrinsic ability of a given cell to accumulate the sensor in the nucleus. To differentiate between these two possibilities, we combined a functional ($Ste7_{DS}$ -NLS-YFP) and a non-functional sensor ($Ste7_{ND}$ -NLS-RFP) in the same cell. We define the Basal Level as the nuclear-to-cytoplasmic ratio of the SKARS before induction (figure 2.12.A). Using this measurement, we observe a high correlation between the nuclear enrichment of the two sensors within a cell, which demonstrates that each cell has an inherent ability to import the sensor (figure 2.12.B). Evidently, in cells displaying a higher nuclear

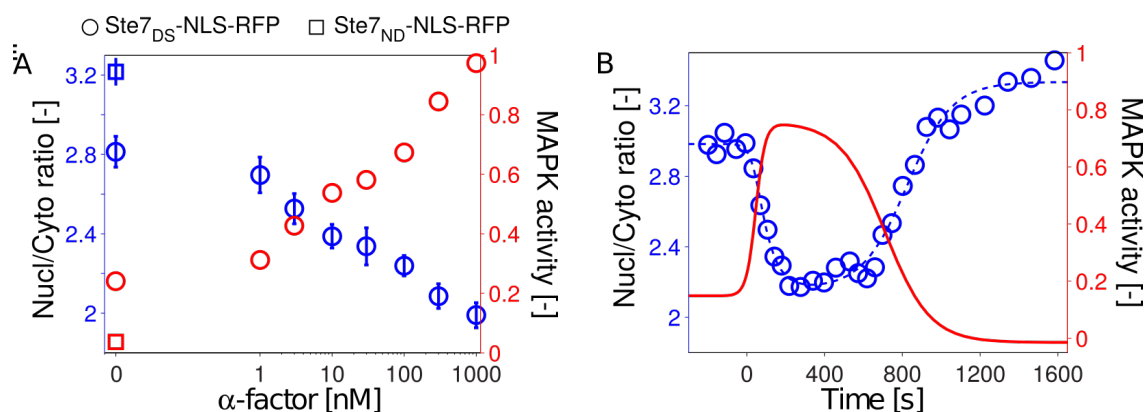


Figure 2.11.: Simulated MAPK activity at various pheromone concentrations and prior and after Fus3-as inhibition. A. Dose-response curve of the nuclear enrichment of the sensor as a function of concentration after 15 minutes of stimulation with pheromone (blue circles). The mean and standard deviation of three measurements are plotted. The corresponding MAPK activity level is calculated (red circles). As reference, the nuclear-to-cytoplasmic ratio of the unstimulated non-docking sensor and its corresponding level of MAPK activity are indicated by blue and red squares. B. Determination of MAPK activity for the experiment from figure 2.6.B. The blue circles correspond to the experimental data points. The dashed blue line represents the fit of those points by the model. The solid red line is the extrapolated MAPK activity for this time-course

enrichment of the sensor, the change in nuclear-to-cytoplasmic ratio upon stimulation is easier to quantify (figure 2.12.A). To allow for a fair comparison between each individual single cell trace, they were normalized by their basal levels. For each individual trace, the initial response (3 to 5 minutes after stimulus) and the final response (last three points of the time-lapse) were quantified (figure 2.13.A-D).

The normalized nuclear-to-cytoplasmic ratios of roughly 300 single cells were sorted based on their final responses and displayed in a heat map where each line corresponds to a single cell trace (figure 2.14.A). In the lower part of the map, cells displaying a large change in nuclear-to-cytoplasmic enrichment upon stimulation are clustered (high final response). The upper part of the map represents a fraction of the population where no response is detected. To discriminate the responding cells from the non-responding ones figure 2.14, we compared the single cell responses of two strains bearing either the docking or the non-docking sensor (Ste7_{DS}-NLS-RFP and Ste7_{ND}-

2. Dynamic single cell measurements of MAPK activity

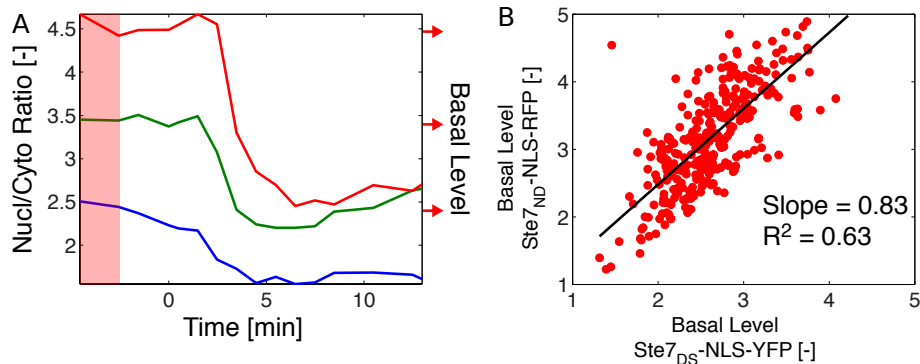


Figure 2.12.: Variability of the basal ratio N/C from cell-to-cell. A. Nucleus to Cytoplasm ratio for three single cell traces. The mean value of the three first points allows to define the Basal Level of the trace ($\text{Nucl/Cyto}(t=-4:-2\text{min})$). B. Correlation between the Basal Level measured in the YFP and RFP channels of a strain bearing two sensors, one with a functional docking sequence ($\text{Ste7}_{DS}\text{-NLS-YFP}$) and one with a non-docking variant ($\text{Ste7}_{ND}\text{-NLS-RFP}$). The high degree of correlation between the two measurements demonstrates that the Basal Level of the sensor is mostly dependent on the intrinsic property of the cells to enrich the sensor and does not depend on a variable constitutive activity of the mating pathway.

NLS-RFP, respectively). Using the non-functional sensor as a reference, we set a threshold to discriminate between the responding cells and non-responding cells bearing the functional sensor (2.15). Roughly 17% of the cells measured were thus characterized as non-responding (2.14.B).

In the group of responding cells, we could also differentiate two types of responses. A small fraction (11 %) of the total cell population displayed a delayed response, characterized by an initial response weaker than the final response (arbitrarily defined as more than a 50 %-fold difference, 2.14.B). 2.14.C represents the mean response of the cells in the defined categories (solid lines) as well as the response of one cell from each sub-population (dotted line), identified by a circle in panel B. Images of these same cells are also provided in panels D, E, and F. The heterogeneity in the dynamics of SKARS between these three populations of cells suggests that they have very different levels of MAPK activity, which may be linked to an intrinsic difference in their ability to respond to mating pheromone.

It is indeed well-established that the signalling activity in the mating pathway is dependent on the cell cycle stage [81, 116]. Cells which are committed to division and have entered the S-phase

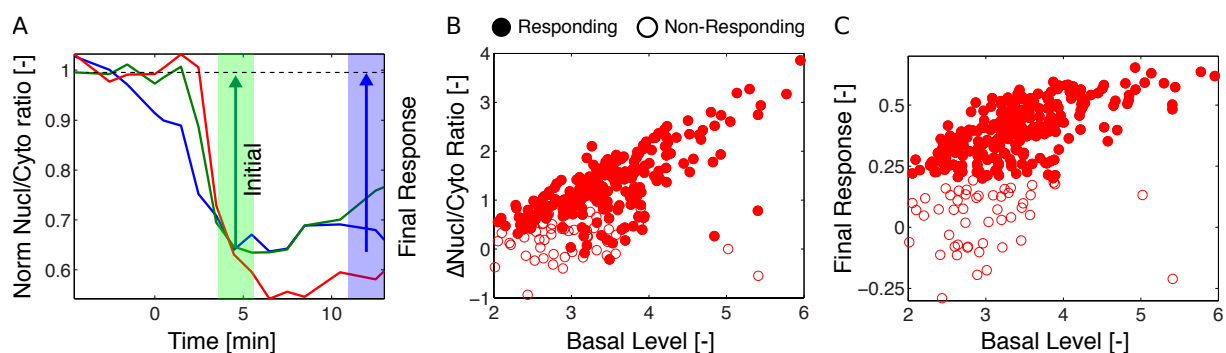


Figure 2.13.: Initial and final response define the dynamic relocation of the sensor at the single cell level. A. Single cell traces are normalized by their Basal Level to allow for a better comparison between individual cell responses. The normalized traces of the three same cells from figure 2.12.A are shown in panel A. The Final Response is calculated as $(\frac{Nucl}{Cyto}_{t=-4:-2min} - \frac{Nucl}{Cyto}_{t=12:15min}) / \frac{Nucl}{Cyto}_{t=-4:-2min}$. The Initial Response is calculated as $(\frac{Nucl}{Cyto}_{t=-4:-2min} - \frac{Nucl}{Cyto}_{t=4:6min}) / \frac{Nucl}{Cyto}_{t=-4:-2min}$. B and C. Correlation between the Basal Level and the difference in Nucleus to Cytoplasm ratio $\frac{Nucl}{Cyto}_{t=-4:-2min} - \frac{Nucl}{Cyto}_{t=12:15min}$. (B) or Basal Level and the Final response (C). The strong bias for the difference in Nuclear/Cytoplasmic ratio as function of Basal Level is corrected by the normalization applied in panel C. Open circles are classified as non-responding cells.

become refractory to signal transduction. To correlate cell cycle stage with the dynamics of the SKARS, we tagged Whi5 and Yox1 with mCitrine in cells bearing the sensor. Whi5 is a repressor of G1 transcription and accumulates in the nucleus of the cells during G1 (figure 2.16.A). It has been used previously as a marker for G1-entry and exit [9]. Yox1 is a transcription repressor that inhibits the expression of cell cycle regulated genes induced in the M and G1 phases [92]. It enters the nucleus upon S-phase entry and remains there until the beginning of G2 (figure 2.16.B). As expected, cells with nuclear Whi5 were predominantly responding (figure 2.17.A, dark blue dots). In contrast, a large fraction of the Yox1 positive cells were non-responding (figure 2.17.B, light blue dots). Cells with cytoplasmic Whi5 were equally split between non-responding and responding cells. Based on the Yox1 data, we can assume that these non-responding cells are mainly S-phase cells (figure 2.17.A, light green dots) and, therefore, the responding ones are G2/M cells (figure 2.17.A, dark green dots). Similarly, we can assume that the Yox1 negative

2. Dynamic single cell measurements of MAPK activity

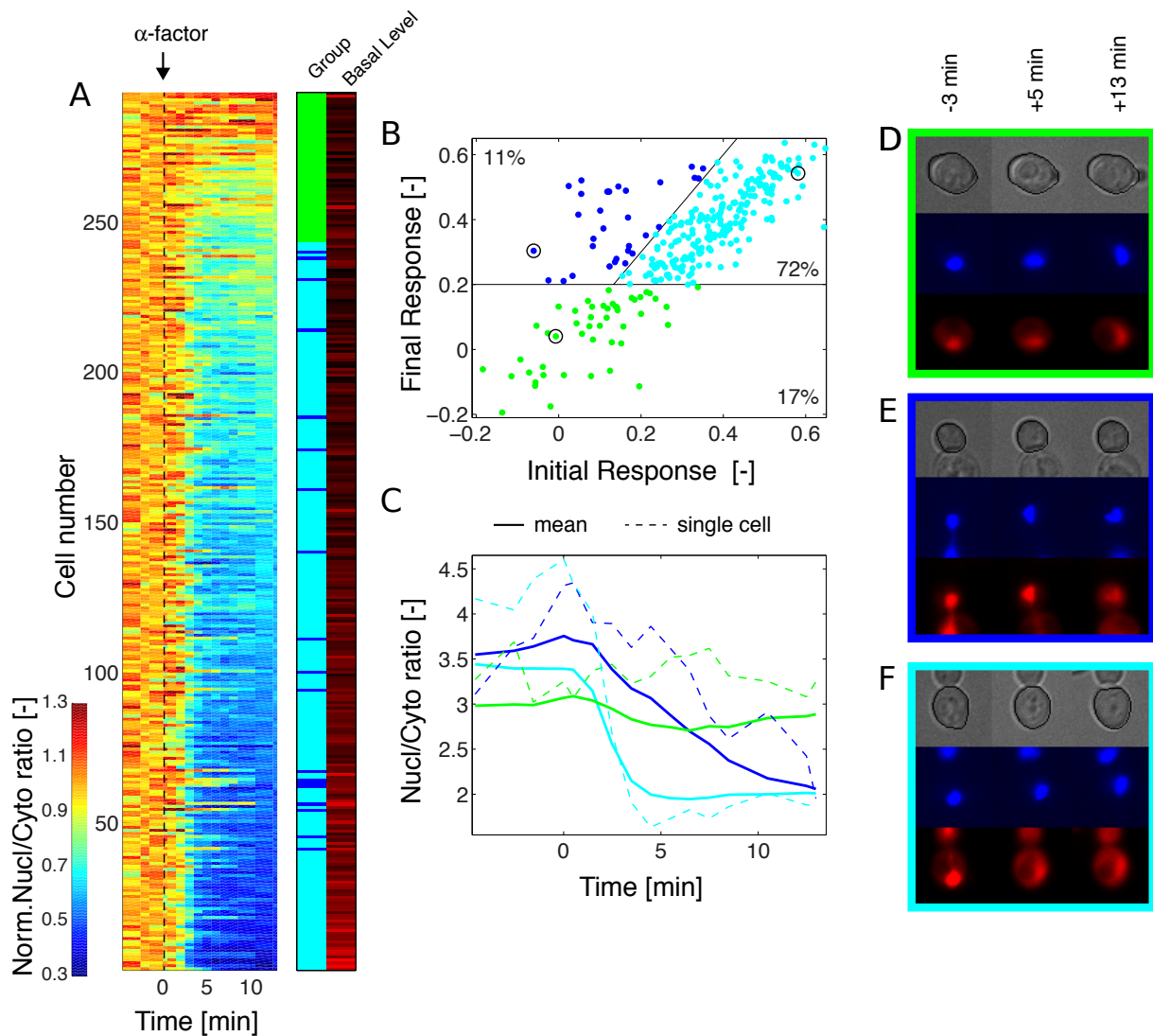


Figure 2.14.: Single cell analysis of MAPK activity upon pheromone stimulation. A Heat map of the response of individual cells to $1 \mu\text{M}$ α -factor. Each line represents the nuclear-to-cytoplasmic ratio of one single cell normalized by its basal level ($N_c = 293$). The cell responses were sorted based on the level of final response (measured at $T = 12$ min). The cells were classified as responding (cyan), non-responding (green), or slow responding (blue). The basal level of each trace is indicated in shades of red (from black to red, increasing basal level). B Scatter plot of initial and final response of the cells. Each dot corresponds to a single cell measurement. The colour indicates to which sub-population the cells belong to. C Temporal evolution of the nuclear-to-cytoplasmic ratio upon pheromone treatment. The solid line represents the mean response of each sub-population. The dashed lines are traces from the three single cells circled in panel (B). D, E, F Images of the selected cells in the brightfield, CFP (histone tag), and RFP (Ste7_{DS}-NLS-RFP) channels at different time points. The dark line in the brightfield image represents the segmented cell contour

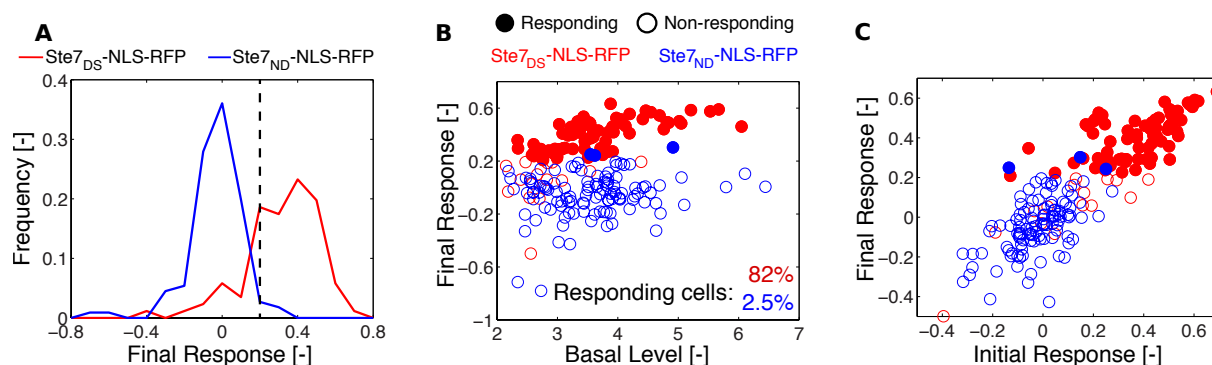


Figure 2.15.: Quantification of single cell response. A. Histogram of the Final Response measured in a population of cells bearing the functional sensor ($Ste7_{DS}$ -NLS-RFP, red) and the non-functional sensor (non-docking, $Ste7_{ND}$ -NLS-RFP, blue). The histogram of the final response in the population allows to set a threshold (dashed line) at 0.2 to minimize the number of cells bearing the non-functional sensor considered as responding. B and C. Correlation between Basal Level and Final Response (B), and Final Response and Initial Response (C) for docking (red) and non-docking (blue) versions of the sensor. The filled circles represent the responding cells. 82% of the cells bearing the functional sensor are characterized as responding. These graphs demonstrate that the difference between a functional and non-functional sensor can also be observed at the single cell level

population, which displays a response, is dominated by G1 cells (figure 2.17.B, dark green dots), while responding cells with a Yox1-positive signal must be in the G2 phase (figure 2.17.B, dark blue dots). Note also that the various population identified using the Whi5 or the Yox1 marker exhibits different MAPK activity level prior stimulation. This values turn to be high for cell in G1 and low for cells in S-G2-M phases. This would suggest that the MAPK activity is differentially regulated depending on the cell-cycle. This result will be further discussed in chapter 3, 3.2.1.

Taken together, these results are in general agreement to what was previously known: G1, M, and G2 cells are permissive to α -factor signalling while S-phase cells are refractory to this stimulus. However, these data also offer some additional insights about this regulation. First of all, there is a clear kinetic difference in the activation of the sensor between G1 cells and G2/M cells. In G1 cells, the sensor exits the nucleus within 3 to 4 minutes after the stimulus, while the G2/M cells seem to display a slower response (figure 2.17.C, dark blue vs. dark green curves).

2. Dynamic single cell measurements of MAPK activity

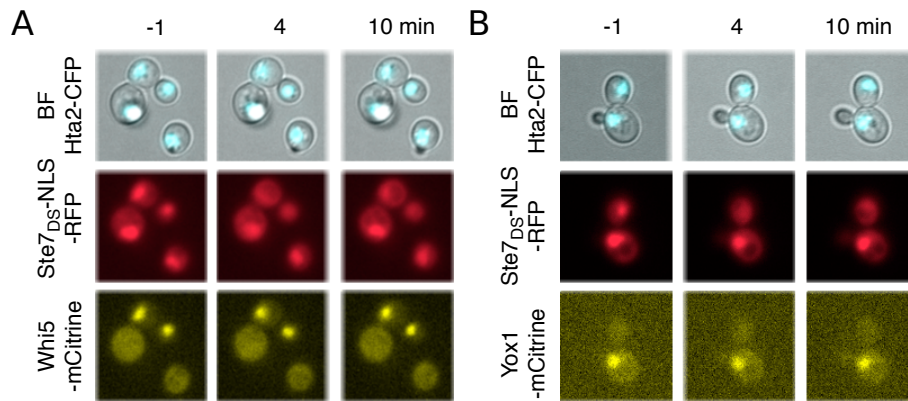


Figure 2.16.: Subcellular localization of the Whi5 and Yox1 cell cycle marker. Yeast cells expressing the $Ste7_{DS}$ -NLS-RFP sensor and Whi5 tagged with mCitrine (A) or Yox1 tagged with mCitrine (B) imaged before and after stimulation with α -factor.

This sub-population of cells is clearly enriched for slow responding cells (figure 2.14.B dark blue dots and figure 2.18.A red dots). This suggests that Fus3/Kss1 activity in this phase of the cell cycle is reduced. The second interesting observation is the fact that almost all sub-populations display an early exit of the sensor, which subsequently returns to basal value for non-responding cells (figure 2.17.C, light green curve and figure 2.17.D light blue curve). This hints at a transient activation of the pathway at early time-points, which cannot be sustained if the cells are not in the proper cell cycle stage.

2.2.4. Combination of sensors

In the previous experiment, SKARS were associated with fluorescently tagged proteins to correlate kinase activity and cell cycle stage. In a similar manner, we can envision to combine multiple SKARSs in the same cell to correlate the activity of different kinases. Indeed, the fluorescent protein in the sensor is an inert bystander of the relocation process and its exchange should not affect the response of the sensor. To verify this statement, we combined an RFP and a YFP versions of the sensor ($Ste7_{DS}$ -NLS-RFP and $Ste7_{DS}$ -NLS-YFP) in the same strain. While there is a slight difference between the YFP and RFP ratio measured with the sensor, the dynamics of the response measured with both sensors are strikingly similar (figure 2.19.A). At

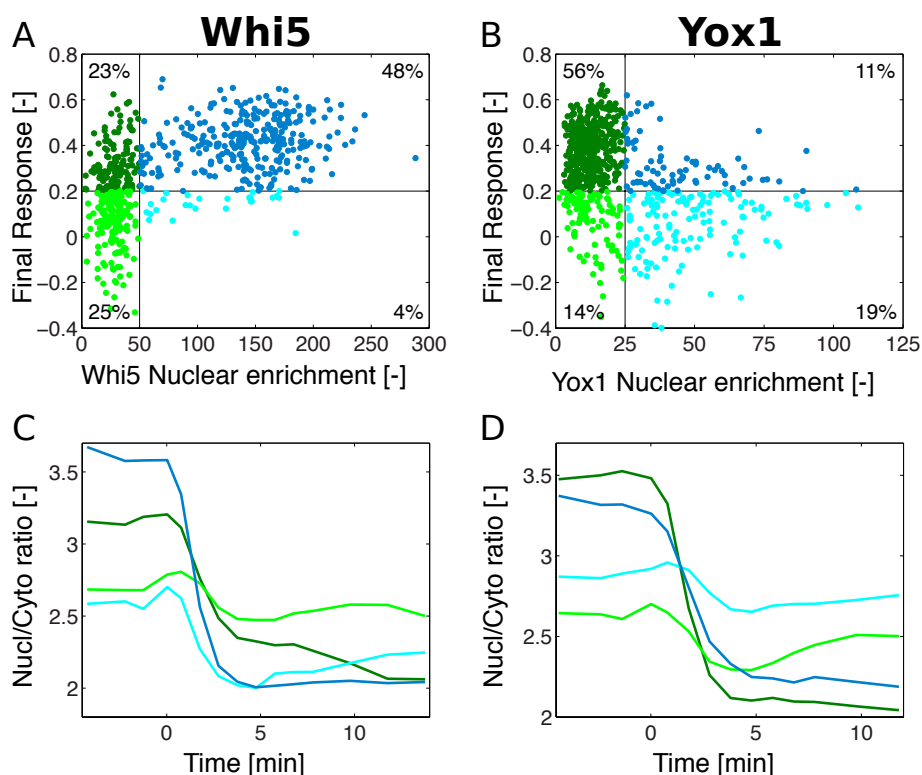


Figure 2.17.: Cell cycle dependent dynamics of signalling in the mating pathway. A, B Correlation between the measured Whi5 (Nc = 616, A) and Yox1 (Nc = 698, B) nuclear enrichment (nuclear – cytoplasmic intensities) measured before stimulation and the sensor’s final response. The scatter plot is split in four quadrants. The blue dots represent cells with an enriched nuclear marker, while the green dots represent cells where no enrichment is detected. The dark and light coloured dots represent, respectively, responding and non-responding cells. C, D Average response of the four sub-populations of cells in the four quadrants delimited on panels c (Whi5, C) and d (Yox1, D). The colour code is the same as in (A) and (B).

the single cell level, we measured a high correlation between the final responses measured with each sensor (figure 2.19.B). The $Ste7_{DS}$ allows the sensing of the combined activity of Fus3 and Kss1. In their analysis of MAPKs’ DSs, Lim *et al.* [101] revealed the difference in structure between the DS of Ste7, which binds both Fus3 and Kss1, and the DS of Far1, that is specific for Fus3. The presence of two prolines in the $Far1_{DS}$ forces the binding to MAPK via a different conformation that is not compatible with the Kss1 docking groove. To test whether we could confer Fus3 specificity to our sensor, we replaced the 11 amino acids in the $Ste7_{DS}$ by the 13

2. Dynamic single cell measurements of MAPK activity

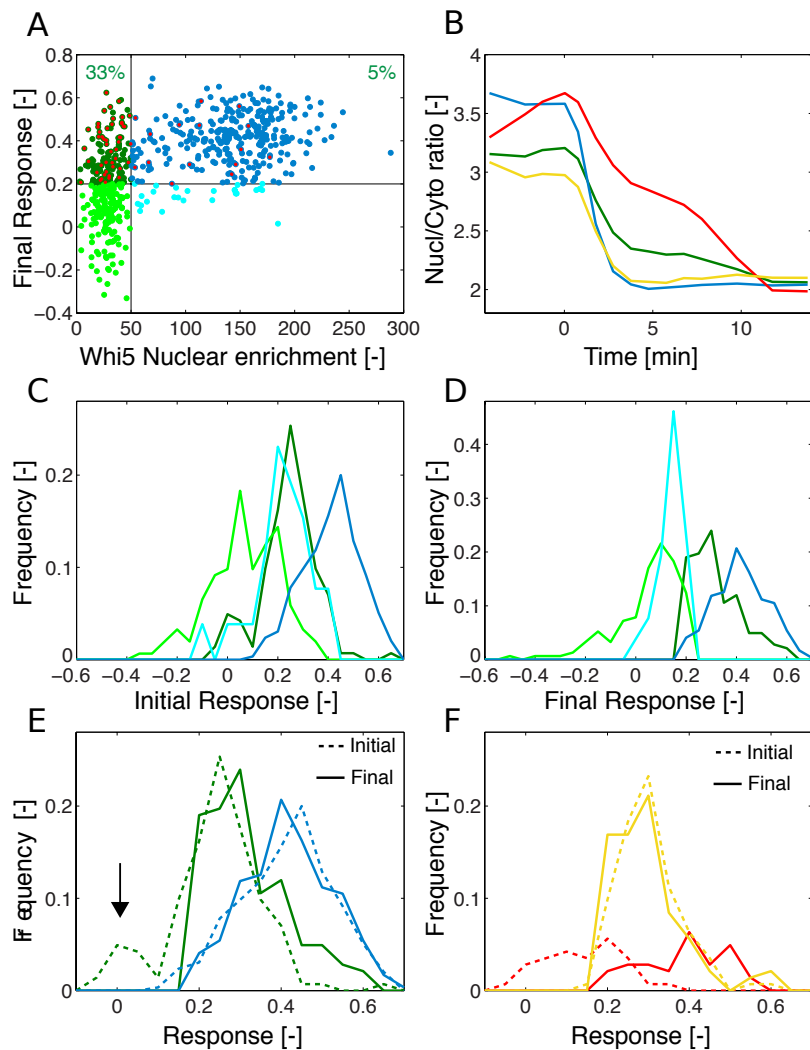


Figure 2.18.: Slow responding cell in G2/M cell cycle stage. A. Same panel as in Figure 5C displaying the Whi5 Nuclear enrichment vs. Final Response of the cell. Cells displaying a slow response are marked with a red dot. 33% of the G2/M cells are characterized as slow responding (only 5% in the G1 cells population). 76% of the slow responding cells are found in the G2/M quadrant. B. Dynamics of Nuclear exit of the SKARS. Blue: average response of G1 Cells. Green: average response of G2/M cells. Yellow: average response of the fast responding cells in G2/M stage. Red: average response of slow responding cells in G2/M stage. C. and D. Histograms of the Initial and Final Response of the four sub-population of cells selected in panel A. The histogram of the slow responding cells (dark green) is the only one that shifts considerably between the initial and final response. E. Comparison of Initial and Final Response histograms for G2/M (green) and G1 (blue) cells. Note the shoulder in the histogram (arrow) denoting a population of cells that have not responded within the first 5 min of the time-lapse but which has disappeared in the Final Response histogram. F. Comparison of Initial and Final Response histograms for G2/M cell with slow (red) or fast (yellow) response phenotype. The slow responding cell display a clear shift in the histogram between Initial and Final Responses.

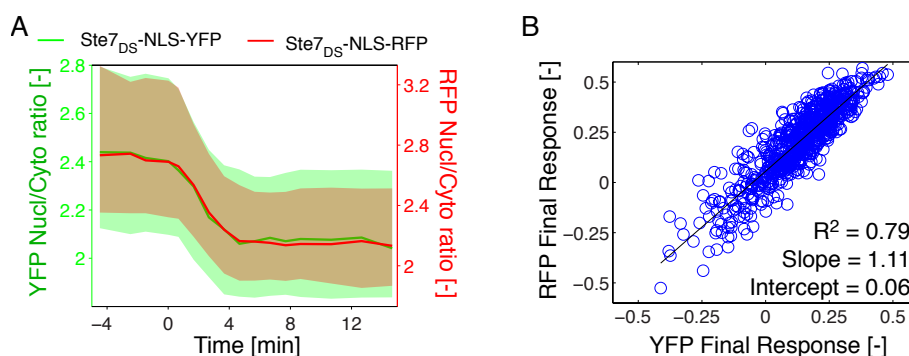


Figure 2.19.: Generation of a Fus3-specific sensor based on the Far1 docking site. A. Combination in the same cell of two sensors bearing the same Ste7_{DS} but tagged with mCherry or mCitrine and stimulated at time 0 with 1 μ M α -factor ($N_c = 660$). The ratios were plotted on two different y-axes (left: Ste7_{DS}-NLS-YFP, right: Ste7_{DS}-NLS-RFP) to allow a direct comparison of the dynamic response of both sensors. B. Correlation of the Final Response in cells bearing the Ste7_{DS}-NLS-YFP and Ste7_{DS}-NLS-RFP sensors.

residues forming the Far1_{DS} (figure 2.20.A). To test the specificity of this sensor, we combined the Far1_{DS}-NLS-RFP and Ste7_{DS}-NLS-YFP sensors in the same cells and quantified their responses in wild-type (WT) and MAPK deleted strains (figure 2.20.B-C). Both sensors relocate in WT and *kss1* Δ backgrounds. As expected, all relocation is abolished in the double MAPK deleted *fus3* Δ *kss1* Δ strain. Interestingly, in *fus3* Δ cells, only the Ste7_{DS}-NLS-YFP sensor exits the nucleus upon α -factor stimulation, demonstrating the specificity of the Far1_{DS} for phosphorylation by the Fus3 MAPK. The histogram of the final response measured in individual cells is displayed in figure 2.20.C. In *fus3* Δ cells, a weak but statistically significant activation of the pathway can be detected. Note also that the basal nuclear enrichment of the Ste7_{DS}-NLS-YFP sensor in this strain is lower, which suggests that, in the absence of Fus3, there is a slightly higher level of MAPK Kss1 activity. This is in agreement with previous observations showing that Kss1 is overexpressed and displays a higher basal activity in a *fus3* Δ background [47]. It is noteworthy to mention that both the dynamics and level of kinase activity in WT and *kss1* Δ cells are very similar, arguing for a predominant contribution of Fus3 to the response of the cells when stimulated with 1 μ M α -factor.

2. Dynamic single cell measurements of MAPK activity

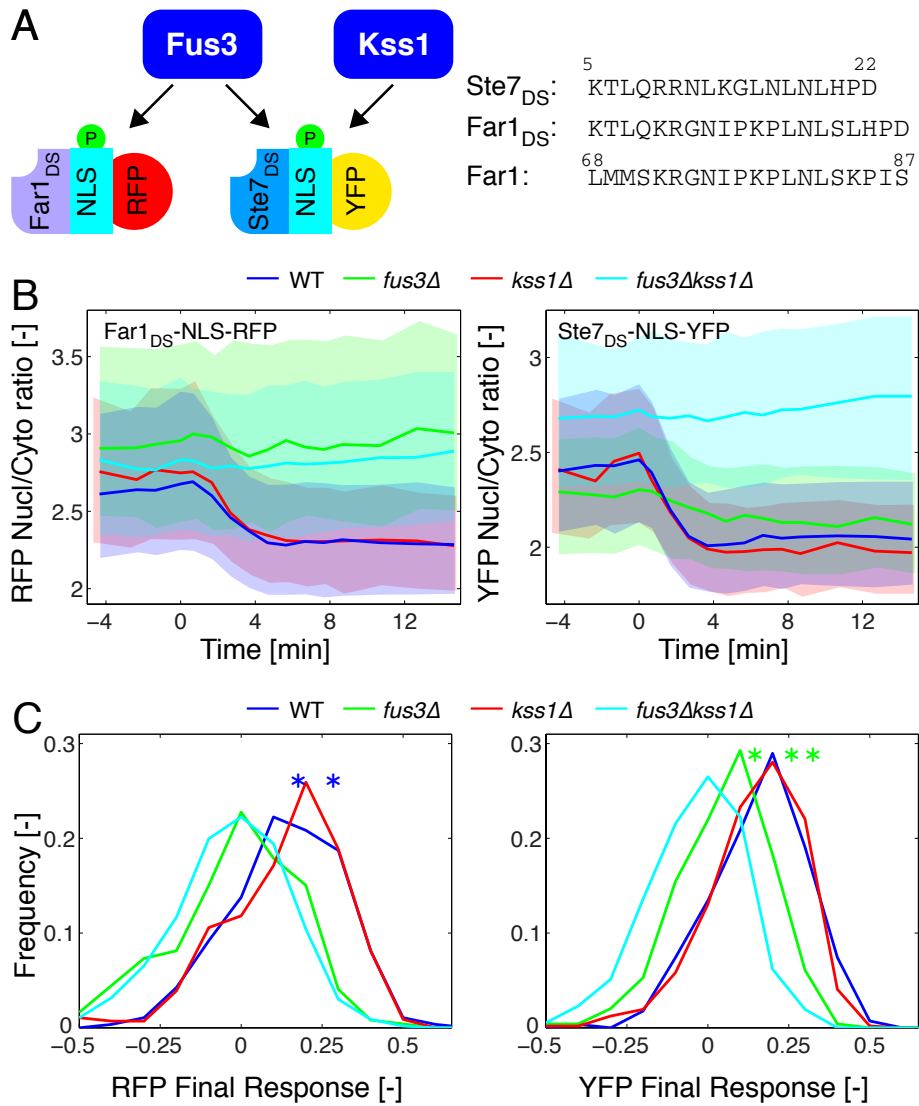


Figure 2.20.: A. Engineering of a Fus3-specific sensor by replacing the Ste7 docking site with the Far1 docking site sequence (Far1_{DS}). B. Response of cells of different background (WT (blue, Nc = 630), *fus3Δ* (green, Nc = 474), *kss1Δ* (red, Nc = 990), and *fus3Δkss1Δ* (cyan, Nc = 952)) bearing the Far1_{DS}-NLS-RFP (left) and the Ste7_{DS}-NLS-YFP (right) stimulated with α -factor 1 μ M. C. Histograms of the final response of cells in the YFP and RFP channel. The asterisks designate distributions that are significantly different (t-test, $P < 0.001$) from the non-responding *fus3Δkss1Δ* control.

2.2.5. Cell wall integrity pathway

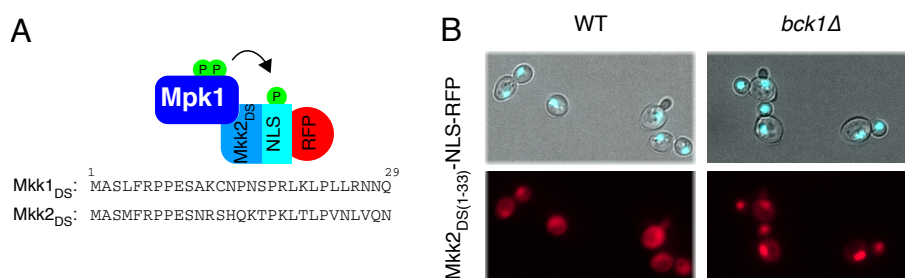


Figure 2.21.: Engineering of a Mpk1-specific sensor. A Schematic of the Mpk1 sensor and alignment of the docking sites present in Mkk1 and Mkk2. A and B. Images of WT (A) and (B) cells bearing the Mkk2_{DS1-33}-NLS-RFP sensor. The cytoplasmic localization of the sensor is signalling dependent.

Since the DS of the sensor dictates its specificity, we next tried to identify a DS for the MAPK of the CWI pathway, Mpk1. Molina *et al.* [57] identified a sequence in the N-terminus of the MAP2Ks Mkk1 and Mkk2 of *S. cerevisiae* that is conserved in other fungi and share some homology with the consensus DS of MAPKs (figure 2.21.A). We therefore cloned the first 33 amino acids of Mkk2 in front of the NLS-RFP construct to generate an Mpk1-specific SKARS. When integrated in cells, this sensor turned out to be mostly cytoplasmic, suggesting that a high basal activity of the MAPK resulted in a constitutive phosphorylation of the sensor. Indeed, this localization was Mpk1 activity-dependent, since deletion of the MAP3K Bck1 leads to an enrichment of the sensor in the nucleus (figure 2.21.B).

To modulate the sensitivity of the sensor, we changed the distance separating the DS and the NLS. Mkk2 N-terminal fragments of different lengths (from 1–27 to 1–150 amino acids) were cloned in front of the NLS, hoping that the distance between the DS and the phosphorylation sites would tune the ability of Mpk1 to phosphorylate the sensor. While we did not detect a simple relationship between the length of the spacer and the basal level of nuclear localization of the SKARS (figure 2.22), we could identify one construct, DS1-100, which displayed the highest enrichment in nuclear fluorescence. Nonetheless, the nuclear enrichment of this SKARS was still highly variable from cell to cell, suggesting that cells within a population can display a wide

2. Dynamic single cell measurements of MAPK activity

range of Mpk1 activities.

To test whether the $Mkk2_{DS1-100}$ sensor could report on Mpk1 activation by acute cell wall stress, cells were subjected to zymolyase treatment. It has been previously reported that in order to activate Mpk1 upon zymolyase stress, activity of the HOG pathway via Ste11 and Pbs2 is required (figure 2.23.A) [10]. Due to the very large difference in basal value between $bck1\Delta$ cells on one side and WT and $ste11\Delta$ on the other, the latter strain offered a better comparison for the response measured in WT cells (figure 2.23.B). When measured at the population level, the

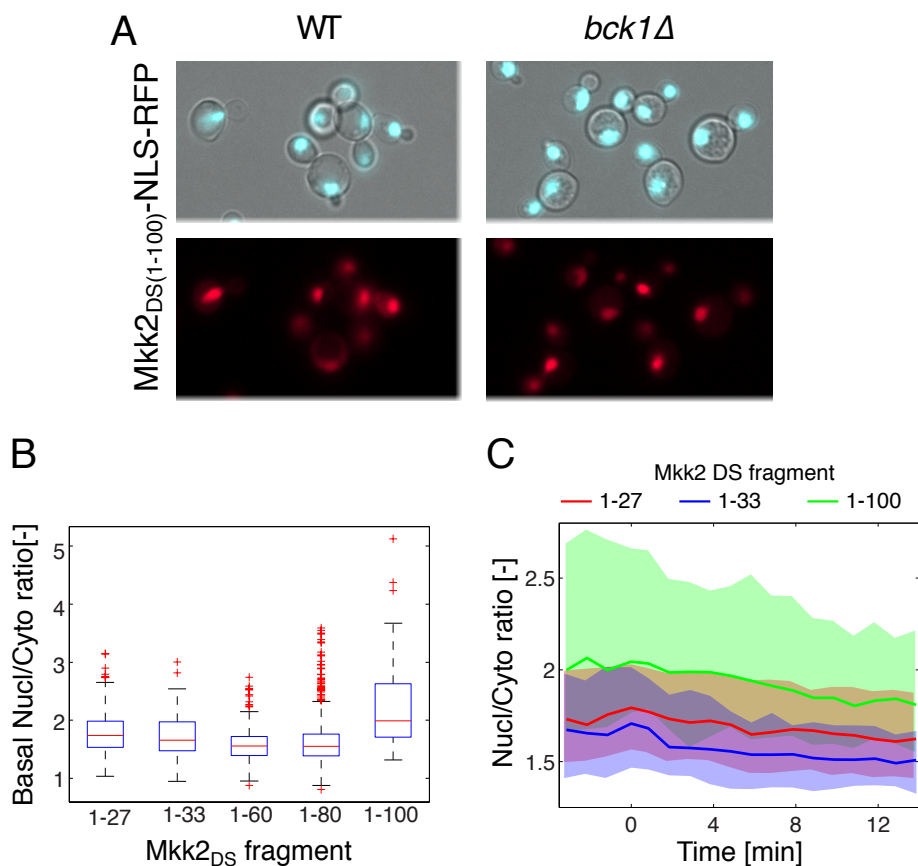


Figure 2.22.: Optimisation of the Cell Wall Integrity MAPK activity sensor. A and B. Images of WT (A) and (B) cells bearing the $Mkk2_{DS1-100}$ -NLS-RFP sensor. The cells with the $Mkk2_{DS1-100}$ -NLS-RFP sensor display a stronger basal nuclear enrichment than cells with shorter versions of the sensor. B. Quantification of the basal level of the sensor as function of the length of the Mkk2 fragment. C. Dynamics of response of three versions of the sensors upon zymolyase stress (3U/ml).

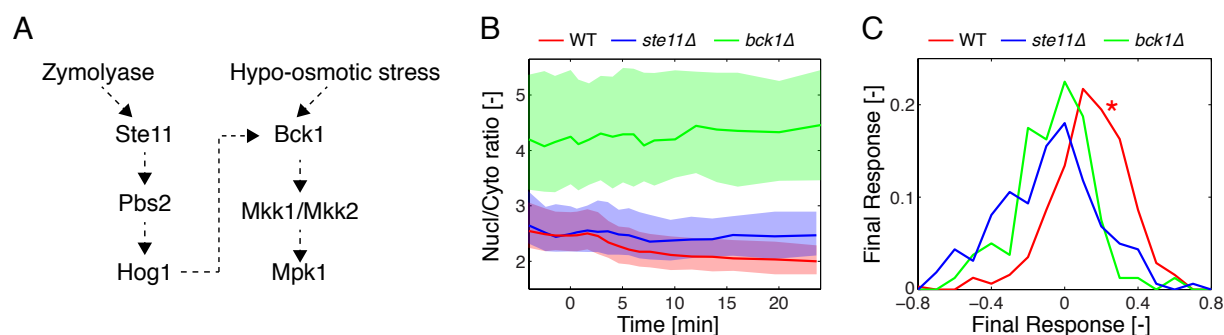


Figure 2.23.: Mpk1 activity dynamics upon zymolyase. A. Scheme of the activation of Mpk1 by zymolyase or hypo-osmotic stress. B. Dynamic localization of the Mkk2_{DS1-100}-NLS-RFP sensor quantified by its change in nuclear-to-cytoplasmic ratio upon stimulation by zymolyase 3 U/mL at time 0 in WT (red, $N_c = 313$), *ste11*Δ (blue, $N_c = 160$), and *bck1*Δ (green, $N_c = 80$). C. Histograms of the final response after zymolyase stress measured in the WT and two deletion strains. In panels C the asterisks designate distributions that are significantly different (t-test, $P < 0.001$) from the *bck1*Δ control.

WT cells stressed with zymolyase displayed a slow gradual relocation of the sensor out of the nucleus. As expected, this translocation was blocked in *bck1*Δ as well as in *ste11*Δ, implying that Mpk1 was not activated in these mutants (figure 2.23.C). Note also that the basal Mpk1 activity in a *bck1*Δ is higher than in a WT background. This would suggest that the CWI pathway is strongly activated in growing condition. This could be explained by the fact that the cell-wall is remodeled to form the bud during the polarized growth [137].

In order to verify that the response of the SKARS was specific to the Mpk1 pathway, we also stressed cells with hypo-osmotic shock, where CWI activation is independent of the HOG pathway (figure 2.23.A). To perform this experiment, cells were grown in medium complemented with 1 M sorbitol. The cells were loaded in a microfluidic chip and the medium was exchanged within seconds by medium containing 0.5 M sorbitol. The sensor transiently exited the nucleus and returned to a stable value slightly lower than the original basal value. Ste11 was not required for this response, as the *ste11*Δ cells displayed a response comparable to the WT cells. In *bck1*Δ cells, only a small drop in the nuclear-to-cytoplasmic ratio was detected corresponding to the expansion of the cell in the lower osmolarity medium (figure 2.24). Note also that the sensor

2. Dynamic single cell measurements of MAPK activity

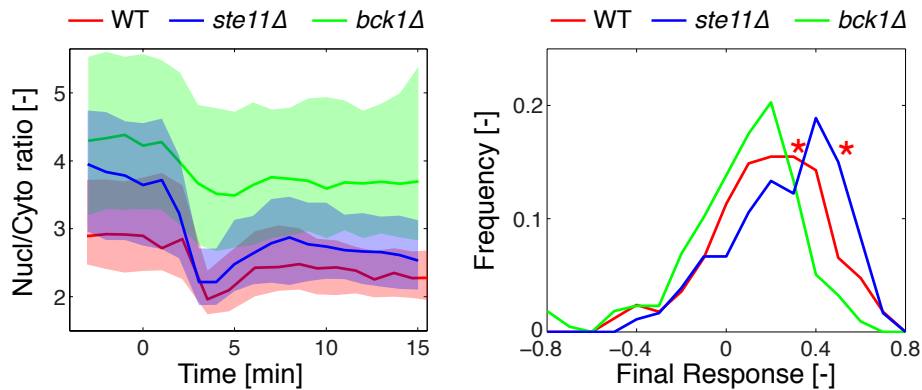


Figure 2.24.: Mpk1 activity dynamics upon hypo-osmotic stress. A. Histograms of the final response after zymolyase stress measured in the WT and two deletion strains. A. Mpk1 sensor relocation upon hypo-osmotic shock performed in microfluidic devices where the sorbitol concentration in the medium is lowered from 1 M to 0.5 M: WT (red, $N_c = 168$), *ste11Δ* (blue, $N_c = 180$), and *bck1Δ* (green, $N_c = 217$). B. Histograms of the final response after hypo-osmotic stress measured in the WT and two deletion strains. In panels B the asterisks designate distributions that are significantly different (t-test, $P < 0.001$) from the *bck1Δ* control.

was more nuclear in cells grown in 1 M sorbitol, implying that the basal activity of the pathway decreased under these conditions and that the deletion of Ste11 also influenced this basal activity in hyper-osmotic medium.

2.2.6. Single cell response to cell wall damage

Because of the wide variety in basal activity of Mpk1 observed in the cell population, we wondered how individual cells responded to zymolyase treatment. Figure 2.25.A represents a 2D-map of the normalized response of more than 300 single cells sorted based on their final response. Using a threshold of 0.2 for the final response, we can split the population in a group of responding (58%, blue) and non-responding cells (green). Figure 2.25.B displays the average nuclear-to-cytoplasmic ratio of the sensor as function of time for these two populations. The non-responding cells have a strikingly lower level of sensor nuclear enrichment at the onset of the experiment denoting a higher basal activity of the pathway in these cells (figure 2.25).

Since it has been reported that the activity of the Mpk1 pathway fluctuates during the cell cycle

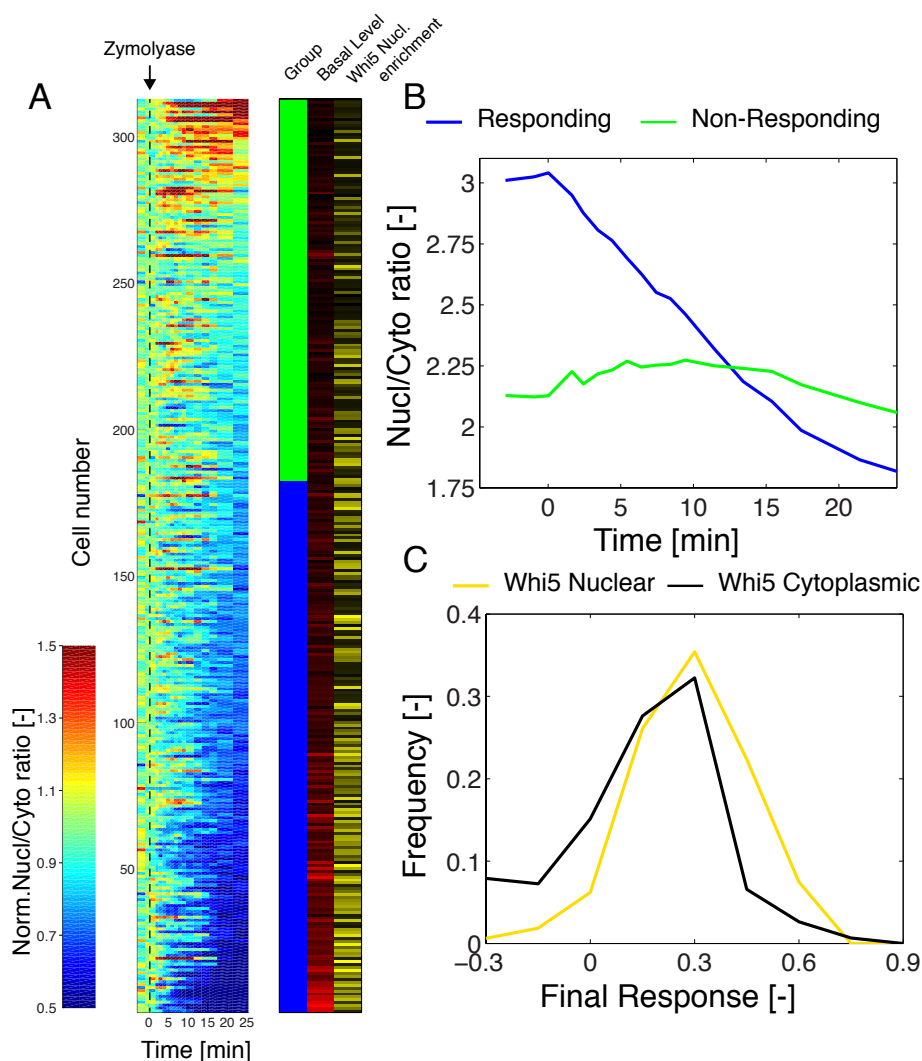


Figure 2.25.: Single cell responses upon zymolyase-induced cell wall damage. A. Heat map of the response of individual cells bearing the SKARS Mkk2_{DS1-100}-NLS-RFP to zymolyase (3 U/mL). Each line represents the normalized response of one single cell ($N_c = 313$). The cell traces were sorted based on the level of final response. This measurement was used to classify the cells in a group of responding cells (blue) and a group of non-responding cells (green). The basal level of each trace is indicated in shades of red (from black to red, increasing basal level). These cells also bear the cell cycle marker Whi5 and its level of nuclear enrichment is indicated in shades of yellow (from black to yellow, increasing nuclear Whi5). B. Histogram of the basal level in responding and non-responding cells. C. Histogram of the final response measured in cells with or without nuclear enrichment of the cell cycle marker Whi5 .

2. Dynamic single cell measurements of MAPK activity

and is higher in phases of polarized growth, we wondered whether the heterogeneity observed in the response to zymolyase was dependent on cell cycle stage [137]. G1 cells in the population were identified with a Whi5-mCitrine tag. The level of nuclear accumulation of Whi5 for each cell is shown in figure 2.25.A; cells with nuclear Whi5 can be found in both the responding and non-responding cells. Figure 2.25.C compares the final response of cells with nuclear and cytoplasmic Whi5. A similar analysis was performed with Yox1-mCitrine cells, where the presence of the

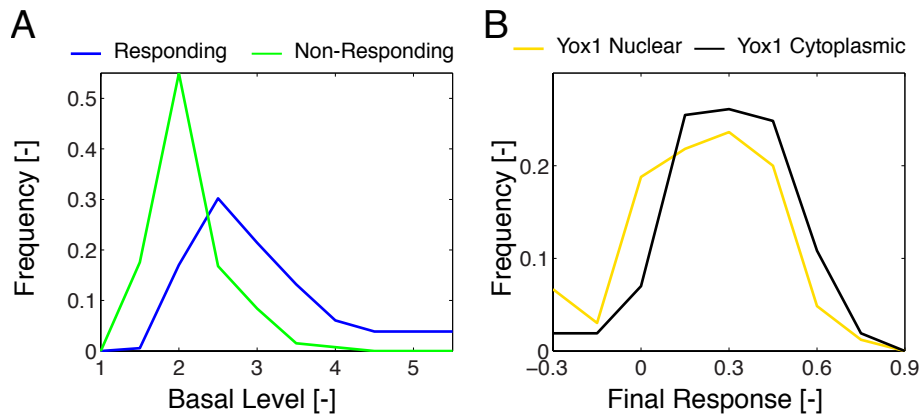


Figure 2.26.: Single cell responses upon zymolyase-induced cell wall damage: Yox1 marker. The experiment from figure 2.25 is performed with a strain expressing the Yox1-mCitrine marker. A. Histogram of the basal level in responding and non-responding cells. B. Histogram of the final response measured in cells with or without nuclear enrichment of the cell-cycle marker Yox1.

fluorescent protein in the nucleus identifies S-phase and early G2-phase cells (figure 2.26). There was a tendency for G1 cells to respond stronger to the stimulus while dividing cells displayed a decreased tendency to respond. However, there was no apparent inhibition of CWI signalling in a cell cycle-dependent manner.

To modulate the basal activity of the pathway, we grew cells in low glucose (0.01 %, figure 2.27). In this medium, the growth rate was slower, thus remodelling of the cell wall occurred on longer time-scales, resulting in a lower constitutive basal activity of Mpk1. Indeed, we observed a global increase in the basal nuclear enrichment of the sensor, resulting from the decreased activity of Mpk1 (figure 2.27B). A larger fraction of the cells stressed with zymolyase under these conditions

displayed an export of the sensor (figure 2.27C). Together, these results indicate that basal activity of the CWI pathway is linked with cell growth rather than the cell cycle. Moreover, in cells where Mpk1 is already activated by growth, we do not detect an additional effect due to the cell wall stress induced by zymolyase within the time-frame of the experiment.

2.3. Discussion

In this chapter, we demonstrate the use of a new set of biosensors to measure the fast dynamics of signal transduction in living single cells. The functional part of the sensor is a double NLS sequence bearing four phosphorylation sites, which results in a three-fold enrichment of the reporter in the nucleus of the cells under basal conditions. This is, however, not a static situation and the sensor constantly shuttles back and forth between the cytoplasm and the nucleus. The import into the nucleus is actively driven by the NLSs while the exit out of the nucleus is a passive mechanism relying on diffusion due to the small molecular weight of the sensor [59]. Upon phosphorylation of the NLS, the import rate into the nucleus will be decreased due to a lower affinity for importin, while the diffusion rate remains the same, resulting in a lower concentration of the nuclear sensor. Note that phosphorylation can occur in both compartments due to the constant exchange between both sensor pools. Therefore, measurement of kinase activity is not restricted to one of these compartments, and the sensor measures the global activity of the enzyme in the cell. Moreover, using a simple mathematical model, it is possible to infer the amount of MAPK activity from the SKARS measurements.

The action of the kinase on the sensor is antagonized by phosphatases. These dephosphorylation events occur on the minute time-scale, as attested by our inhibition of Fus3 experiment (figure 2.6). Since the signal transduction event in the MAPK cascade occurs on a similar timescale, the SKARS are perfectly suitable to record these fast signalling events. Our sensor ultimately measures the balance between kinase and phosphatase activities on the phosphorylatable residues on the NLS. In MAPK pathways, signalling results in a change in the activation

2. Dynamic single cell measurements of MAPK activity

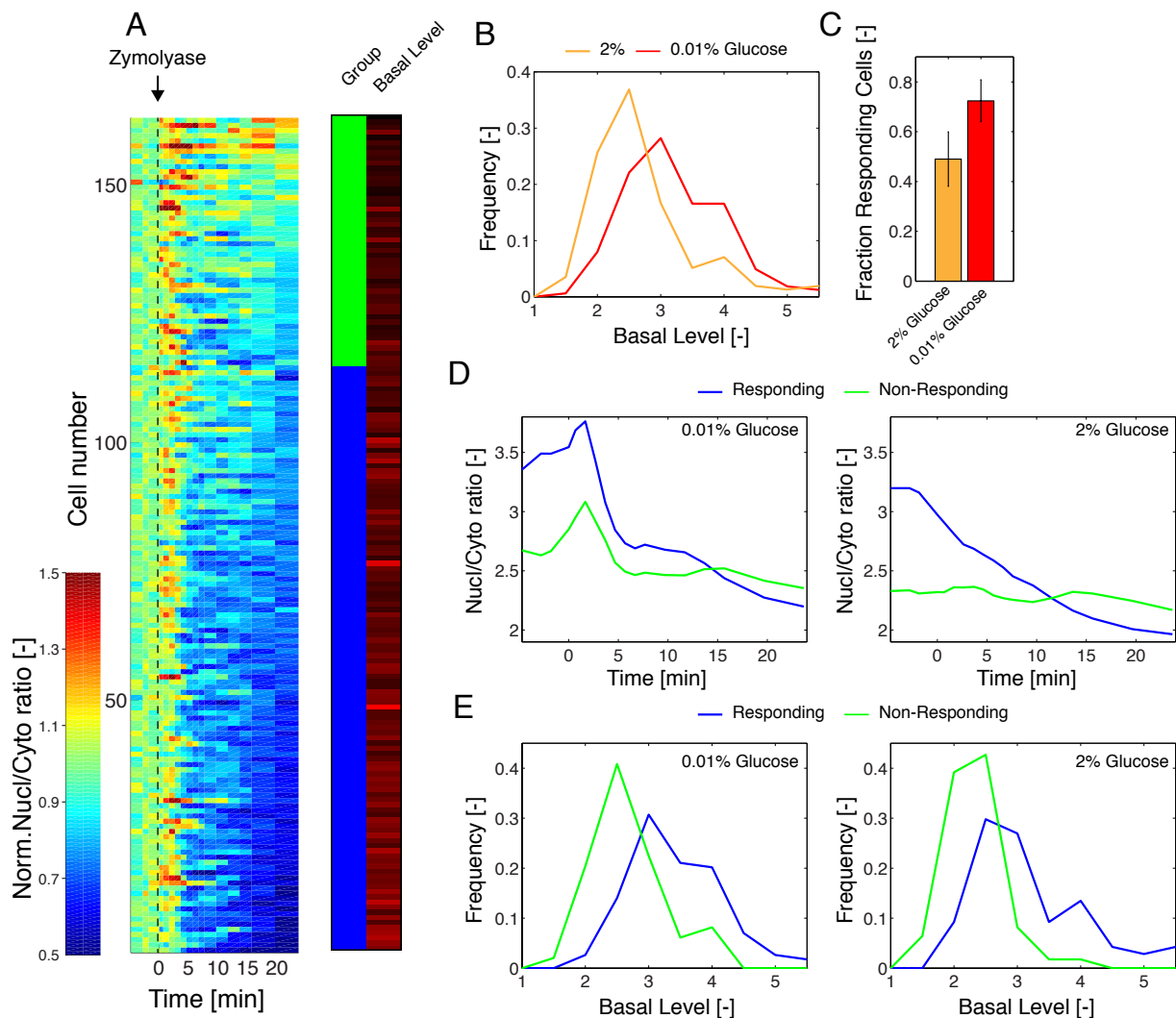


Figure 2.27.: Single cell analysis of Mpk1 activation by zymolyase in low glucose concentration. A. Heat map of the response of individual cells bearing the SKARS Mkk2_{DS1-100}-NLS-RFP to zymolyase (3U/ml). Each line represents the normalized response of one single cell ($N_C = 163$). The cell traces were sorted based on the level of Final Response. This measurement was used to classify the cells in a group of responding cells (blue) and a group of non-responding cells (green). The Basal Level of each trace is indicated in shades of red (from black to red, increasing basal level). B. Histogram of the Basal Level of nuclear enrichment in 0.01% and 2% glucose. C. Fraction of responding cells in 2% and 0.01% glucose. Mean and standard deviation of four experiments are shown. D. Time-course of the Nuclear to cytoplasmic ratio for responding and non-responding cells at 0.01% and 2% glucose. E. Histogram of the Basal Level for responding and non-responding cells grown in 0.01% and 2% glucose.

of the MAPKs while the phosphatases possess a relatively stable and constitutive activity. Part of the variability observed with our sensor could possibly arise from differences in phosphatase activity between individual cells.

Förster Resonance Energy Transfer (FRET) probes have been generated to monitor the activity of kinases in cells [124, 38, 79]. In comparison, the SKARS possesses two main advantages. First, the requirement of the FRET probe to use two fluorophores together with the limited number of available FRET pairs makes it difficult to combine two different FRET sensors in the same cell. In comparison, our system uses a single fluorescent protein and we have showed the correlated measurements of two reporters in the same cell. This number could be increased to three or four by combining different fluorescent protein spectral variants [110].

The second advantage of our system lies in its modularity. The optimization of the FRET sensor is a difficult task because the orientation of the two fluorophores has to be adjusted and depends directly on the structure of the sensor's active site [39, 62]. In the SKARS, the substrate site and the fluorescent protein are independent of each other, and can therefore be interchanged without affecting each other. Indeed, the fluorescent moiety was exchanged between mCherry and mCitrine without affecting the dynamics of the response. Similarly, we could exchange the $Ste7_{DS}$ with a $Far1_{DS}$ or $Mkk2_{DS}$ to confer specificity of the sensor towards Fus3 or Mpk1, respectively. We also demonstrated that the sensitivity of the sensor can be tuned by changing the distance between the DS and the phosphorylatable residues in the NLS.

Interestingly, NLSs as well as MAPK DSs are conserved domains throughout all eukaryotes. This implies that a similar strategy can be adopted to develop sensors for higher eukaryotes. In fact, other kinase sensors based on phosphorylatable NLS or nuclear exclusion sequences have been described in the literature both in yeast and in higher eukaryotes by using small domains of proteins known to relocalize [115, 31]. In parallel to the development of our biosensor, Regot *et al.* [99] have used a similar strategy to quantify MAPK activity in mammalian cells. This underscores the wide applicability of the approach presented here. In this work, we used a synthetic biology approach to design *de novo* a MAPK substrate that can undergo relocation.

2. *Dynamic single cell measurements of MAPK activity*

Using a similar strategy, we can also envision measuring other enzymatic activities in living cells. Extending the range of available SKARS for other kinases should be relatively straightforward if they require a DS and possess a short consensus motif. Other kinases with longer consensus phosphorylation sites could also be monitored provided that phosphorylatable residues can be placed close enough to the NLS to influence its association with the importin.

2.4. Conclusion

Using these biosensors to probe MAPK activity in the mating and cell wall integrity pathways, we could reveal a large heterogeneity in the response between cells within an isogenic population. For the mating pathway, this variability can be explained by extrinsic differences between cells. While it has been known that the response to mating pheromone was cell cycle-dependent with an inhibition of the pathway during the S phase, we could demonstrate with these sensors that there is also a different kinetic activation of the pathway between a fraction of G2/M cells and cells in the G1 phase. In the S phase, the scaffold protein Ste5 is phosphorylated by the Cln2/Cdc28 complex to prevent its recruitment at the plasma membrane via the PM domain [116]. It remains to be seen whether the same mechanism is involved in the observed difference in the kinetics between G1 and G2/M cells. In the CWI pathway, a heterogeneity in the response can also be observed between individual cells. It cannot be attributed to cell cycle-specific cues, but rather to the general growth of cells that induce more or less basal activity of the Mpk1 MAPK.

These two examples confirm the notion that MAPK pathways are not isolated signal transduction cascades, but are embedded in the global signalling network of the cell. MAPK pathways can integrate these intra-cellular signals to modulate their output, and in turn the MAPK activity can impact on cellular processes such as the cell cycle, metabolism, or growth. The ability to measure MAPK activity in single cells provided by the SKARS enables us to uncover these regulations and provides the opportunity to identify the mechanistic links that connect MAPK pathways to other cellular processes. In general, the SKARS technology enables the direct mea-

measurements of enzymatic activity in living cells and as such can become an important tool for system biology. Its use will allow the identification of new regulatory mechanisms present in these signalling cascades and, in turn, will enable to build more accurate mathematical models of the dynamic events taking place in these pathways.

3. Dynamic single cell study of the mating and cell-cycle cross-inhibition mechanism.

3. Mating and cell-cycle cross-inhibition mechanism.

3.1. Background

Mating process. Unicellular yeasts are powerful model systems to understand the cell-fate decision making. In *Saccharomyces cerevisiae*, when two haploid cells of opposite mating type ($MAT-a$ and $MAT-\alpha$) are in close proximity, two paths can be taken: divide or mate. All cells in a mating mixture secrete pheromones to indicate their relative position to the surrounding potential partners. Once the pheromone is sensed, the future partners arrest their cell cycle progression in G1 and start a chemotropic polarisation leading to the formation of a bulge (shmoo) oriented toward each other [128, 7, 107, 27]. The shmooes grow until cells touch each other. Following this, both fuse and mix their DNA content to form a diploid cell. The resulting diploid faces a new choice influenced by the environmental conditions. If the environment is suitable for growth, the cell divides. However, under nitrogen deprived conditions, the diploid cell starts the meiosis and forms haploid spores that will wait for better conditions to germinate [73].

As we can see, the budding yeast life cycle contains various steps in which cells have to choose between multiple fates. This cell-fate decision is mostly controlled through signalling cascades, such as MAPK pathways, that are well conserved among eukaryotes [96, 107, 89, 44]. To sum up, the mating is a prototypical process extensively studied as it requires the regulation of conserved signalling cascades.

The mating MAPK pathway. The signalling cascade activated during the mating is very well characterised 3.1. The pheromone binds a receptor (Ste2) that promotes the conversion of GDP into GTP on the α subunit (Gpa1) of an heterotrimeric G protein. The nucleotide exchange leads to the dissociation of Gpa1 from the β - γ subunit (Ste4-Ste18)[128]. The free Ste4-Ste18 complex promotes signal transduction by activating the PAK-like kinase Ste20 [67] and the scaffold protein Ste5 [55]. The Ste5 forms a complex with a conserved MAPK pathway module composed of Ste11, Ste7 and Fus3 [128, 7, 107]. The localisation of Ste5 at the membrane brings the MAPK module close to the MAP4K Ste20 that triggers a phosphorylation cascade.

Ste20 activates the MAP3K Ste11, which activates the MAP2K Ste7 that then activates the two MAPK Fus3 and Kss1. Active MAPKs spread the signal to various substrates. Among them we find transcription factors such as Dig1, Dig2 and Ste12, which regulates the transcription of approximately 200 genes [103, 7, 107]. Some of these genes encode for signalling components but also for proteins involved in cell polarity and fusion [103].

Mating and cell cycle cross-inhibition. Although Fus3 is thought to be the most important MAPK, the mating can still occur if Kss1 is expressed alone [106]. This suggests that both MAPKs have some redundant functions. However, only Fus3 activates the Cyclin Kinase Inhibitor (CKI) Far1. Far1 is one of the most important targets of the mating pathway. Once activated by Fus3, this protein regulates the Cyclin Dependent Kinase (CDK) Cdc28 in G1 by outcompeting with the cyclins Cln1/2. The Far1 CKI prevents a proper binding of the CLN to their substrates. Moreover, Far1 is thought to directly inhibit the activity of Cdc28. This results in the inhibition of the CDK and therefore the arrest of the cell cycle

progression in G1 [91, 87]. In parallel, the cell cycle was reported to inhibit the mating through two major mechanisms. The first one consists in the degradation of Far1 at the transition from G1 to S-phase (also named as the START checkpoint) and requires a complex formed by the CDK and the first expressed late-G1/early-S Cyclin Cln3 [72, 53]. The second mechanism was discovered by the group of Peter Pryciak in 2007 and consists in the direct inhibition of the

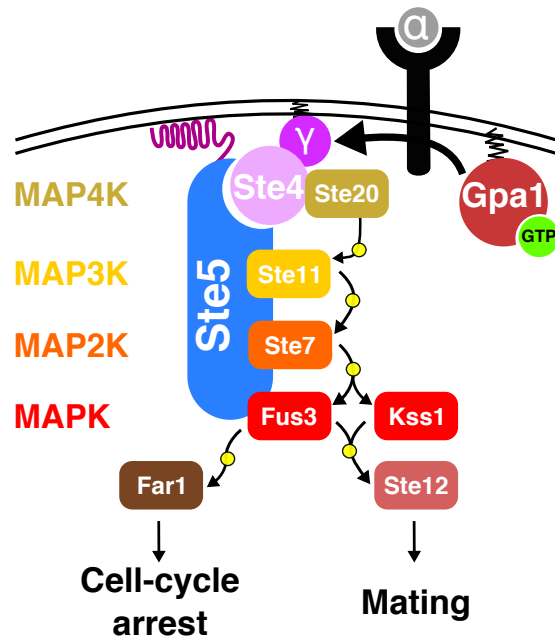


Figure 3.1.: Schematic representation of the *Saccharomyces cerevisiae* mating pathway.

3. Mating and cell-cycle cross-inhibition mechanism.

MAPK pathway through the scaffold protein Ste5. First of all, they identified a plasma membrane interaction domain (PM) at the N-terminus end of Ste5 that is required to enhance the signal transduction through the MAPK pathway [93]. Interaction of this domain with the membrane acts in synergy with the interaction with the G_{β} subunit and stabilises the scaffold at the membrane [131]. In addition, they found that this PM is phosphorylated in S-phase by the complex CDK-CLN Cdc28-Cln1/2. This leads to the detachment of the MAPK module from the G_{β} and thus to a lower signal transduction efficiency [116]. To conclude, the mating and the cell cycle are tightly linked by a cross-inhibition mechanism.

Current assay limitations. Although the current model of cross-inhibition mechanism is well established, the available tools are limited in term of qualitative and quantitative data acquisition. Far1 dependent arrest of the cell cycle was observed using halo assay or through inhibition of the Cdc28-Cln1/2 activity [88, 87]. In these conditions, the arrest was studied at the whole population level. On the other hand, cells in culture do not progress synchronously in their cell cycle. This can be a problem, as the dynamic MAPK activity might be different in each cell cycle phase [26, 25]. Thus, synchronisation strategies, using either Cdc28/Cdc15 thermo-sensitive mutant strains or chemicals such as hydroxyurea, are commonly used to study the mechanism of inhibition of the mating pathway driven by the cell cycle [116, 11, 72]. In addition, phosphorylation of the Ste5 scaffold protein by Cdc28-Cln2, and the downstream effect on the signalling cascade activity, were described using Western Blot or gene expression reporter methods in strains overexpressing cyclins [129, 116]. Consequently, all these methods either use very artificial conditions and report the behaviour of the whole population, or do not specifically measure the activity state of signalling cascades. These are major limitations, since the cell cycle and mating cross-inhibition mechanism induce an heterogeneous pheromone response. A proper study of this mechanism requires single cell level measurement.

Recently, some groups attempt to clarify the MAPK activity pattern in all phases of the cell cycle. The group of Andre Levchenko measured the mating MAPK activity at the single cell level

using a FRET sensor. The group of Jan Skotheim, tracked the cell cycle progression of single cells based on the Whi5 sub-cellular localisation. Although these two groups acutely measured either the mating pathway or the cell cycle progression, they quantified less efficiently the second (cell shape observation to identify the cell cycle stage, and transcriptional reporters or protein accumulation at the shmoo tip to measure mating pathway activation. [19, 29, 28].

By combining synthetic biology, live cell imaging and computational data analysis, we propose to revisit the model describing the relationship between mating and cell cycle through dynamic measurements of the MAPK and the CDK activities, both simultaneously, and in live single cells.

3. Mating and cell-cycle cross-inhibition mechanism.

3.2. Result

3.2.1. SKARS and Whi5: MAPK and CDK activity sensors.

Whi5 and SKARS: Structure and behaviour. In order to study how mating and cell cycle interact with each other, we choose to quantify the activity state of the signalling cascades that regulate these two processes. Moreover, as the cell cycle progression is different from cell to cell, we performed this analysis at the single cell level. Cell shape observation and fluorescent gene expression reporters are the most common strategies used to monitor cell cycle progression and mating activation. However, these strategies have several weaknesses that limit their reliability to report the dynamic activity state of a given signalling cascade [72, 80, 3, 86]. To counteract this problem, we imagined a system in which the difference of fluorescent protein in and out of the nucleus is translated in kinase activity. Such approach has the advantage to directly probe one particular node of a signalling cascade using a process that is dynamically closer to phosphorylation kinetic than to transcription. In the context of our study, two independent sensors will be used to simultaneously measure the activation states of the mating MAPK and the cell cycle master regulator Cdc28 activity in each individual cell.

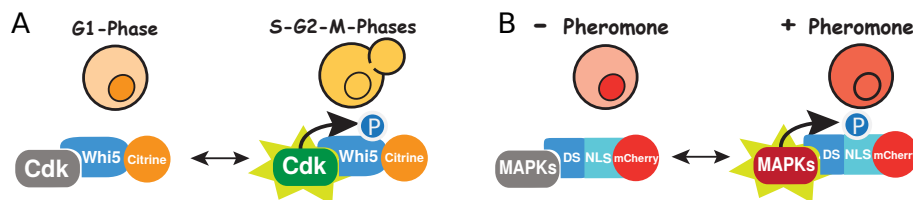


Figure 3.2.: Schematic representation of the cell cycle CDK activity sensor (Whi5) and the synthetic mating MAPK activity sensor (SKARS).

As explained in the chapter [Introduction](#), Whi5 is a repressor of G1 genes transcription [23, 21] and has been previously used as a marker for G1 entry and exit [9, 25]. The nuclear shuttling of the protein is controlled by the Cyclin Dependent Kinase (CDK) called Cdc28, that phosphorylates the transcription factor (TF). In G1, Whi5 is in its non-phosphorylated nuclear form, as the CDK is not active (figure 3.2.A). Once the cell transits from the G1 phase to the S-phase

(START checkpoint), the CDK phosphorylates Whi5 and triggers its cytoplasmic accumulation. In order to visualise this dynamic sub-cellular change, the endogenous Whi5 protein was tagged on its C-terminus with the mCitrine fluorescent protein.

To measure the dynamic activity of the mating signalling cascade we use the SKARS technology described in the [chapter 2](#) [30]. We use the $Ste7_{DS}$ -SKARS configuration to report the kinase activity of the two MAPKs Fus3 and Kss1 (figure 3.2.B).

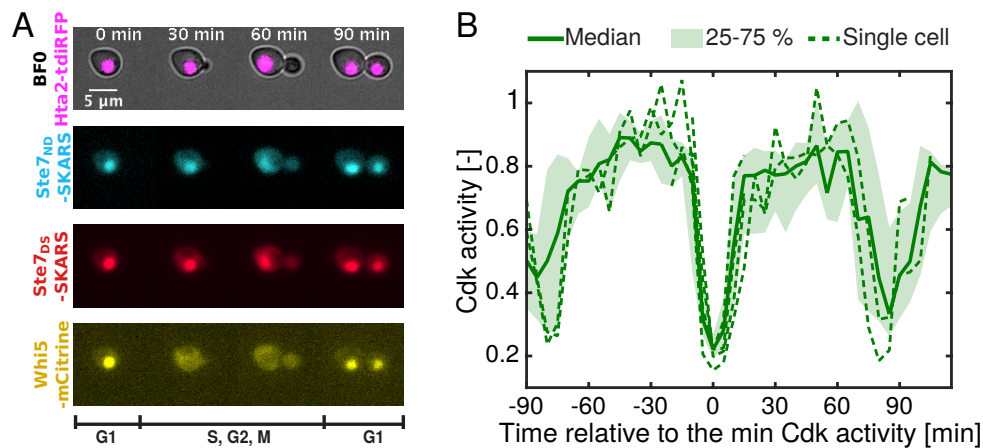


Figure 3.3.: A. Fluorescent microscopy images of cells observed during time lapses experiment. Pictures show WT cells expressing a Hta2-tdiRFP (nucleus), a $Ste7_{ND}$ -SKARS-mCFP (Corrector), a $Ste7_{DS}$ -SKARS-mCherry (MAPK sensor) and a Whi5-mCitrine. Each fluorescent channel was acquired every five minutes for two hours. B. CDK activity reported as function of the time relative to G1-entry. Time lapse movie from A. was analysed using the YeastQuant platform (See appendix Material and methods 55 and [85]). The CDK activity corresponds to the fluorescent intensity ratio between the cytoplasm and the nucleus of Whi5. 70 cells that exhibit at least one impulse of CDK activity were selected. The time of impulse appearance is considered as the time point 0 minutes and serve as a temporal reference (see exp procedure and FigSup1).

Whi5 sub-cellular localisation reports on the dynamic of CDK activity. To confirm that both sensors exhibit the expected sub-cellular localisation at the single cell level, we express the two systems into the yeast strain W303 and ran two hours time lapse (TL) experiments using an epi-fluorescence microscope. Figure 3.3.B shows one representative cell that expresses the

3. Mating and cell-cycle cross-inhibition mechanism.

Whi5-mCitrine (Yellow) and Ste7_{DS}-SKARS (Red). In order to identify the nucleus area, we also tagged the Hta2 histone with a tandem dimer infra-red fluorescent protein (tdiRFP, purple). In the first frame, the cell shows a strong yellow nuclear staining. This signal disappears after 30 minutes but reappears at 90 minutes. The loss of nuclear fluorescence correlates with the bud appearance at 30 minutes (S-G2-phases) and ends once the cell completes the cytokinesis (compare Whi5-mCitrine channel with BF0 Hta2-tdiRFP). This demonstrates that Whi5 translocates from the nucleus to the cytoplasm after S-phase entry and re-enters into the nucleus after G1-entry as expected.

The Whi5 nuclear translocation depends on the phosphorylation driven by the CDK [9, 25]. To quantitatively report on the activity level of the CDK we used the YeastQuant platform to segment and track the nucleus and the cytoplasm of hundreds of cells along the time lapse movies [85] (figure 2.4). The CDK activity was defined as the ratio of fluorescence intensity between the cytoplasm and the nucleus in the yellow channel. This calculation was performed at each time point and for all the cells tracked from the beginning to the end of the experiment. The dynamic of CDK activity appears to be extremely heterogeneous between cells. Each single cell shows shifted negative pulses of CDK activity consistent with the fact that the cell cycle progresses independently from cell to cell (figure 3.4A). These delayed signals are problematic to observe a similar general trend of CDK activity. To overcome this problem, cell traces were aligned based on the time at which the CDK activity reaches its minimal value (G1 phase). This procedure will be further referred as “synchronisation”. This synchronisation strategy is very efficient also for cells that transit through G1 (figure 3.4.A, B).

We applied this method to confirm that the Whi5 oscillation period correlates with the reported growth speed of budding yeast. As shown in figure 3.3.B, the average synchronised CDK activity oscillates periodically (filled line). This is confirmed at the single cell level, as individual traces exhibit a similar trend (dotted lines). The period separating two negative pulses agrees with the reported time required for a cell to start and complete one cell cycle (i.e. 90 minutes). Consequently, the dynamic of CDK activity deduced from the Whi5 sub-cellular localisation,

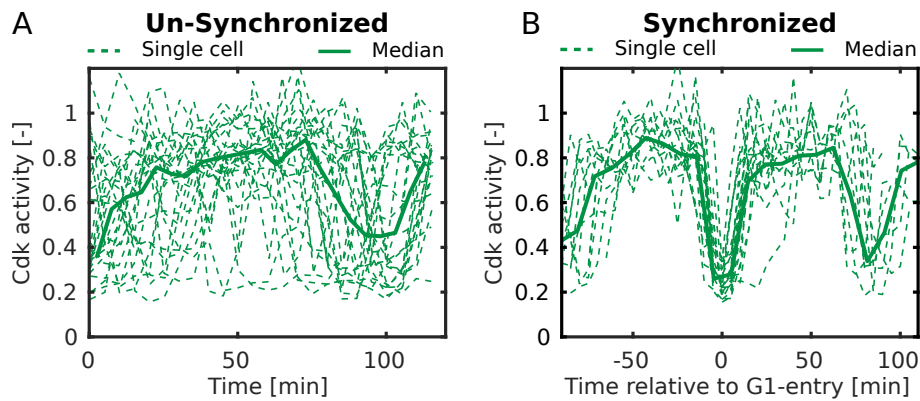


Figure 3.4.: Synchronisation of CDK activity based on the time cells enter G1. WT cells expressing SKARS and Whi5 sensor were imaged for 2 h with 5 minutes intervals. Images were analysed using the YeastQuant platform and the CDK activity was calculated as the yellow fluorescent intensity ratio between the cytoplasm and the nucleus for each individual cell and at each time point (A, B). A. Cells were selected since their CDK signal shows at least one impulse event. The CDK activity of the selected cells was reported as function of time. B. The time at which the CDK activity traces reaches its minimum value was taken as a temporal reference ($t=0$). The CDK activity traces from B were plotted related to these values.

acutely reports on the cell cycle progression of each individual cell. Moreover, the *in silico* cell synchronisation based on the G1 entry is an extremely powerful method to get a representative picture of cell behaviour at a given cell cycle stage.

Correction of the SKARS signal. The $Ste7_{DS}$ -SKARS presented in the previous chapter is used to measure the MAPK activity of Fus3 and Kss1. For simplification, this construct will be further referred as "SKARS" [chapter 2](#). A red nuclear staining is observed at all frames of the time lapse experiment performed in [figure 3.3.A](#). This confirms that in basal conditions the sensor is actively imported into the nucleus at all cell cycle phases. However, a small decrease in nuclear intensity can be observed at 60 minutes. To find out whether this is due to cell cycle dependent regulation of the MAPK basal activity, a non-functional SKARS containing point mutations in its interaction domain was used as an internal control (CFP channel, [figure 2.5](#), [figure 3.3.A](#)). For simplification, this construct will be further referred as "Corrector". [Figure 3.3.A](#) shows a

3. Mating and cell-cycle cross-inhibition mechanism.

nuclear staining reduction at 60 minutes in the Corrector channel. Thus, the Corrector is not imported into the nucleus with the same efficiency throughout the cell cycle.

To completely reject the involvement of the mating pathway in the reduced nuclear importation of the SKARS and the corrector, we performed the same experiment in a *ste5Δ* strain, a mating signalling dead mutant. We then decided to focus on the sub-population of cells that enters in G1, since the largest nuclear signal change seems to happen in this cell cycle phase transition. After

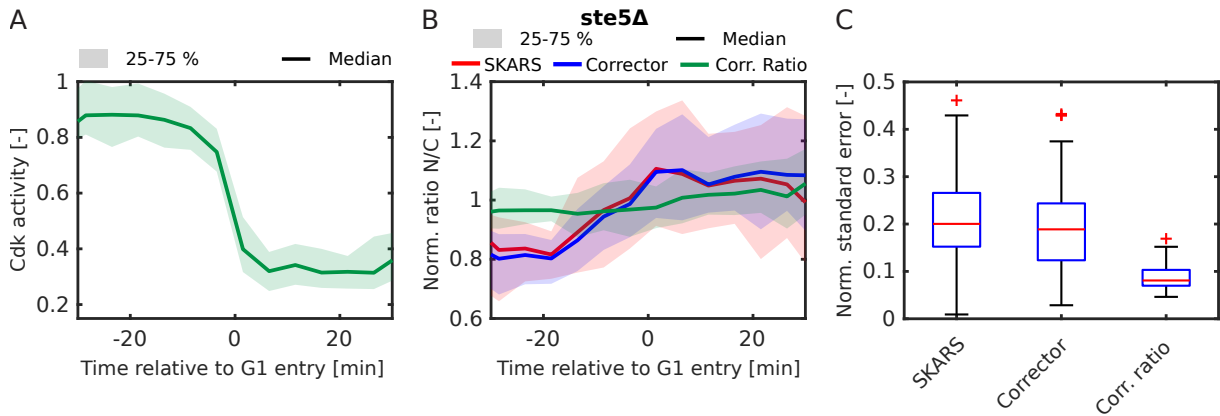


Figure 3.5.: Optimization of the MAPK activity quantification. Time lapse experiments and image analysis was performed as previously described (45 minutes long, 3 minutes interval). A. Synchronised CDK activity signals. CDK activity of cells entering in G1 plotted relative to the start of the CDK signal degradation. B. Dynamic sub-cellular localisation of SKARS and Corrector at S-G2-M to G1 phases transition. SKARS and Corrector values from A were extracted and N/C ratio of both sensors were calculated. Noise attenuation was obtained by calculating the ratio between the N/C ratio of corrector divided the N/C ratio of SKARS (Corr. Ratio). For comparison, N/C ratios and Corr. ratio were normalised relative to their respective mean and then plotted relative to the time cells enter in G1 as in A. C. N/C ratio noise reduction. Standard errors of normalised N/C ratio and corrected ratio along the time axis calculated for all tracked cells and plotted as boxplot.

CDK activity based synchronisation (figure 3.5.A), the corresponding normalised SKARS and Corrector N/C ratio are plotted relative to the time of G1 entry (figure 3.5.B). The *ste5Δ* mutant exhibits a 40% increase of the N/C ratio of both SKARS and Corrector during the entry into G1 (figure 3.5.B). This goes in the direction of the qualitative observations done in figure 3.3.B and confirms that the sensor's nuclear import efficiency changes from S- to G1-phase. However, no

differences between SKARS and Corrector N/C ratio is observed. The corrected ratio median ($\frac{Corrector_{N/C}}{SKARS_{N/C}}$) remains flat with a reduced 25-75 percentile shaded area. This confirms that the SKARS and Corrector ratios show the same dynamic and that both signals can suppress each other (figure 3.5.C). Consequently, SKARS signal is subjected to small fluctuations independently on Fus3 and Kss1 activity. This noise is reduced by two folds when SKARS and Corrector signals are combined. Based on this analysis, we will now on consider the corrected ratio as the MAPK activity.

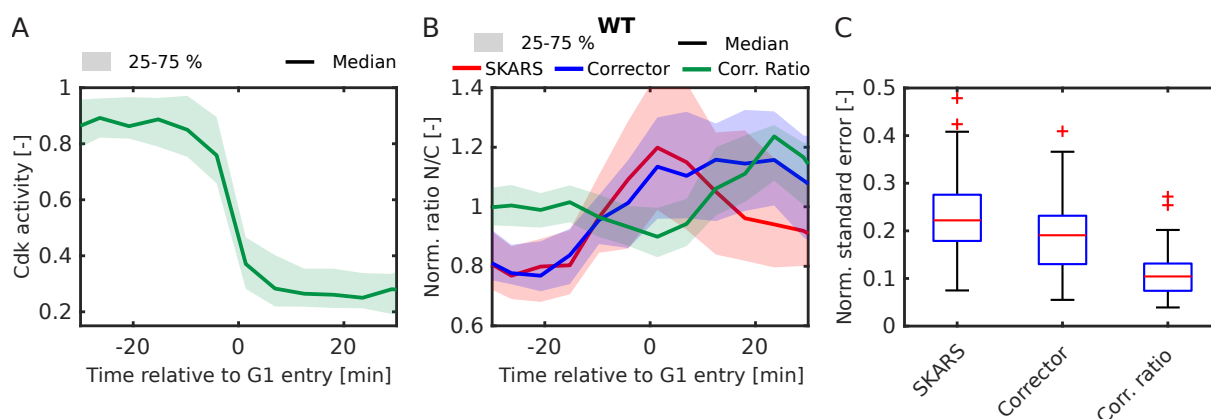


Figure 3.6.: Dynamic MAPK activity in unstimulated conditions. Time-lapse and analysis were performed as in figure 3.5 but in a WT background.

Same analysis as performed in figure 3.5 was reproduced in a WT background. Interestingly, the SKARS and the Corrector signals do not overlap when cells finish to enter in G1 (10-30 min, figure 3.6.A and B). As a consequence, the corrected ratio shows an oscillation pattern. The 25-75 percentile area surrounding the Corrected ratio median remains constant along the time. This suggests that we removed artifactual noise from the SKARS signal using the Corrector internal control. The oscillation pattern observed from the corrected ratio suggests that in absence of pheromone, the MAPK activity is regulated in a cell cycle-dependent manner. In growing conditions, kinases are down regulated at the interplay between S-G2-M and G1.

3. Mating and cell-cycle cross-inhibition mechanism.

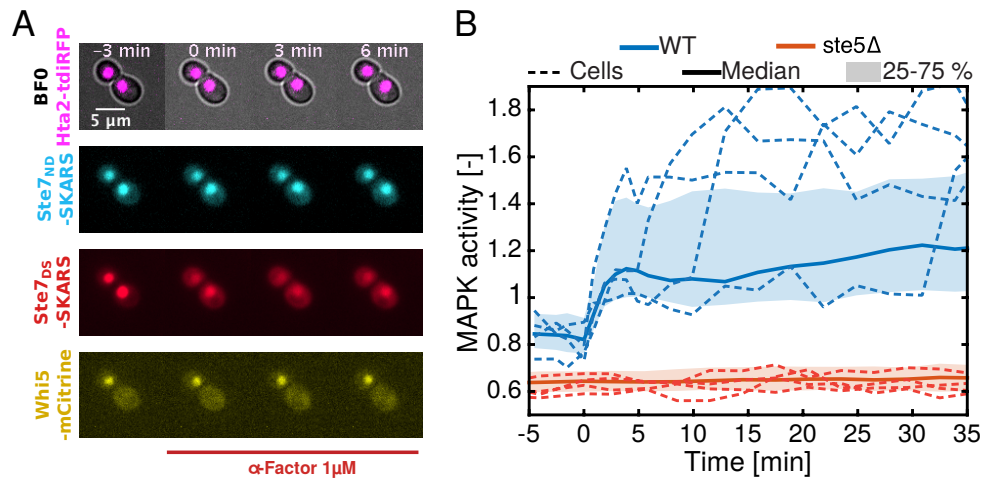


Figure 3.7.: A. SKARS sub-cellular localisation prior and after pheromone treatment. The strain from figure 3.3 is imaged every three minutes for 45 minutes. α -factor is added nine minutes after time-lapses start. This is referred as the time point 0. Pictures show two representative cells. B. MAPK activity reported as function of time. Time-lapse movies from A. and from a mating signalling dead mutant strain (*ste5* Δ) are analysed as previously. The MAPK activity corresponds to the Corrected Ratio described in figure 3.5 and 3.6.

The corrected SKARS signal reports on the activity of the mating MAPK. We have previously shown that the SKARS sensor accumulates into the cytoplasm of cells stimulated with exogenous pheromone (2.2.1, figure 2.3, [30]). To confirm this, we performed time lapse experiments in which cells were stimulated with 1 μ M of α -factor 6 minutes after the beginning of the imaging (figure 3.7.A). Cells show a strong nuclear red signal. Immediately after pheromone addition (time point 0), the nuclear red signal decreases. The corrector, however, remains nuclear during the time-lapse, as well as the Hta2-tag. Consequently, stimulation of cells with pheromone induces a cytoplasmic accumulation of the SKARS.

The loss of nuclear signal is stronger in the upper cell which imply that both cells exhibit different MAPK activation after stimulation. In order to confirm this heterogeneous MAPK activation, we performed time lapse movies with the WT or with a mating signalling dead mutant (*ste5* Δ). In *ste5* Δ background, the median and random chosen single cell traces show the same constant low MAPK activity before and after pheromone treatment. This is consistent

with the fact that, in this mutant, the mating pathway is broken (figure 3.7.B). On average, the MAPK activity in WT background increases and reaches a plateau in less than five minutes following stimulation. At the single cell level, we can see that the MAPK activity increases to an intermediate value (25% increase of the signal right after stimulation) followed by a delayed two-fold increase (figure 3.7.B, WT cells). These results show that even though cells are exposed to the same pheromone concentration, they do not activate the mating pathway with the same dynamic, suggesting that the environmental change is not perceived in the same way.

To sum up, SKARS and Whi5 report on the dynamic activity of the mating MAPKs Fus3 and Kss1 and the CDK Cdc28 respectively. The measurement of both pathways is obtained for hundreds of individual living cells and with a temporal resolution of two minutes. This high temporal resolution enables to track rapid signal dynamic changes, often missed with classical protein expression reporters' strategies. The use of the Whi5 TF as a sensor enables to track the cell cycle progression without synchronizing cells with chemicals or genetically engineered mutants. On the MAPK side, we improved the SKARS technology using a Corrector as a permanent internal control and reduced the single cell trace noise by two-folds. This SKARS optimisation leads to the observation that the cell cycle regulates the mating not only in pheromone stimulated conditions but also in normal growing conditions. Overall, these results show that SKARS and Whi5 can be used to measure mating and cell cycle signalling cascade activity simultaneously and in the same cell.

3.2.2. Single cell analysis of the MAPK activity signal.

Dynamic activity of the mating MAPKs in G1- and in S-phase. It was reported that the mating pathway cannot be activated in all the cell cycle phases [81, 53, 50, 72, 129]. To confirm that the MAPK pathway is targeted by this cell cycle-dependent regulation, we performed time lapse experiments with pheromone stimulation as in figure 3.7 and extracted the MAPK activity during the cell cycle progression. The imaged strain expressed the same fluorescent markers as

3. Mating and cell-cycle cross-inhibition mechanism.

in figure 3.7 and did not express the pheromone protease Bar1, so that cells were continuously stimulated with the same concentration of pheromone [8, 27]. After image quantification, MAPK and CDK activities were calculated. We then performed a cell clustering based on the dynamic CDK activity of each individual cell and reported the average MAPK activity corresponding to each group.

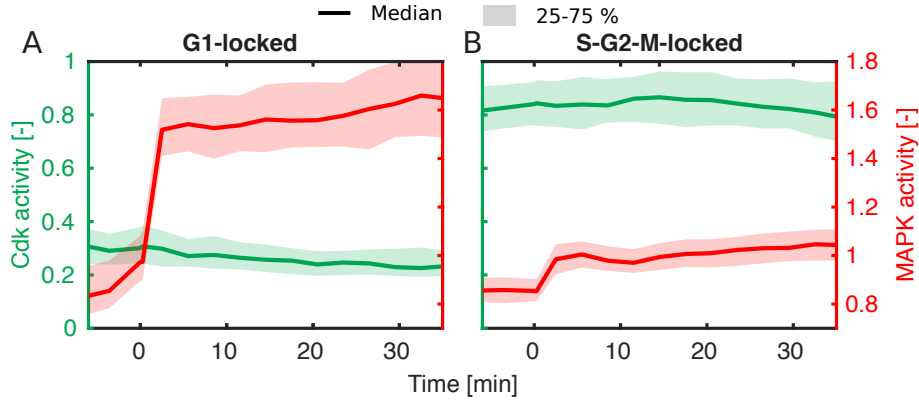


Figure 3.8.: Pheromone induced MAPK activation of cells in G1 or S-G2-M phases. Time-lapse experiment of 45 minutes with 3 minutes intervals were performed as in figure 3.7 on a strain deleted for the gene encoding the Bar1 protease. MAPK and CDK activities were calculated for 738 cells tracked from the beginning to the end of the time lapse. Single cells were sorted in different clusters by comparing their CDK activity pre-/post-stimulation: (i) low/low : G1-locked. (ii) high/high : S-G2-M. (iii) low/high is S-entry. (iiii) high/low : G1-entry. Both CDK and corresponding MAPK activities were averaged and are plotted on two independent axis in relation to the time of pheromone addition (filled line: median, shaded area: 25-75 percentile). The figure shows CDK and MAPK activity of G1-locked (A, cell fraction: 20%) and S-G2-M (B, cell fraction: 35%) cells. Both CDK and corresponding MAPK activities are averaged and plotted on two independent axis relative to the time of pheromone addition (filled line: median, shaded area: 25-75 percentile).

The first two clusters contain cells with a sustained low or high level of CDK activity and correspond to cells that remain either in G1 (G1-locked, figure 3.8.A) or in S-G2-M (S-G2-M-locked, figure 3.8.B) respectively. G1-locked cells exhibit a sustained low CDK activity. The corresponding MAPK activity shows a two folds increase in less than five minutes post stimulation, followed by a stabilisation of the signal until the end of the experiment (figure 3.8.A). Unlike for the G1-locked cells, we observe only a minor MAPK response of the S-G2-M-locked

cluster (1.25 fold increase). Consequently, the mating pathway is strongly activated in G1 and much less in S-G2-M. These results support the reported observations showing that the mating is not induced during the S-phase. Moreover, we are able to show that the inhibition mechanism consists in the reduction of the MAPK activation after pheromone stimulation without its complete abrogation.

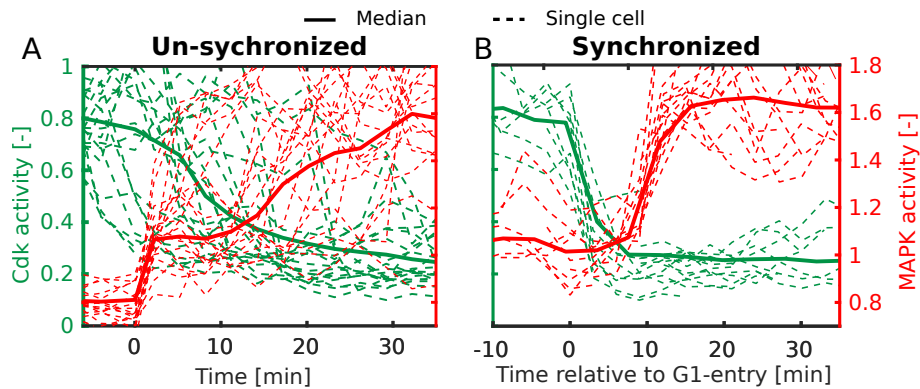


Figure 3.9.: CDK and MAPK activities relative to G1-entry. WT cells expressing SKARS and Whi5 sensors were imaged for 45 minutes with three minutes intervals. $1\mu\text{M}$ α -factor was added to the well nine minutes after the acquisition start. Cells entering in G1 were selected as the CDK signal start above 0.55 and end below this threshold. A. The dynamic of CDK and MAPK activities of randomly selected cells from the G1-entry cluster are plotted relative to the time of induction. E. The last time point at which the CDK activity remains below 0.55 is taken as a temporal reference. CDK and MAPK activities from A are plotted relative to this reference time.

Cells entering G1 exhibit heterogeneous MAPK signal patterns. As discussed in the previous paragraph, the Whi5 sensor allows cell cycle progression tracking of individual cells. While previous studies relied on chemical synchronisation to study signalling in various cell cycle phases, our strategy enables us to use the natural variability of the sample. This is an interesting feature that provides information about cells during their transition between cell cycle stages.

Cells exposed to pheromone while they are in S-phase, do not stop their progression, but were reported to complete their cell cycle to G1 [81]. We found indeed that 30% of the population of cells tracked from beginning to the end of the time lapse experiment enters in G1 after α -factor

3. Mating and cell-cycle cross-inhibition mechanism.

addition. This entry happens in a delayed manner, as cells are not synchronised in their cell cycle progression. The corresponding dynamic of MAPK activity seems to follow the same trend, as single cell red curves are shifted from each other (figure 3.9.A). These results suggest that in this cluster, the average MAPK activity relative to the time of induction does not illustrate well how the pathway is dynamically activated at the single cell level (figure 3.9.A, compare red median and red single traces).

As the difference of MAPK activity between S-G2-M-locked cells and G1-locked cells, we thought that plotting MAPK activity relative to the time at which cells enter in G1 would enable to observe a more representative pattern than the signal of each single cell. To do this, we performed cell synchronisation based on the CDK activity as previously described (figure 3.9.B). After synchronisation, the CDK activity traces are well aligned. The corresponding MAPK channel also shows a good overlap of single traces, suggesting that the major change of MAPK activity occurs at the transition between S-G2-M and G1 and not after pheromone treatment.

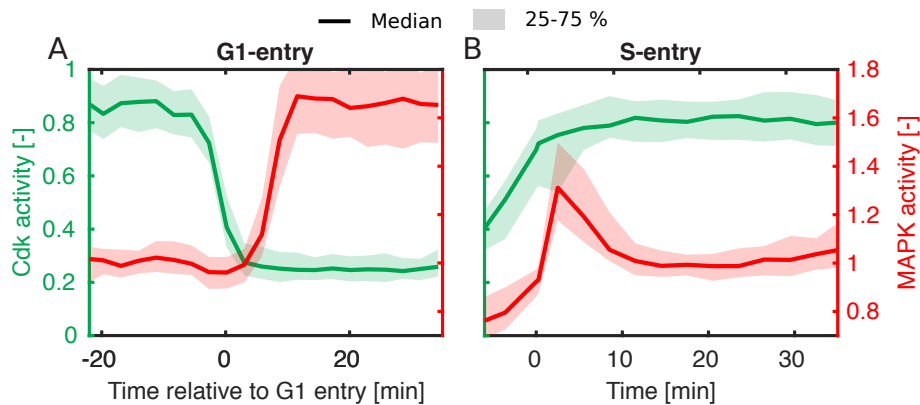


Figure 3.10.: MAPK activity of cells in transition between cell-cycle phases. The figure presents the MAPK activity of two clusters obtained from the experiment described in figure 3.8. CDK activity of G1-entry cells drops post-stimulation (A, G1-entry, 33%). S-entry cells show the opposite signal pattern (B, S-entry, 10%). Both CDK and corresponding MAPK activities are averaged and plotted on two independent axes relative to the G1-entry time (G1-entry) or relative to the pheromone addition (S-entry). Time points prior stimulation are removed from the analysis after synchronisation of the G1-entry cells traces.

MAPK is activated only in G1 We observed that S-G2-M-locked cells slightly activate the mating pathway (figure 3.8.B). One question that can be addresses is how the dynamic activity of the MAPK evolves when cells enter in G1 after stimulation. To obtain this information, we first identified cells that enter in G1 and then synchronised their MAPK and CDK traces in relation to the G1-entry time point. Note also that the time points preceding the stimulation were rejected from the analysis in order to focus only on the period in which cells were exposed to pheromone. The CDK and MAPK activities are then plotted as in figure 3.8. Prior the CDK activity drop, the MAPK activity is at the level of the S-G2-M phase cells. Then, activity increases to the level of the G1-locked during the CDK signal degradation. Interestingly, MAPK activity starts to increase only when the CDK activity reaches its minimum level. This indicates that the mating signalling cascade recovers its full activation capacity after cells have completed their cell cycle. These last results dissent from previous studies which instead reported that during G2 the mating pathway activity increases gradually [19, 129, 81].

In addition to start a new transcriptional program and recruiting the polarisation machinery to form the shmoo, MAPK activation also induces to cell cycle arrest in G1 [91, 87]. Consequently, we do not expect to find cells that enter in S-phase after being stimulated with pheromone. Surprisingly, about 10% of the population exhibits a low CDK activity before stimulation and high CDK activity after stimulation. Even more surprisingly, although the CDK activity is almost at its maximum value during stimulation, the corresponding MAPK signal shows a pulse pattern with a peak at 75% of the G1-locked maximum value and a recovery that stabilises at the level recorded for S-G2-M cells (figure 3.10.B). Consequently, we see that a significant part of the population is committing to S-entry but remains still transiently sensitive to exogenous pheromone addition. Thus, small temporal windows separate the phase of choice between G1-arrest and cell-cycle commitment and the phase during which the MAPK is inhibited by the cell cycle.

3. Mating and cell-cycle cross-inhibition mechanism.

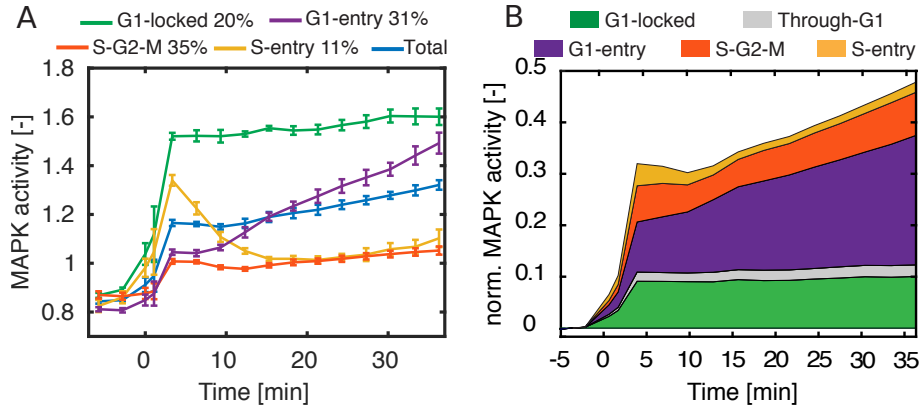


Figure 3.11.: Contribution of cluster signals to the average MAPK activity. A. Dynamic MAPK activity of the four main cell-cycle clusters. The blue curve represent the MAPK activity recorded for the whole population. Line correspond to means of medians from at least three replicates. Error bars are standard deviations. B. MAPK activity from A. are plotted relative to the fraction of cells in each sub-population. Each coloured area represent the cumulative effect of the signal of the given cluster plus the signal of the cluster located below it.

Cell-to-cell variability of the MAPK signal is a downstream effect of delayed cell cycle progression. A clustering based on the CDK activity enables us to identify four cell populations exhibiting different MAPK dynamic patterns. To confirm the relevancy of these clusters and compare their mating pathway dynamic activation with the one of the whole population, we perform the clustering on four independent replicates and calculate the mean of the replicates median MAPK activity for each cluster (figure 3.11.A). Dynamic MAPK activities is very similar from replicate to replicate, independently on the cluster. In addition, 95% of the cell population is well sorted in the four clusters. The last 5% is a group of cells defined as transiting “through G1” as they transiently activate the CDK. For the time being, this cluster is ignored because most of the cells show noisy CDK activity. Altogether, the various MAPK activity patterns observed result from cell cycle regulatory mechanisms only.

The average dynamic MAPK activity shows a similar trend to the one previously observed using western blot assay [54, 43, 77, 136]. The average signal first shows a five minute-long sharp increase, followed by a small overshoot ending at 10 minutes and a sustained slower increase

(figure 3.11.B,). To investigate the contribution of all clusters to the average MAPK activity, we plotted the cumulative MAPK activity in relation to the fraction of cells in each sub-population. The major sub-populations contributing to the first fast increase are the G1-locked and the S-G2-M clusters. The sustained increase of the signal is generated by G1-entry cells which progressively accumulate in G1. The small overshoot is due to the presence of the S-entry population (figure 3.11.B). All of this shows that the average MAPK activity signal can be divided in four main signals. Average population analysis allows to observe the response of a whole population into a given condition. Single cell analysis, however, enables to observe the variability of the response in this condition.

To sum up, our single cell analysis strategy enables to extract data from one time-lapse experiment that summarise decades of observation on the mating and cell cycle cross-inhibition. Although the mating pathway is heterogeneously activated from cell to cell, we succeed in summarising this variability by sorting cells into five well-represented categories. The CDK activity based clustering confirmed that cells in S-phase induce four times less the mating MAPK pathway than those in G1. Moreover, we show that the full activation capacity is reached only during G1 and that a small fraction of cells committed to S-phase transiently activates the signalling cascade. All MAPK activity signals from these clusters show very different patterns. Thus, considering the average MAPK activity is not enough to well determine the fate of each individual cell in this experimental condition. Finally, the five clusters isolated from the CDK kinase dynamic exhibit different dynamic MAPK activity signals that are representative of how the mating pathway gets activated at the single cell level.

3. Mating and cell-cycle cross-inhibition mechanism.

3.2.3. The mating pathway regulates the cell cycle in a pheromone dose-dependent manner.

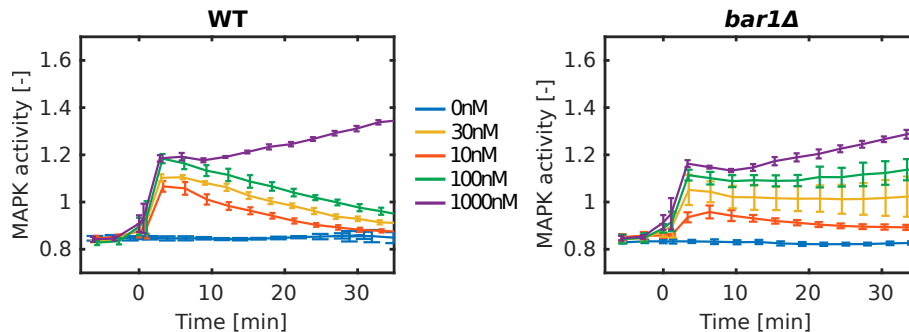


Figure 3.12.: MAPK signal degradation induced by the Bar1 protease. Time-lapse experiments are performed as in figure 3.7 on WT and *bar1Δ* cells. Stimulation was applied with various α -factor concentrations. MAPK activity is calculated, averaged and plotted relative to the induction time for the whole population. Each curve is the mean of at least three replicates. Error bars are standard deviations.

MAPK activation is pheromone dose-dependent. Individual cells secrete pheromone to indicate their relative position in a mating mixture [8, 27, 58]. The pheromone can freely diffuse into the environment, leading to the formation of a concentration gradient around the cell. The cells respond to this gradient by forming a shmoo. The mating pathway activity was reported to gradually change depending on the pheromone amount [46, 77]. In order to confirm this, we performed the same experiment as in 3.2.2 with increasing concentrations of α -factor and quantified the corresponding MAPK activity.

At the whole population level, WT cells stimulated with $1\mu\text{M}$ of pheromone exhibit an average kinase activity signal similar to what we already observed in figure 3.11. The MAPK signal first reaches a peak in less than three minutes, then slightly drops to slowly increase again in the end (figure 3.12.A). Stimulation with media without α -factor leads to a flat curve as expected. At intermediate pheromone concentrations, we observe a reduction of the signal peak as the α -factor concentration drops. This suggests that the MAPK pathway is activated in a dose dependent manner as reported [46, 136]. At these intermediate concentrations, we observe a slow signal

degradation until reaching the pre-stimulation value. This slow and constant loss of MAPK activity might be induced by pheromone degradation driven by the protease Bar1 (see 3.2.2). To confirm this, we performed the same set of experiments in a strain deleted for the gene encoding this protease. As expected, the signal drop disappears at all intermediate concentrations in this background (figure 3.12.B).

To summarise, the MAPK is activated in a pheromone dose-dependent manner. Thus, we can artificially tune the level of MAPK activity. Although the Bar1 protease induces a MAPK signal degradation, this loss of signal can be circumvented using a strain deleted for the gene encoding this protein. Thus, in the following experiments, the *bar1* Δ background will be our reference strain and will be referred as WT.

The mating dependent cell cycle arrest in G1 is MAPK activation dose-dependent The MAPK activity of cells stimulated with a saturating concentration of pheromone shows various dynamic patterns depending on the cell cycle stage. In order to see how these patterns evolve at intermediate pheromone concentrations, we performed the cluster analysis described in the paragraph 3.2.2 on the experiments shown in figure 3.12.B. Independently on the concentration used to stimulate the cells, we found the four clusters described in figure 3.8 and 3.10. Except for the G1-locked cluster, the dynamic MAPK activity signal shows a similar trend at all tested concentrations. However, we observed a reduction of the signal amplitude as the pheromone concentration drops (figure 3.13). This suggests that the MAPK can respond in a dose-dependent manner to a range of pheromone concentrations independently on the cell cycle phase. Thus, the cell cycle regulates the activation capacity of the mating MAPK signalling cascade, but not its sensitivity to a range of pheromone concentrations. The G1-locked cluster shows a slow signal decrease at intermediate α -factor concentrations. This drop cannot be due to pheromone degradation as cells do not express the Bar1 protease. Negative feedback loop mechanisms acting on the signalling cascade were previously described and may explain such MAPK activity degradation [136, 48, 77, 127].

3. Mating and cell-cycle cross-inhibition mechanism.

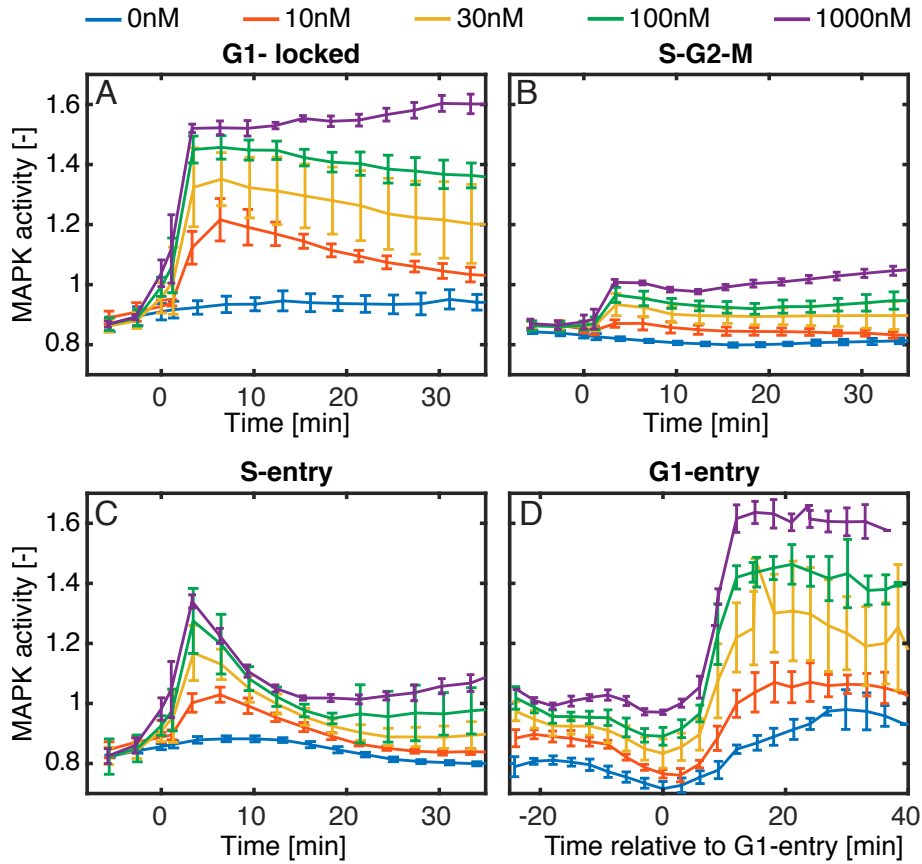


Figure 3.13.: MAPK activity level is pheromone dose-dependent in all phases of the cell cycle. Experiments from figure 3.12.B are analysed using the clustering strategy described in the section 3.2.2. Each line is the result of the mean of at least three replicates' medians at a given α -factor concentration. Error bars are standard deviations.

In the paragraph 3.2.2, we briefly mention a population of cells that transits through G1 during the time-lapse experiment. When exposed to a saturating concentration of pheromone, this cluster exhibits a noisy dynamic Cdk and MAPK activity 3.2.2. However, this noise is decreasing at intermediate α -factor concentrations. In addition, we observe that the MAPK activity of cells in this cluster never exceeds 1.1, while in G1 the MAPK activity can reach 1.6 (figure 3.14.A). This last observation suggests that cells transit through G1 because the MAPK is not enough activated to block the cell cycle progression.

We have shown that the MAPK activation is pheromone concentration-dependent. Knowing

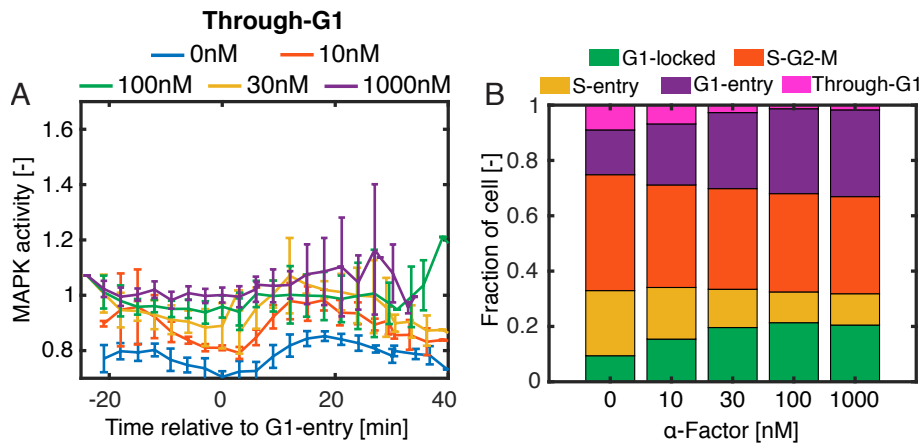


Figure 3.14.: Clusters cell fraction change depending on pheromone concentration. The dynamic MAPK activity of cells transiting through G1. Experiments from figure 3.12.B are analysed using the clustering strategy described in the paragraph 3.2.2. Cell transiting through G1 during the time lapse experiments are identified as they exhibit a pulsed of Cdk activity. Single cell traces were synchronised as already described in figure 3.9 for the G1-entry population. The corresponding dynamic MAPK activity of at least three replicates is averaged and plotted as in figure 3.13. B Fraction of cells in each cluster depending on the pheromone concentration. Each cell fraction value is the mean of at least three replicates.

that activation of the mating MAPK leads to cell cycle arrest in G1, we would expect that the distribution of the cells in each cluster change depending on the α -factor concentration (figure 3.14.B). As the α -factor concentration increases, the fraction of cells into the G1-locked and the G1-entry groups increases, while it diminishes for the S-entry and the Through-G1 clusters. In summary, we observe an enrichment of cells in G1 in a pheromone dose-dependent manner. Knowing that the mating pathway activation increases with the pheromone concentration, this two results indicate that the capacity to arrest the cell cycle in G1 is MAPK activity level-dependent.

MAPK activity level-dependent regulation of the cell cycle commitment. The cell cycle commitment is defined as the time when cells pass the START checkpoint to enter in S-phase. In the cell cycle, this check point is positioned where the mating cannot stop the cell cycle progression. This corresponds to the time before the cyclin Cln1 and Cln2 get expressed [50, 81].

3. Mating and cell-cycle cross-inhibition mechanism.

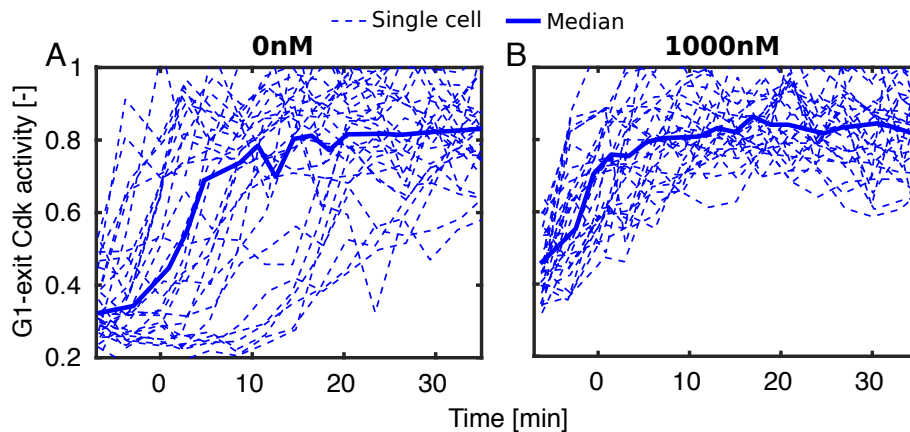


Figure 3.15.: Dynamic Cdk activity of cells entering in S-phase prior and after stimulation. Cdk activity of single cells from one replicate of figure 3.13.C is potted as function of time. An equivalent number of single traces is randomly selected in both conditions.

The pheromone dose-dependent accumulation of cells in G1 that we observe suggests that the choice between G1 arrest and cell cycle progression can be influenced. To confirm this, we focused on the CDK activity of single cells in the S-entry cluster and stimulated either with control media or with saturating concentration of pheromone. The CDK activity of cells stimulated with media increases in a delayed manner figure 3.15.A. On the opposite, traces of cells stimulated with 1000nM of α -factor exhibit a synchronised accumulation of CDK activity (figure 3.15.B). Knowing that cells entering in S-phase and stimulated with saturating concentration of pheromone can still activate the mating pathway (figure 3.13.C), we can hypothesize that, after reaching a given CDK activity threshold, the mating pathway is not strong enough to promote the arrest in G1.

In order to see whether this CDK threshold changes depending on the pheromone concentration, we extracted the CDK activity prior stimulation (Initial CDK activity) from each single cell entering in S-phase and used boxplots to observe the distribution of these values depending on the α -factor concentration. The dispersion of the initial CDK values decreases while the median value increases with the pheromone concentration. The replicate medians follow the same trend as the median of the replicates used to produce the boxplots (figure 3.16.A). Consequently, the level of CDK activity required to enter in S-phase changes depending on the activity level of the

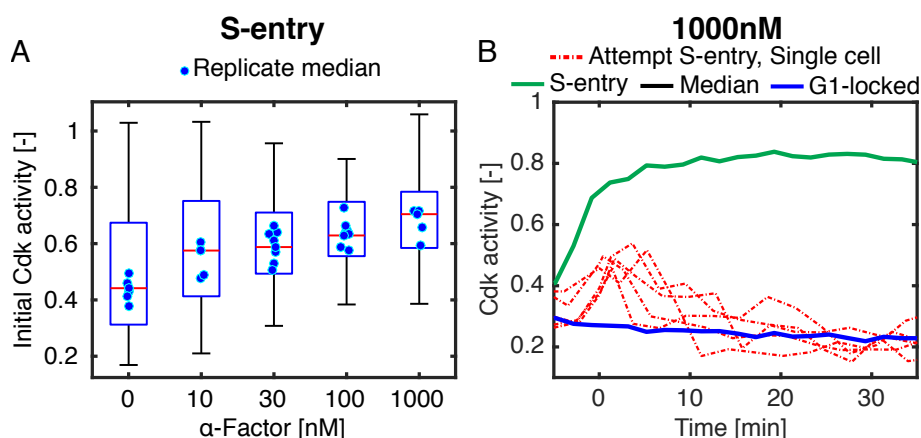


Figure 3.16.: Maximum CDK activity required to commit to cell cycle. A. Basal CDK activity depending on the pheromone concentration. Initial CDK activity is defined as the average CDK activity prior stimulation. The distribution of the initial CDK activity of S-entry cells from one replicate of figure 3.13.C is plotted as boxplot. The additional dots correspond to the median initial CDK activity of all replicates at a given concentration. B. CDK activity of cells attempting to enter in S. CDK activity of the G1-locked cells from the 1000nM replicates are combined. The “Attempt S-entry” group is defined as the cells that belong to the G1-locked cluster from figure 3.13.C and have an initial CDK activity above 0.35. The “G1-locked” cluster contains cells from the G1-locked cluster shown in figure 3.13.C and an initial CDK activity below 0.35. The “S-entry” cluster contains cells from the S-entry cluster shown in figure 3.13.C. The corresponding dynamic CDK activity of these three groups are averaged and plotted. Four single cell traces are plotted to support the relevancy of the median.

MAPK.

We went further in this analysis and tried to identify cells that attempt to enter in S-phase but remain blocked in G1. In order to find out whether this population exists, we compared the initial CDK activity of cells stimulated with 1000nM and belonging to the G1-locked cluster. We found a small fraction of cells slightly shifted above the major part of the population with an initial CDK activity higher than 0.35 (data not shown). When focusing on the dynamic CDK activity of this population, we observe that some traces show a transient increase in CDK activity right after stimulation, suggesting that cells start to enter in S but fail and remain in G1 (figure 3.16.B). This fraction of cells failing to enter in S are well identified at 1000nM of

3. Mating and cell-cycle cross-inhibition mechanism.

α -factor. However, the identification appears more challenging at intermediate concentrations, as the proportion of these cells remains extremely low. This is probably because the arrest in G1 occurs at low CDK activity levels.

To sum up, we confirmed previous observations showing that the mating pathway is activated in a pheromone dose-dependent manner. However, we found that the capacity of the cells to be sensitive to a gradual range of pheromone is conserved in all cell cycle phases. This suggests that the cell cycle does not interfere with the capacity of the mating pathway to be sensitive to intermediate concentrations of pheromones.

We also confirmed that the mating pathway inhibits the cell cycle progression by promoting the arrest in G1. Moreover, our single cell analysis showed that the fraction of cells entering in S-phase post-stimulation is reduced with the increase of pheromone concentration. This suggests that CDK and MAPK compete to balance the cell choice toward either the arrest in G1 or the entry into S. Consequently, the START checkpoint is not defined by a single CDK threshold value. This threshold can vary and depends on the level of activated MAPK.

3.2.4. Far1 and CDK activities are both required for the mating and the cell cycle cross-inhibition mechanism

The CKI Far1 is required to arrest cells in G1. We confirmed in the paragraph 3.2.3 that the mating regulates the cell cycle by promoting the arrest in G1. The molecular basis of this inhibition was established 25 years ago. Only one protein links the MAPK and the CDK, the CKI Far1 [88]. Far1 is a specific substrate of the MAPK Fus3 [101]. Once it gets phosphorylated by the mating MAPK, Far1 binds and inhibits the complex CDK-CLN Cdc28-Cln2 [88, ?]. This inhibition occurs by preventing the interaction of the CDK-CLN complex with its substrate or by directly blocking the kinase activity of the Cdc28 [91]. To confirm that Far1 is necessary for pheromone-dependent inhibition of the cell cycle, we performed the dose-response experiment shown in figure 3.13 in *far1* Δ background.

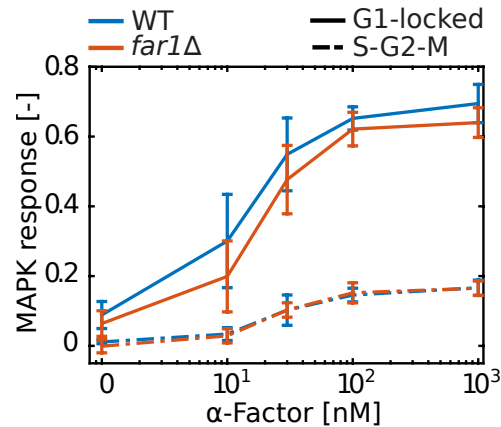


Figure 3.17.: Pheromone dose-dependent activation of the MAPK in *WT* and *far1* Δ . The strain shown in figure 3.13 was deleted for *FAR1* and measured in the same conditions as the *WT* in a dose-response experiment. MAPK response is defined as the MAPK activity reached 5 min post-stimulation minus the average MAPK activity pre-stimulation, and plotted as function of pheromone concentration. Error bars are standard deviations of at least three replicates.

The deletion of the gene coding for Far1 should not disturb the activation capacity of the MAPK module, nor its sensitivity to gradual pheromone concentrations, as this protein is located downstream of the MAPK in the signalling cascade. To confirm this, we performed time lapse dose-response experiments with *WT* and *far1* Δ strains and extracted the mean MAPK activity response in the first five minutes post-stimulation. We then plotted this parameter in relation to the α -factor concentration (figure 3.17). As expected, a similar increase of the MAPK response is observed for both *WT* and *far1* Δ . In addition, the response of G1-locked and S-G2-M cells are similar in both backgrounds. These results attest that the absence of Far1 has no impact on the MAPK activation capacity or sensitivity and that inhibition of the mating pathway in S-phase still occurs.

To determine whether Far1 is required to prevent the cell cycle commitment, we looked at the fraction of cells in G1 at the end of time lapse experiments. In *WT* background, this percentage is increasing in a pheromone dose-dependent manner, ranging from 30% at 0nM up to 50% at 1000nM. In *far1* Δ , however, the cell fraction is sustained around 30% at all α -factor

3. Mating and cell-cycle cross-inhibition mechanism.

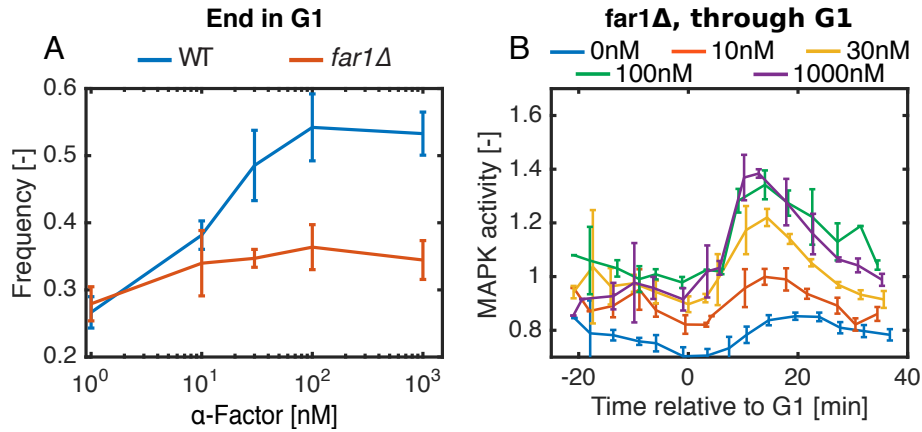


Figure 3.18.: *far1Δ* cells do not arrest in G1. The experiment is performed as in figure 3.17. A. The percentage of cells in G1 at the end of the time lapse movie is plotted as function of pheromone concentration. Error bars are standard deviations of at least three replicates. B. The MAPK activity of cells passing through G1 is plotted as in figure 3.14.A. Solid lines are means of the median of at least three replicates. Error bars are standard deviations of replicate medians.

concentrations (figure 3.18.A). Consequently, the lack of the CKI Far1 abrogates the capacity of cells to accumulate in G1 post-stimulation. As we showed that the mating pathway can still be inhibited in S-phase in *far1Δ* background, we would expect that the MAPK gets activated when cells transit through G1. Indeed, we found that the cluster “Pass-through G1” transiently activates the mating MAPK (figure 3.18.B). Altogether, these results suggest that the CKI Far1 is required to arrest cells in G1 upon pheromone stimulation, but that has no role in the mating pathway inhibition mechanism in S-G2-M.

CDK activity is required to inhibit the mating pathway. Our single clustering analysis confirmed previous studies showing that the mating pathway is inhibited in S-G2-M (3.2.2). Moreover, it was reported that mating genes and MAPK pathway components are down regulated when the S-phase Cln1/2 are overexpressed [129, 81]. Overexpression of Cln2 also leads to the hyperphosphorylation of the scaffold protein Ste5, that detaches from the plasma membrane and thus releases the core components of the mating pathway from the pheromone receptor complex[116]. Finally, cells expressing a thermo-sensitive allele of the CDK (*Cdc28-ts*) show a good rate of

fusion after release from restrictive temperatures compared to permissive temperatures [100]. This indicates that inhibition of the mating pathway in S-G2-M may require the kinase activity of the CDK Cdc28.

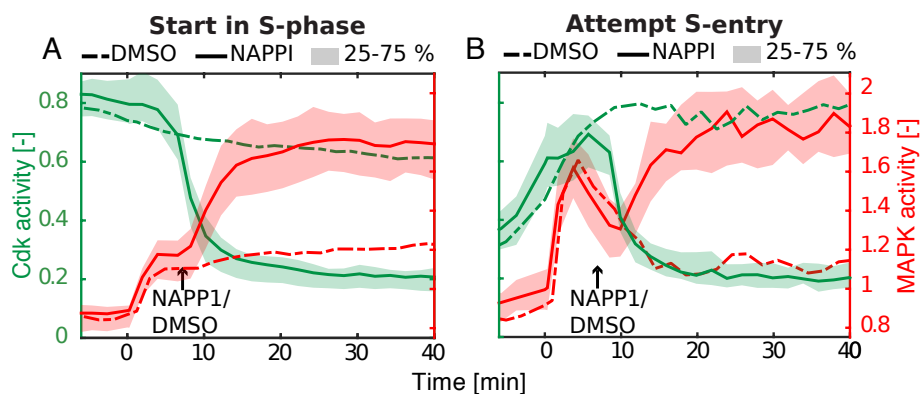


Figure 3.19.: Dynamic CDK and MAPK activities after Cdc28-as chemical inhibition. A. Strain expressing Whi5 and SKARS reporters and an ATP analogue sensitive allele of Cdc28 (Cdc28-as) is imaged every two minutes for 50 minutes. Cells are stimulated with 100nM α -factor at minute 0 and then with the ATP analogous NAPP1 (10 μ M final) or DMSO (0.04% v/v final) 6 min later. MAPK and CDK activities are plotted for cells starting in S-G2-M phase (mean $CDK_{t<0min} < 0.5$, A), or entered in S-phase pre-pheromone addition (mean $CDK_{t<0min} < 0.5$ and mean $CDK_{0min<t<6min} > 0.5$, B).

To confirm that the activity of Cdc28 is required to reduce the mating MAPK activation capacity, we performed time lapse experiments on a strain expressing a genetically engineered Cdc28 allele that can be chemically inhibited using the ATP analogue NAPP1. Cells starting in S-G2-M before stimulation were selected, and dynamic MAPK and CDK activities were plotted relative to the time of pheromone addition. Cells show a drop of the CDK signal, reaching the level of G1-locked cells. This decrease occurs in less than five minutes post NAPP1 addition. The DMSO control experiment shows a sustained high level of CDK activity as expected. This suggests that the Cdc28-as is quickly inhibited by the ATP analogous, mimicking an entry into G1. MAPK activity slightly increases in the first six minutes following pheromone addition. This signal pattern is characteristic of cells in S-G2-M as discussed in figure 3.19.A. However, after addition of the inhibitor, the MAPK activity signal recovers the level shown by cells locked in

3. Mating and cell-cycle cross-inhibition mechanism.

G1, and this in less than 15 minutes. Altogether, these results show that the reduced MAPK activation capacity of cells in S-G2-M phases can be unlocked through the inhibition of CDK activity. Thus, the inhibition of the MAPK in S-G2-M stages is regulated by the activity state of the CDK.

We have shown in figure 3.10.B that cells committed to S-phase entry exhibit a transient MAPK activity. To find out whether the late inhibition of the MAPK is induced by CDK activity dependent mechanism, we recovered the data of the experiment performed in figure 3.19.A and focused on a sub-population of cells that is entering in S-phase after inhibition. We successfully identified cells that increase their CDK activity prior DMSO/NAPPI addition. This increase continues after stimulation with DMSO and saturates at the CDK activity level of S-G2-M cells. Moreover, the MAPK channel shows a transient activity pattern, typical of cells entering in S phase post pheromone stimulation (figure 3.10.B). This confirms that we succeed in identifying the cell cycle committed cells using the first 12 minutes of the time lapse only. After NAPPI addition, however, a sudden drop in CDK activity can be observed. In this condition, we can also observe that the MAPK inhibition is broken about 5 min after the signal reaches the peak. Consequently, the MAPK activity inhibition that occurs at the transition between G1 and S can be prevented by inhibiting the CDK. Therefore, the mechanism triggering the inhibition of the MAPK activity when cells enter in S is regulated by the activity of the CDK Cdc28.

To sum up we first showed that the Far1 protein is required to arrest cells in G1 and that this inhibition occurs in a pheromone dose-depend manner. Subsequently, we showed that inhibition of the mating pathway in S-G2-M phase requires the activity of the CDK Cdc28. The molecular basis of the MAPK inhibition might involve a direct regulation of protein activity, since the MAPK activation rate after CDK inhibition release is fast. Altogether, these results suggest that the mating and the cell cycle cross-inhibition mechanism are ruled by the competition between the MAPK-dependent activation of Far1 and the CDK activity.

3.2.5. CDK Inhibition of the mating pathway

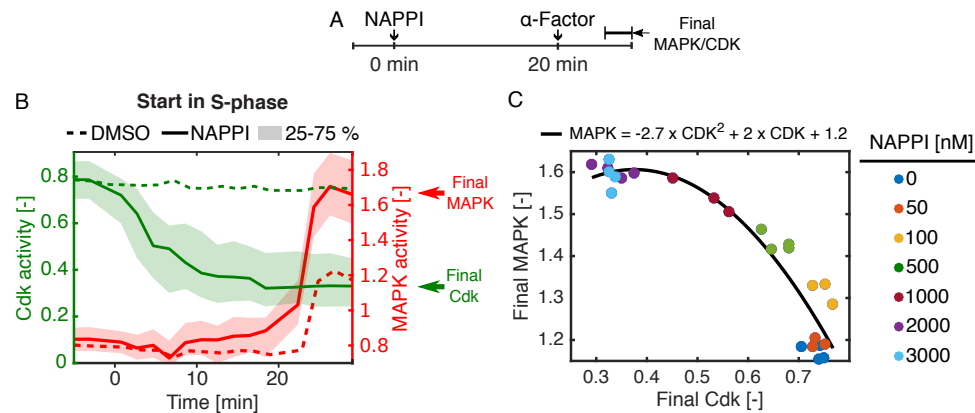


Figure 3.20.: Final MAPK activity at various concentrations of CDK inhibitors. A. Experimental setting. The strain expressing the Cdc28-as allele is imaged for 40 minutes. CDK is inhibited with different concentrations of NAPPI at time 0 min for 20 minutes. α -Factor is then added at saturating concentration (750nM final) and cells are imaged for 15 additional minutes. B. Dynamic CDK and MAPK activities of cells starting in S-phase at two extreme NAPPI concentrations. Curves show the resulting cells that are stimulated with NAPPI at 3000 nM (filled line) and 0 nM (dotted line). Lines correspond to the median value at each time point and areas correspond to 25-75% percentiles. C. Correlation between final MAPK and final CDK. MAPK and CDK activity levels in the last five minutes of the time lapse are extracted for each individual cell, averaged by calculating the median and compared using a scatter plot. The fitting to a polynomial function is performed on the experiments from 100nM to 3000nM NAPPI (black line).

MAPK activation capacity is correlated with CDK-activity . We showed that the cell cycle down regulates the MAPK activity during the S-G2-M-phases in a CDK activity-dependent manner (paragraph 3.2.4). In order to determine whether this inhibition mechanism is correlated with the activity in a dose-dependent manner, we set an experiment in which the CDK activity is artificially controlled. Therefore, the Cdc28-as strain was first inhibited with NAPP1, until the CDK activity reached a desired signal, and then cells were stimulated with saturating concentration of pheromone. For the analysis, we extracted the MAPK and CDK activities obtained in the last five minutes of the time lapse (25-35 min, Final MAPK and Final CDK, figure 3.20.B.) Note that the MAPK activity level reached at 3000 nM NAPPI corresponds to the level observed

3. Mating and cell-cycle cross-inhibition mechanism.

for the G1-locked cluster figure 3.20.B. This confirms that NAPPI releases the MAPK from the CDK-dependent inhibition.

To further determine whether the MAPK activation capacity is linked to a precise CDK activity value, we compared the Final MAPK and the Final CDK obtained at various inhibitor concentrations. Overall, these two parameters fit very well to a 2nd order equation (figure 3.20.C). Altogether, this steady-state analysis shows that the inhibition of the mating pathway is CDK activity level-dependent.

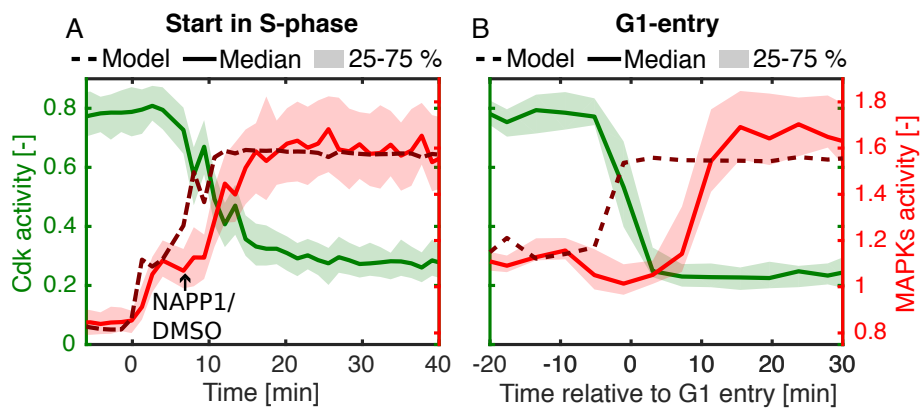


Figure 3.21.: Dynamic MAPK activity estimation from CDK activity. A. Model and MAPK activity fit after CDK inhibition. Dynamic CDK and MAPK activities from one replicate of the assay described in figure 3.19 are plotted. CDK activity of cells starting in S-phase is used as input for a model based on the equations obtained from figure 3.20 (See Appendix B). Solutions of the equations define an estimation of the corresponding MAPK activity for each single cell at each time point. The modelled MAPK activity values are averaged using medians and plotted in the same y-axis as the measured experimental MAPK activity. B. The model fits with the MAPK activity for cells entering in G1. Strain from A. is imaged as in figure 3.10 without performing any CDK inhibition. Cells are stimulated at time point 0 with 750nM α -factor (final concentration). Dynamic MAPK and CDK activities of cells entering in G1 are extracted, synchronised and plotted. MAPK activity is estimated as in panel A and the corresponding median values are plotted.

Modelling of the MAPK activity inhibition mechanism. The NAPPI dose-response experiment we previously performed shows that the MAPK activity depends on the CDK activity. As these conclusions are based on steady-state experiments, we now ask whether this relationship

is conserved in a dynamic system. To answer this question, we used the result from the dose-response experiment and developed a simple model that estimates the MAPK activity based on the CDK values (Appendix B). Modelled and real dynamic MAPK activities were first compared in conditions where the CDK is inhibited post pheromone treatment (figure 3.21.A). After pheromone addition, the real MAPK activity recorded for cells starting in S-phase slightly increases up to the level reached in S-G2-M. During CDK inhibition, the MAPK activity increases for 10 min and stabilises at the level observed for the G1-locked cells. The MAPK activity signal of the model fits well with the experimental data. Thus, the model confirms the MAPK and CDK activity correlation in a dynamic system as well.

We then applied our model to a situation in which the CDK activity drops naturally: the G1-entry transition phase. We performed classical time lapse movies on the *Cdc28-as* strain. Using the model, we then estimated the MAPK activity of cells entering in G1 using their CDK activity values. While the estimated signal increases during the CDK signal degradation, the real MAPK activity signal first shows a little transient degradation and then increases again to reach the same steady-state value as the model. We thus conclude that different mechanisms regulate the MAPK pathway in S-G2-M and during G1-entry. Moreover, these various mechanisms might be differentially sensitive to the CDK activity.

To sum up, by controlling the activity level of the CDK and observing the corresponding MAPK response, we found that the cell cycle inhibits the mating pathway in a *Cdc28* activity dose-dependent manner. The analysis performed in steady-states conditions enabled us to establish a simple model, which estimates the mating pathway activation capacity relative to a given CDK activity level. In conditions where the CDK is inhibited, the model fits well the experimental data, but cannot explain the dynamic activation of the MAPK during G1 entry. Thus we can hypothesise that the cell cycle regulates the mating pathway through multiple mechanisms.

3.2.6. Molecular mechanism of mating inhibition in S-G2-M.

3. Mating and cell-cycle cross-inhibition mechanism.

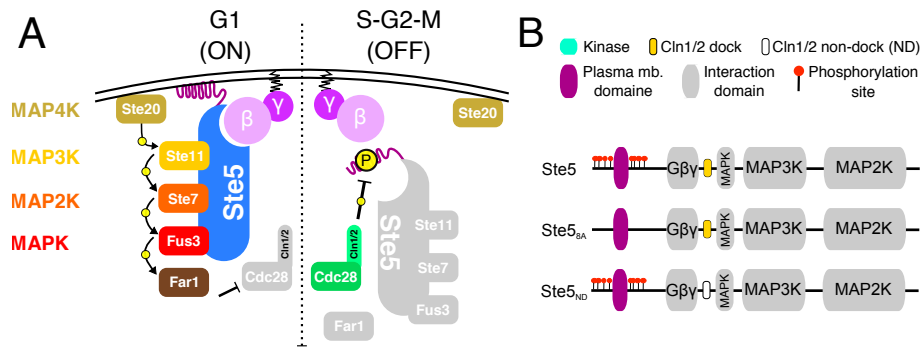


Figure 3.22.: A. Current model of the mating and cell cycle cross-inhibition mechanism. B. Schematic linear representation of the structure of Ste5 scaffold protein and the variant used in the study (adapted from Pope, P. A. & al [91]). B. The Ste5_{8A} variant is obtained by replacing the phosphorylated Serine/Tyrosine surrounding the PM domain by the Alanine (position: 4,11, 29,43, 69, 71, 81, 102). The Ste5_{ND} variant is obtained by replacing the LLPP motif at position 278 by a stretch of four Alanines. Both alleles replace the original *STE5* chromosomal copy, and they are thus expressed under the original promoter. In addition, the *BAR1* protease gene is deleted, in order to avoid early MAPK signal degradation.

The Ste5 scaffold protein is regulated during the cell cycle progression. Our previous analysis confirmed that Cdc28 activity is required to inhibit the mating pathway in S-G2-M. However, we also showed that the CDK may regulate the MAPK through multiple intermediates. The current model states that, in mating condition, the Ste5 scaffold protein binds to the protein Gβγ dimer, so as to promotes the recruitment of the core components of the MAPK pathway at the membrane [116, 131, 119, 93]. Ste11 is relocated in proximity of the membrane-anchored Ste20 and the cascade of phosphorylation can start [7] (figure 3.22.A). In 2007, Peter Pryciak and co-workers established that the CDK, in complex with the cyclin Cln2, regulates the localisation of the Ste5 scaffold protein [116]. Indeed, Ste5 possesses a N-terminus plasma membrane interacting domain (PM) that acts in synergy with the Gβγ binding [131] (figure 3.22.A-B). In G1, Ste5 PM domain is bound to the membrane. In S-phase, however, the CDK-CLN complex phosphorylates the serine and tyrosine surrounding Ste5 PM domain, promoting the detachment of the signalling components from the membrane(figure 3.22.B). Thus, signal transduction through the mating pathway cannot occur anymore.

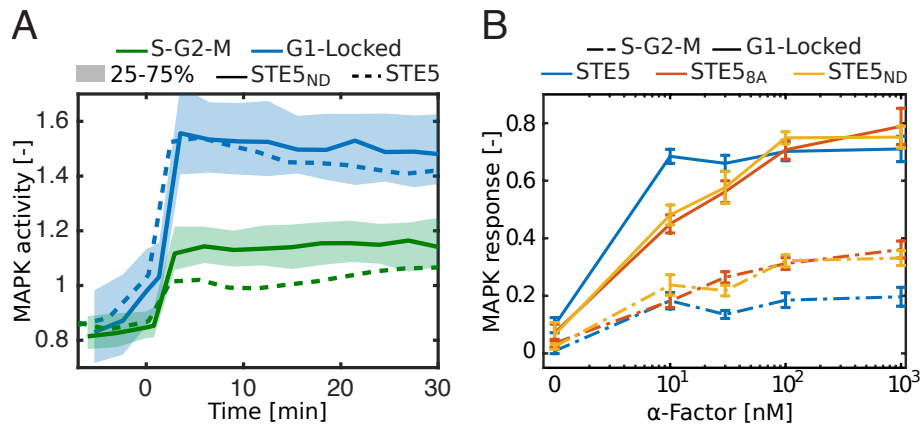


Figure 3.23.: MAPK activity response in mutants expressing non-phosphorylatable Ste5. The dose-response experiment from figure 3.13 is reproduced on strains expressing Ste5, Ste5_{8A} or Ste5_{ND} alleles. A. Dynamic MAPK activity of G1-locked and S-G2-M cells. Cells were stimulated with 1 μ M α -factor at time 0. B. Single cell MAPK responses following stimulation are calculated and plotted as in figure 3.17.A. Values correspond to the means of at least three replicates and error bars are standard deviations.

Although this model, explaining how the cell cycle regulates the mating pathway, is well accepted, no studies confirmed it at the single cell level. For this reason, we performed dose-response experiments as in figure 3.13 on strains expressing two alleles of Ste5 previously described [13, 116]: a CDK non-phosphorylatable mutant (Ste5_{8A}) and a cyclin non-docking (Ste5_{ND}) mutant [131, 91, 90, 14]. We compared MAPK activity reached by cells expressing the Ste5 alleles when they are either in G1 or in S-G2-M. Cells expressing the Ste5 or the Ste5_{ND} alleles show similar dynamic MAPK activities when they are in G1 phase (figure 3.23.A). However, the strain expressing the Ste5_{ND} exhibits, during the S-phase, a higher and sustained MAPK activity compared to the strain expressing the WT allele. The same response is observed in cells expressing the Ste5_{8A} (data not shown). This confirms the results from Strickfaden & al, 2007 [116], suggesting an improved activation of the mating pathway in S-phase, when Ste5 cannot be phosphorylated. Surprisingly, the MAPK activity of S-G2-M clusters from both Ste5 mutants does not stabilise at the level of the G1-locked clusters. We confirmed this difference by the comparison of the S-G2-M and G1-locked MAPK response at intermediate pheromone concen-

3. Mating and cell-cycle cross-inhibition mechanism.

trations (figure 3.24.B). At all tested concentrations, Ste5 mutants display a weaker ability to signal in S-G2-M than in G1.

Altogether, these results suggest that the cell cycle regulates the mating through the regulation of the phosphorylation state of the scaffold protein Ste5. However, as mutant expressing non-phosphorylatable Ste5 alleles still show reduced MAPK in S-G2-M phases compared to G1 suggesting that additional mechanism occur to inhibit the mating pathway in this cell cycle stage.

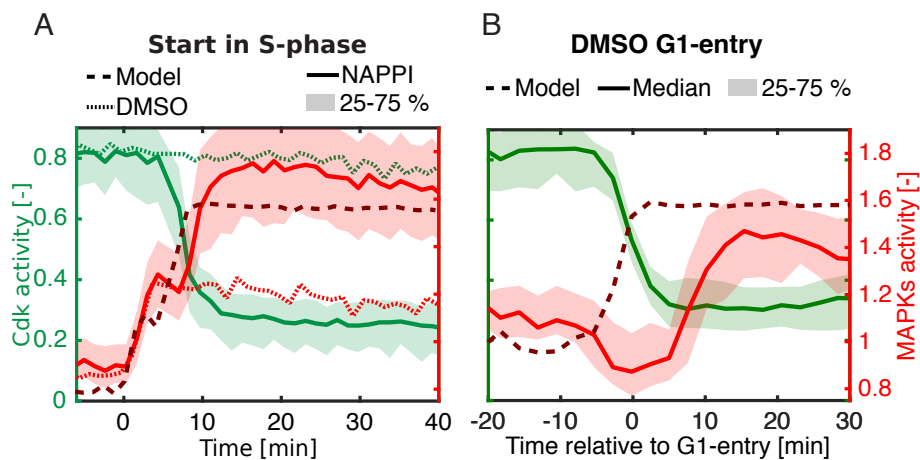


Figure 3.24.: MAPK activation after CDK inhibition in the $Ste5_{ND}$ strain. A. *Cdc28-as* strain expressing the $Ste5_{ND}$ and deleted for *BAR1* is imaged and analysed as in figure 3.21.A. The curve represents MAPK and CDK activities of cells in S-phase in the beginning of the experiment. B. The DMSO control experiment from A is analysed as in figure 3.21. Curve represent the CDK and MAPK signal of cell entering in G1 post pheromone addition. For both panel, filled and dotted lines correspond to medians of single cells traces.

The inhibition of Ste5 is CDK activity-dependent. The Ste5 phosphorylation by the CDK is not sufficient to explain a complete inhibition of the mating pathway in S-G2-M phases. In order to determine whether the remaining mechanisms are CDK activity dependent, we tried to observe whether S-G2-M cells expressing $Ste5_{ND}$ alleles reach the maximum MAPK activity after *Cdc28-as* inhibition with NAPP1 (figure 3.24). We focused our analysis on the $Ste5_{ND}$ because the $Ste5_{8A}$ possesses unmutated potential phosphorylation sites. In the ND allele, however,

the Cln2 binding site mutation may totally abrogates the phosphorylation by the Cdc28-Cln2 complex. Cell starting in S-phase prior pheromone addition activates the mating pathway at intermediate level. As expected, the intermediate MAPK activity reached in this mutant is higher compared to the one observed in the WT (Ste5 ND : 1.2, WT: 1, compare figure 3.24.A with figure 3.21.A). After CDK inhibition, the MAPK activity increases and stabilises at the level of the G1-locked cluster. This suggests that additional mechanism(s) of inhibition of the mating pathway require the CDK activity. These results confirm that Ste5 phosphorylation only partially explains the inhibition exerted by the CDK and that additional CDK activity-dependent mechanisms are still required.

We observe in figure 3.21.B that the MAPK is transiently inhibited just before completing the cell cycle. To determine whether the phosphorylation of Ste5 contributes to this signalling cascade down regulation, we recovered the data from the DMSO control experiment used in figure 3.24.A, and observed how the MAPK is activated while cells enter in G1 (figure 3.24.B). The model does not support the data at high CDK activity level (before G1 entry). Moreover, both modelled and experimental MAPK signals are delayed when the CDK activity drops, and the MAPK negative overshoot observed during CDK signal degradation is even amplified. This last result suggests that an independent and stronger inhibition of the mating pathway occurs at the transition between S-G2-M and G1 phases. Altogether, these results suggest that the Ste5 phosphorylation driven by the CDK in S-G2-M phases contributes to inhibit the mating pathway, but it is not sufficient to completely abolish it.

Cdc28 does not regulate the mating through the MAP2K or the MAP4K We previously concluded that the CDK might target multiple components to inhibit the mating in S-phase. In this section, we will investigate two potential targets of the CDK. As suggested by Ammerer and colleagues, the regulation of the cell cycle can happen through Ste11 or downstream components (Ste7, Fus3) [129]. We first tested the role of the MAP2K Ste7. This kinase is essential for signal transduction, since a deletion of the encoding gene causes the cells to be completely insensitive to

3. Mating and cell-cycle cross-inhibition mechanism.

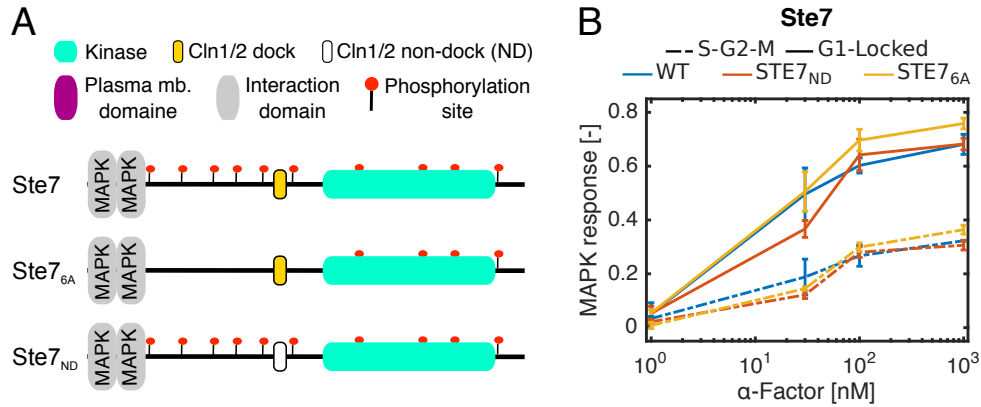


Figure 3.25.: Potential inhibition of the MAPK through Ste7. A. The Ste7_{6A} variant is obtained by replacing the serine/tyrosine phosphorylation sites by an alanine (Amino acid numbers: 105, 130, 167, 116, 137, 149). The Ste7_{ND} variant is obtained by replacing the region coding for the SISLPPL motif at protein position 156 with a sequence coding for alanines. Both alleles replace the original WT copy of *STE7*. Note that strains express also the Ste5_{ND} allele. Alleles are thus expressed under the *STE7* native promoter. B. Single cell MAPK responses after stimulation are calculated and plotted as in figure 3.17.A. Values correspond to means of at least three experimental replicates and error bars represent standard deviation.

pheromones[19]. The MAPK Fus3 is also known to regulate the MAP2K by phosphorylation, so as to reduce the signalling cascade sensitivity [35]. Moreover, Ste7 is known to be ubiquitinated in a pheromone-, cell cycle- and Ste11- (MAP3K) dependent manner [?, 127]. Finally, when analysing the sequence of Ste7, we found a LPPL motif [13] that resembles to the typical Cln1/2 docking site found in Ste5. In order to see whether the cell cycle regulates the mating pathway through Ste7 in S-phase, we constructed strains expressing variants of this protein. Note that these strains also express the Ste5_{ND} allele, in order to observe only the potential effect of the CDK on Ste7. In the first tested allele (Ste7_{6A}), all the phosphorylation sites located outside the kinase domain are replaced by an alanine. The second Ste7 variant (Ste7_{ND}) is mutated for the potential Cln1/2 DS (LPPL motif, figure 3.25.A). We then performed time lapse experiments and analysis as described in figure 3.23.B. We do not observe any difference of MAPK activity response between the WT background and the strains expressing the Ste7 variants (figure 3.25). Thus, the cell cycle does not regulate the mating pathway in S-G2-M

phases through a CDK-dependent phosphorylation of Ste7.

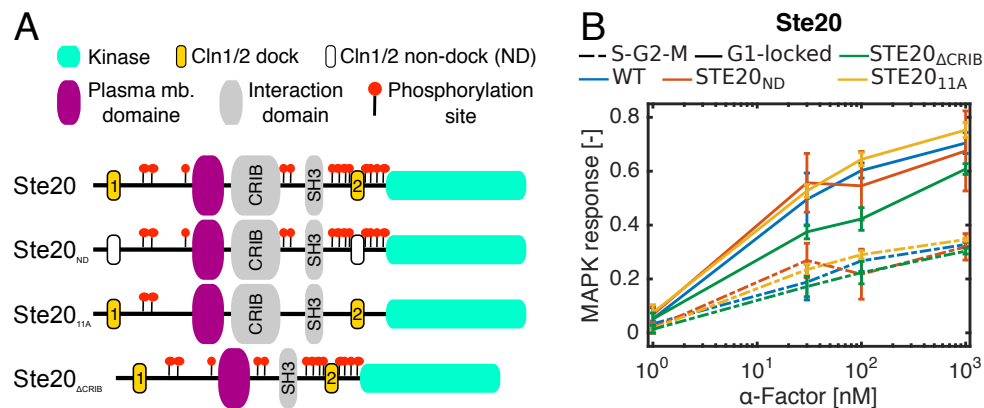


Figure 3.26.: Inhibition of the MAPK through Ste20. A. The Ste20_{11A} variant is obtained by replacing the serine/tyrosine phosphorylation sites by an alanine (positions: 269, 418, 423, 492, 502, 512, 517, 547, 555, 562, 573). The Ste20_{ND} variant is obtained by replacing the coding sequences of the SLDDPIQF and the PLPPIPP motifs at protein positions 87 and 535 with sequences of same length coding for alanines. Both alleles are inserted into the strain expressing the Ste5_{ND}, at the original *STE20* chromosomal locus. *STE20* variants are thus expressed under their native promoter. B. Single cell MAPK responses following stimulation are calculated and plotted as in figure 3.17. Values correspond to means of at least three experiments and error bars represent standard deviation.

It was demonstrated that a strain with inhibited Cdc42 or its master regulator Cdc24 does not activate the mating during the S-phase, suggesting that the cell cycle target a mating pathway component located downstream of Cdc42 [22]. Ste20 PAK-like kinase (MAP4K) might be a good target for cell cycle regulation. Its phosphorylation, localisation and activity are regulated in a cell cycle-dependent manner [66, 13]. Ste20 contains a well-known Cln2 DS at the N-terminus of the protein, that enables a direct phosphorylation of the protein by the CDK [13] (figure 3.26). We also found a second potential DS motif surrounded by eight phosphorylation sites. Phosphorylation of these sites is thought to open the protein, so that the CRIB domain of Ste20 can bind the active GTP bound form of Cdc42. This open conformation is also thought to be important to promote signal transduction through the mating pathway [64]. We tested the response to pheromone of strains expressing Ste20 variants mutated for their phosphorylation

3. Mating and cell-cycle cross-inhibition mechanism.

sites, for both Cln DS, or with a CRIB domain deleted allele (figure 3.26). Note that these strains also express the Ste5_{ND}. In all the tested constructs, G1-locked cells activate much more the MAPK than the S-G2-M cells, as in the WT background. Thus, the cell cycle does not regulate the mating pathway through Ste20.

To sum up we confirmed in this section that Ste5 scaffold protein is an entry point for the cell cycle to regulate the mating pathway. The CDK-CLN complex phosphorylates the protein and promotes the detachment of the Ste5-Ste11-Ste7-Fus3 complex from the membrane [116]. However, we found that this model is not sufficient to explain the MAPK inhibition in S-G2-M phases. We concluded that additional mechanism(s) act in addition to the Ste5-dependent mechanism. We tested two potential CDK targets, the PAK-like kinase Ste20, also known at the MAP4K, and the MAP2K Ste7, by expressing phosphorylation sites and using Cln1/2 DS derivative mutants. However, none of these alleles have improved S-G2-M MAPK activity compared to strains expressing the WT allele. Thus, the mechanism acting in parallel with the CDK-dependent Ste5 phosphorylation has still to be uncovered.

3.3. Discussion

Cell fate decision making: mate or divide. Using combination of synthetic biology and live fluorescence microscopy, we accurately monitored the dynamic kinase activity of both mating MAPKs, Fus3 and Kss1, after pheromone stimulation and in function of the cell cycle progression. With this strategy we confirmed that the activation capability of the mating pathway is maximal during G1. This result supports the fact that in mating assays, two opposite mating types undergo fusion only during this cell cycle phase. Biologically, this makes sense since cells contain one copy of each chromosome and the polarisation machinery can be fully exploited to shmoo toward the partner. Therefore, this process implicates an arrest of the cell cycle progression in order to allow the starting a new transcriptional program and the polarisation.

We monitored the cell cycle arrest in G1 upon stimulation with pheromones and inferred that the START checkpoint is not defined only by the CDK activity threshold [50, 81]. Indeed, we demonstrated that the arrest in G1 is also MAPK activity dose dependent. Thus CDK and MAPK compete to drive the cell choice either toward arrest in G1 or cell cycle commitment. We attempted to quantify this relationship between CDK and MAPK activities to be able to anticipate the cell choice. However, we were limited by the fact that daughter cells can stay longer in G1 independently on the MAPK activity level [26, 25]]. Consequently, it is difficult to identify mating-induced G1 arrest events. This issue could be solved by imaging for a longer period prior stimulation and focusing the analysis on cells that enter in G1 prior pheromone addition. Lineage tracing methods could also be used in order to separate mother cells from daughter cells [126, 102].

The delay between cell cycle commitment and MAPK activity inhibition rises another important question: how much active Far1 is required to arrest the cell cycle? This question can be partially addressed in *cln3Δ* background since this cyclin was reported to be responsible for cell cycle dependent degradation of Far1 [53]. Alternatively, we could think about constitutively express a stable version of Far1 [72]. In this condition, we would abrogate the cell cycle depen-

3. Mating and cell-cycle cross-inhibition mechanism.

dent regulation of Far1 and the arrest would be only the downstream consequence of the MAPK activation. Then, by expressing the CKI with constitutive promoters of increasing strength, we would be able to define how much Far1 is required to block the cell cycle progression.

Another possibility would consist in correlating the Far1 expression and degradation with the capacity of commitment to cell cycle. Tagging Far1 with a fluorescent protein (FP) is not a good option, since the signal would be subjected to artifacts mostly due to the FP maturation time. This problem can be bypassed using the dPSTR technology we developed in our lab [3]. The dPSTR would be fused to the *FAR1* promoter and supplemented with the fragment of CKI responsible for its cell cycle dependent degradation. In combination with the Whi5 marker, Far1 protein levels could be monitored across the cell cycle phases by reporting the nuclear accumulation of the dPSTR into the nucleus prior and after pheromone treatment.

Inhibition of the mating pathway in S and G2 phases Our study showed that inhibition of the mating pathway in S-G2-M phases is CDK activity dose-dependent and confirmed that one target of the CDK Cdc28 is the Ste5 scaffold protein. However, we realised that the molecular mechanism proposed by the group of Pryciak is not sufficient to explain how the MAPK is inhibited in S-G2-M phases[116]. Thus, other mechanisms have to be uncovered.

Two articles have narrowed down the number of potential targets of the cell cycle at proteins located either downstream of Cdc42 in the signaling cascade [22], or downstream/in parallel of Ste11. We thus attempted, without success, to verify a potential direct regulation of Ste20 (MAP4K) and Ste7 (MAP2K) by Cdc28. Another potential target currently under investigation is the adaptor protein Ste50. This scaffold links the MAP4Ks Ste20 and Ste11. Some mutants of Ste50 protein were shown to differentially activate the mating pathway compared to WT[56]. Moreover, this protein contributes to the crosstalk between pathways and contains a multitude of potential phosphorylation sites targeted by the MAPKs Fus3, Kss1 and Hog1 [134]. For example, Hog1-dependent phosphorylation in hyper-osmotic stress condition dampens the mating pathway [76]. Consequently, Ste50 is a key component required to maintain MAPK pathway specificity.

Therefore, this protein could be an entry point to regulate the mating pathway in S-G2-M phases. Finally, we cannot reject the hypothesis that Ste5 can be regulated through other paths. We tested the hypothesis of the membrane detachment through the phosphorylation of the Ste5 PM domain [93, 116, 119], but other putative phosphorylation sites and a second cyclin docking site are located close to domains known to interact with the MAP3K, the MAP2K and the MAPK.

We observed that in S-G2 the MAPK activity is reduced and not completely abrogated. This slight activation of the mating pathway may explain why some groups have reported that the signalling cascade can be activated in G2[19]. We can imagine that this low activity may contribute to prepare the cells for mating when they enter in G1. Preliminary results showed that some promoters involved in mating, such as the P_{FAR1} or P_{AGA1} are induced in S-G2, although not as efficiently as in G1. This would mean that mating genes respond differentially depending on the level of activated MAPK. Overall, investigation of the regulation of mating dependent genes in function of the cell cycle stages opens a wide possibility of further investigations, and this thank to our strategy.

Transient MAPK inhibition during G1 entry Finally, our data suggest that the MAPK is down-regulated during the CDK signal degradation at G1 entry. It was shown that CDK activity must drop to enable an exit from the M-phase [97]. Consequently, we hypothesise that the transient inhibition of the mating pathway occurs during the M-phase. Our results suggest that the MAPK, or one or multiple upstream signalling cascade components, are transiently inhibited at G1 entry and this independently on the Ste5 phosphorylation.

Although the regulation of the mitosis in budding yeast is well documented, it remains difficult to make a direct link between the mating pathway components and regulators of the M-phase. It was reported that transcription of many MAPK pathway component genes are regulated in a cell cycle dependent manner [80]. However, the transient inhibition occurs in less than 20 minutes, which is fast for a transcriptional regulation.

Two other components might make the link between the M-phase and the mating. These are

3. Mating and cell-cycle cross-inhibition mechanism.

the Ste20 PAK-like kinase and the scaffold protein Bem1. Both are known to localise at the septum[69]. In mating condition, Bem1 is implicated in shmoo formation but is not required for MAPK activation [17]. On the contrary, Ste20 has a clear role in the mating pathway. We tested various expressing Ste20 alleles but we did not observe any MAPK activity signal difference compared to WT (data not shown). Considering this, the MAP4K might not be implicated in the pathway inhibition during the M-phase and the potential targets might be either downstream to it or part of the receptor branch.

Following this last idea, the α -subunit of the G-protein, Gpa1, could be a interesting candidate. The phosphorylation of this protein is promoted in G2-M by the Elm1 kinase[61] and is poly-ubiquitinated in G1 [125]. The Elm1 kinase is a well know regulator of cell morphology and is located at the bud neck. Moreover, a deletion of this protein leads to filamentous morphology that can be compensated by a Cdc28 mutant that lacks some functional phosphorylation sites[32]. To conclude, Gpa1 might be a good target for the cell cycle to control the mating pathway activity in M-phase.

The last hypothesis we can draw is that the transient inhibition is not induced by a mechanism that specifically target the mating pathway. Indeed, we mention previously that the CDK activity must drop to exit M-phase [97]. To achieve this, a huge pulse of active phosphatases (Cdc14 and PP2A) is released and inhibits directly the CDK [52] and its substrate. Thus, we can suggest that these phosphatase inhibits the mating pathway through unspecific dephosphorylation of the signalling cascade components.

3.4. Conclusion

In this chapter, we described a single cell analysis of the mating and cell cycle cross-inhibition mechanism. By combining synthetic biology with live single cell imaging and computational data analysis, we succeeded in measuring in each individual cell the kinase activity of the cell cycle regulator Cdc28 and the mating pathway MAPKs Fus3 and Kss1 . Our strategy enabled to iden-

tify four main MAPK dynamic activity patterns linked to cell cycle position. We confirmed that the mating pathway induces cell cycle arrest in G1 through the Far1 CKI and that the cell cycle inhibits the mating pathway through the phosphorylation of the Ste5 scaffold protein. However, we found that additional uncovered CDK activity dependent mechanisms act in addition to the Ste5 phosphorylation in S-G2-M phases. Finally, we found that MAPKs are strongly down regulated during the transition between S-G2-M and G1 phases, suggesting that another mechanism induces the inhibition of the mating pathway independently on Ste5 phosphorylation. Further investigations will have to uncover these parallel mechanisms and test their relevance on mating efficiency.

4. General discussion

4. General discussion

SKARS Cell-to-cell variability has become an important field of investigation during this last decade. Indeed, an isogenic population can exhibit either a uniform response or a heterogeneous behavior from cell-to-cell. These observations have important implications in the signal transduction field, as the cell fate is the result of the processing of intra/extracellular cues by signalling cascades. Signal processing by signalling cascades is defined by a sequence of reactions driven by molecular mechanisms specific to the current physiological state of the cell. Dynamic single cell analysis of signalling cascade activity is thus required to define the molecular processes leading to a given cell fate. FACS and single cell mass spectrometry show only snapshots of the state of a cell, while fluorescent based reporters are mostly limited by the maturation time of the fluorophore. Thus, despite important technical progresses, investigating the activity state of signalling cascades at the single cell level remains difficult.

In the first chapter, we described a new approach based on a synthetic fluorescent biosensor that can act at the same time scale as the signal transduction and reports the activity state of a kinase from a signalling cascade. This synthetic fluorescent biosensor, that we called SKARS, is composed of three domains: a docking site (DS), a nuclear localization sequence (NLS) and a fluorescent protein (FP). The DS enables a specific interaction with the kinase of interest and the NLS promotes the active transport of the sensor into the nucleus. Once activated, the kinase inhibits the NLS by phosphorylation and promotes the cytoplasmic accumulation of the sensor. Thank to time lapse microscopy, we can deduce the dynamic activity of this kinase by calculating the ratio of fluorescence intensity between the nucleus and the cytoplasm. Bioinformatic analysis allow to perform this measurement in hundreds of individual cells, enabling us to probe the activity state of the signalling cascade upstream from the measured kinase.

The first version of the SKARS was built to measure the activity of the mating MAPKs Fus3 and Kss1. Then, we adapted the SKARS to probe the MAPK Mpk1 from the CWI pathway. We easily achieved this by replacing the original interaction domain by the DS of the Mpk1 upstream regulator, Mkk2. This shows that only minor changes in the structure of SKARS are required to measure another MAPK. Although we designed sensors to measure the activity of various

MAPK, one can envision to use the SKARS technology to measure other kinases. The only limit consists in finding a regulator or a substrate which contain a very well-defined interaction domain. If no interaction can be found, a possible solution would be to use interacting peptides to artificially promote the interaction of the biosensor with the kinase [122]. For instance, SynZips are hetero-specific synthetic coiled-coil peptides that work by pairs and specifically interact with each other. The idea would consist in using one SinZIP to tag the kinase of interest and replace the SKARS DS by a complementary peptide. Overall, this strategy would enable to enlarge the spectrum of measurable kinases.

The straightforward structure of SKARS also enables to overcome the species barriers. Indeed, NLS signals are reported to be functional in broad number of organisms, like mammalian cells. Moreover, MAPK phosphorylation sites are also widely conserved. We recently developed SKARS for three MAPK from mammalian cells, ERK, JNK and p38. For this, we used their known upstream regulator DS that we inserted in our yeast sensor. In fact, similar MAPK sensors has been designed during the SKARS developpement. The KTR biosensor from the Corvet lab have a very similar structure, although it possesses an additional nuclear export signal [99, 138]. We are currently comparing the range of sensitivity of the KTR and SKARS. The preliminary result of Min Ma, a Post-Doc from our lab, suggest that the KTR saturates its signal at a lower level than SKARS, meaning that our design seems to better translate higher kinase activity level. Consequently, our SKARS technology might be a good alternative to KTR.

Application The SKARS technology offers many possibilities of application. In this study, we used this bio-reporter to record the activity of mating MAPK following exogenous pheromone stimulation. The same kind of investigation can be done with mammalian cells in the context of drug discovery for cancer therapy. Indeed, a drug can be tested for its effect on MAPK activation and, at the same time, the downstream behaviour can be observed. We can also imagine to observe the emergence of cancer cell resistance to some drugs and try to correlate it with a particular MAPK activity signal pattern.

4. General discussion

The MAPK activity signature that is recorded by SKARS provides interesting information about the kinetics of signal transduction through signalling cascades. However, the measured kinase activity pattern often results from the combination of multiple inputs, since signalling pathway are all interconnected. Thus, in some cases, the signalling cascade must be isolated to describe its various kinetics properties. Recent studies have described optogenetic systems such as the CIBN/CRY2 from *Arabidopsis thaliana* [60] or the photo-dissociable tetrameric green fluorescent protein Dronpa145N[138], that allows a controlled activation of a pathway. These methods consist on promoting the oligomerisation of two proteins by illuminating cells at a precise wave length. Using this technique, the Michael Lin lab has artificially generated various Akt kinase activity patterns and correlated this with specific cell behaviours. On the other hand, the group of Takeaki Ozawa combined the SKARS homologue (KTR) with his optogenetic system, and uncovered a direct and rapid inhibitory feedback loop from ERK to MEK1.

These last examples illustrate a second straightforward property of our biosensors. The SKARS technology can be combined with other biosensors. The combination of multiple sensors can be extremely useful in the context of the study of cross-talks between signalling cascades. In the chapter two, we presented an experimental setting where the yeast mating MAPK and the cell cycle progression were both probed at the same time using a SKARS sensor and the Whi5 transcription factor respectively. Based on our quantitative measurements, we confirmed that the two physiological processes are interconnected at the level of signalling cascades. The mating pathway promotes the cell cycle arrest in G1 by activating the Far1 CKI, while the CDK Cdc28 inhibits the MAPK during the S-G2-M cell cycle phases. Our single cell analysis confirmed that the CDK targets the Ste5 scaffold protein by phosphorylating its PM domain [116]. However, we revealed that other mechanisms occur in S-G2 phases. In M-phase, the MAPK activity seems to be regulated through a mechanism that could not require the phosphorylation of Ste5. Consequently, parallel measurements of multiple kinase activities in live single cell enable to extract high resolution data, allowing to understand how signalling cascades cross-interact dynamically.

We chose to investigate the cross-talk between mating and cell cycle by combining a natural CDK sensor with the SKARS. Other proteins, such as the MAPK Hog1 in yeast, or the mammalian transcription factors NF- κ B, are known to change their sub-cellular localisation depending on the activation of MAPKs. However, not all MAPKs, MAPKs' substrates and regulators exhibit such a behaviour. In Chapter 1, we proved that this problem can be solved by combining multiple SKARSs tagged with different fluorescent proteins into the same yeast cell. Preliminary data from Min Ma, suggest that this strategy can also be applied in mammalian cells as well (also supported by data from the Corvert Lab[99]).

Although the combination of SKARS sensors is an interesting feature that can be applied to study the cross-talks between signalling cascades, the biosensor is also fully compatible with other synthetic bio-reporters. Indeed, Delphine Aymoz, a PhD student in our lab, has developed the synthetic translational reporter dPSTR, that is fully compatible with the SKARS technology [3]. In the context of the response to pheromones, we can imagine to correlate the MAPK activity with the induction of particular genes. Combined with the Whi5 marker, this gene regulation can be monitored in parallel with MAPK activity and during the cell cycle progression. Because of technical issues due to overlapping of FP emission spectrum, not enough fluorescent channels are available to combine these three sensors. One possible solution to counteract this problem would be to direct the phosphorylation-dependent relocation of the sensor to another cell compartment. Inspired from the work of Nadim Mira, a former lab member, we can imagine a bipartite synthetic protein, with one component constitutively located at the plasma membrane and a second one that would interact with its partner after being phosphorylated by the MAPK. In such situation, the MAPK activity is converted in a relocation signal from the cytoplasm to the plasma membrane. We are currently investigating this in the lab.

The SKARS sensor might be combined with another biosensor that enables to quantify the number of mRNA molecules using the Ms2 or PP7 phage coat proteins [65, 12]. We can imagine to observe the number of produced transcripts following the activation of a promoter regulated by the MAPK. We can also imagine to probe the signalling cascade activity and both the down-

4. General discussion

stream transcriptional and translational responses with the SKARS, our dPSTR and the pp7 system respectively. Using simultaneously these three types of sensors, we would be able to get fantastic information about how these three cellular processes interact with each other and drive the cell fate decision in a given environment.

Overall, the synthetic biology field has promoted the emergence of new techniques enabling to probe key cellular processes in live single cells. The study of single cell behaviour has been limited for a long time by the capacity to observe the development of the cell in its natural environment. In the context of mating process study in yeast, we can already observe the fusion process while extracting the MAPK activity and tracking the cell cycle progression of individual cells. In mammalian cells, however, this is more complicated, since single cells evolve in a tissue that has complex structure and composition. This major limitation is about to be broken-down by the recent progresses done in the microscopy field, that have led to the emergence of new techniques such as three-dimensions live microscopy or intra-vital microscopy. We strongly believe that SKARS might play a role in the future investigation based on these techniques. We can imagine to study the MAPK activity of single cells during the development of model organisms such as zebrafish (*D. rerio*) or the nematode *C. elegans*, or to probe the MAPK activity of cancer cells directly inside the tumors' macro-environment. We are currently collaborating to invest this path.

Conclusions In this thesis we presented a synthetic bio-reporter that allows accurate measurements of signalling cascade activity, dynamically and at the single cell level. The sensor is actively imported into the nucleus when the signalling cascade kinase is OFF, and accumulates into the cytoplasm when the kinase is turned ON. This subcellular localisation change is used as a proxy for kinase activity measurements through the calculation of a ratio of fluorescence intensity between the nucleus and the cytoplasm. We apply this technique in the context of the study of the yeast mating MAPK and cell cycle cross-inhibition mechanism and proved that the current model describing how the cell cycle regulates the mating pathway is incomplete.

This first example of application of such system led us to conclude that the SKARS can be applied in numerous fields of research by combining this probe with other bio-reporters. Combination of multiple SKARSs enables to study cross-talk between pathways such as the MAPK pathways. In addition, the SKARS can also be combined with transcriptional or translational fluorescent based reporters in order to assess how some promoters would respond to various dynamic signalling cascade activity patterns.

To conclude, the SKARS synthetic protein is a tool that can be used to comprehend how individual cells process intra- and extracellular signals and how this leads to a particular cell fate.

5. Material and methods

5. Material and methods

Strains and plasmids Yeast strains and plasmids are listed in table A.1table A.2. SKARS plasmids were constructed by cloning the different parts of the sensor into a pRS304 or pRS306 vector backbone [113]. They were expressed from the constitutive promoter P_{RPS2} , cloned using SacI-HindIII restriction sites. The DS from *STE7*, *FAR1*, and *MKK2* were amplified either from yeast genomic DNA or synthesised and subsequently cloned between HindIII and XbaI sites. To generate the 2xNLS sequence, two oligos were synthesized, annealed, and cloned in the vector by enzymatic restriction with XbaI and BglII. The fluorescent proteins mCherry, mCitrine_{A206K,L221K} or CFP were cloned between BglII and XhoI. A CYC1 terminator was cloned between XhoI and KpnI.

In chapter 3, the sensor and the corrector were assembled by cloning the *STE7*₁₋₃₃-NLS-NLS-*mCherry* or the *STE7*_{ND}-NLS-NLS-*CFP* (HindIII-KpnI) sequences downstream the P_{RPS6b} promoter into the pSIVURA (SacI-KpnI) [132]. The plasmid pED141 containing both sensor and corrector was obtained by cloning the P_{RPS6b} -*STE7*_{ND}-NLS-NLS-*CFP* into the second MCS of pED92 (AatII-SphI). The plasmids were transformed in W303 yeast background bearing a Hta2-CFP nuclear marker (ySP37) or the Hta2-tdiRFP (yED136).

Genomic deletions were constructed in cells bearing the sensors using KAN or NAT resistance cassettes [40, 70]. In the chapter 2, Whi5 and Yox1 were tagged with mCitrine using pKT139 plasmid [111]. In the chapter 3, Whi5 was tagged with mCitrine using pGTT-mCitrine_{A206K,L221K} plasmid [132]. Plasmids containing the coding sequence of Ste5, Ste20 and Ste7 were obtained by amplification of a chromosome fragment spanning from about -100bp (into the promoter) to the end of the ORF and cloned using PacI-NheI sites into the pGTH-CFP, replacing the fluorescent protein. Mutated variants were then obtained by replacing a fragment of the gene by a synthesised double-stranded DNA containing the desired mutation. Plasmids were integrated into the genome of yeast by homologous recombination replacing the NAT or KAN cassettes used to delete the genes.

Sample preparation The cells were grown in saturated overnight cultures at 30°C in synthetic medium (YNB: CYN3801, CSM: DCS0031, ForMedium) . They were diluted in the morning to OD₆₀₀ 0.05 and grown for at least four hours before starting the experiments. For experiments in wells, 96-well plates (MGB096-1-2LG, Matrical Bioscience) were coated with a filtered solution of Concanavalin A (0.5 mg/mL, 17-0450-01, GE Healthcare) for 30 min, rinsed with H₂O, and dried for at least 2 hours. Before the experiment, the cultures were diluted to an OD₆₀₀ of 0.05, and briefly sonicated. A volume of 200 µL of culture was loaded into each well. Cells were left settling 15-45 minutes before imaging. To stimulate the cells, 100 µL of inducing solution was added to the wells. For α -factor stimulation, 1 µM final concentration. Zymolyase (120491-1, AMS Biotechnology) stress was applied at 3 U/mL final concentration. To inhibit Fus3_{as} or Cdc28_{as} (chapter 2, chapter 3), a 25 mM stock solution of NAPPI (A603004, Toronto Research Chemical) in DMSO was diluted in SD-medium to 40 µM. The solution was added to the wells to obtain a final working concentration of 10 µM. In control experiments, cells were treated with DMSO 0.16 % in SD-full.

For the dose-response experiment from figure 2.11, the pheromone stimulation was performed in Eppendorf tubes. Specifically, 200 µL of cell culture was mixed with 100 µL of α -factor to reach a final concentration between 0 and 1 µM. Immediately after mixing, 200 µL of this suspension was loaded into a coated 96-well plate. After 15 minutes of incubation, images from ten different were acquired.

For the hypo-osmotic stress experiment in microfluidic device (figure 2.24.A-B), cells were grown overnight in SD medium containing 1 M sorbitol, diluted in the same medium to OD₆₀₀ of 0.05, and grown for at least 4 hours before the beginning of the experiment. Cells were diluted to an OD₆₀₀ of 0.25 if necessary, and 200 µL of culture was loaded in a microfluidic chip (Y04C, CELLASIC Corp). SD medium with 1 M sorbitol and containing fluorescein-dextran (D3305, Invitrogen) 1 µg/mL was added into flow chambers 1 and 2. SD medium with 0.5 M sorbitol and containing fluorescein-dextran 0.5 µg/mL was added to wells 3 and 4. To allow a rapid switch between the media, the pressure was set at 3 psi in wells 1 and 2 and at 0.3 psi in wells 3 and

5. Material and methods

4. At the desired time, the high and low pressures were inverted to load medium into the cell imaging chamber.

Microscopy Images were acquired with a fully automated inverted epi-fluorescence microscope (Ti-Eclipse, Nikon), controlled by Micromanager software [117] and placed in an incubation chamber set at 30 °C, with a 40× oil objective and appropriate excitation and emission filters. The excitation was provided by a solid-state light source (SpectraX, Lumencor). The images were recorded with a sCMOS camera (Flash4.0, Hamamatsu). A motorised XY-stage allowed recording multiple fields at every time points. CFP (40 ms), RFP (100 ms), and YFP (100 ms (chapter 2) or 300 ms (chapter 3)) and two brightfield (10 ms) images were recorded at time intervals between 1 and 5 minutes.

Data analysis Time-lapse movies were analysed with the YeastQuant platform [85] (figure 2.4). The cell nuclei were segmented by thresholding from CFP images. The contour of the cell around each detected nucleus was detected using both brightfield images. The cytoplasm object was obtained by removing the nucleus object expanded by two pixels from the cell object. The nuclei were tracked across all the frames of the movie. Multiple features of each object were quantified. Dedicated scripts in Matlab R2016b (The Mathworks) were written to further data analysis. Only cells tracked from the beginning to the end of the movie were taken into consideration. In addition, for single cell analysis, a quality control was applied on each trace and only the traces with low variability in nuclear and cell area, CFP nuclear fluorescence, and RFP cellular fluorescence were kept for further analysis.

For each cell, the average nuclear intensity in the fluorescent channel corresponding to the SKARS was divided by the average intensity in the cytoplasm for every time point, in order to generate the single cell trace. The basal level was calculated as the mean of the three first time points of the nuclear-to-cytoplasmic ratio. The nuclear-to-cytoplasmic ratio was normalised by division with the basal level. The final response was calculated as 1 minus the average of the last three time-points of normalised nuclear-to-cytoplasmic ratio. The initial response and

the MAPK response were calculated as 1 minus the average of three time-points shortly after the stimulus (3–5 minutes after α -factor addition). The initial CDK activity was defined as the average of three time-points shortly before the stimulus (3-6 minutes before α -factor stimulus). For the Cdc28_{as} NAPP1 dose response experiment, final MAPK and CDK activities were defined as the average of the time-points after α -factor addition (4-10 minutes after stimulus). All these quantities are unitless numbers, since they are ratios between fluorescence intensities obtained from the microscope camera. We used the symbol [-] to represent this lack of units.

Mathematical model In [chapter 2](#), we used the SimBiology toolbox of Matlab (R2014a) to simulate the model. The details of the reactions implemented and constant rate used are provided in the [Appendix B](#). To extract the MAPK activity based on the experimental nuclear-to-cytoplasmic ratio, an equation representing the MAPK activity as a function of time had to be provided. The parameters of this equation ([table B.3](#)) were then optimised to obtain the best fit of the experimental data. In the [chapter 3](#), simulations of the model was obtained using a Matlab (R2016b) scripts. Details of the procedure for the modelling are in the [Appendix B](#).

Bibliography

- [1] Steven J. Altschuler and Lani F. Wu. Cellular heterogeneity: do differences make a difference? *Cell*, 141(4):559–63, may 2010. [1](#), [1](#)
- [2] Kazuhiro Aoki, Yuka Kumagai, Atsuro Sakurai, Naoki Komatsu, Yoshihisa Fujita, Clara Shionyu, and Michiyuki Matsuda. Stochastic ERK activation induced by noise and cell-to-cell propagation regulates cell density-dependent proliferation. *Molecular cell*, 52(4):529–40, nov 2013. [1](#), [1](#), [1](#), [1](#), [1](#), [1](#), [1](#)
- [3] Delphine Aymoz, Victoria Wosika, Eric Durandau, and Serge Pelet. Real-time quantification of protein expression at the single-cell level via dynamic protein synthesis translocation reporters. *Nature Communications*, 7:11304, 2016. [1](#), [3.2.1](#), [3.3](#), [4](#)
- [4] Gábor Balázsi, Alexander van Oudenaarden, James J. Collins, Alexander van Oudenaarden, and James J. Collins. Cellular Decision Making and Biological Noise: From Microbes to Mammals. *Cell*, 144(6):910–925, mar 2011. [1](#)
- [5] Rodrigo Baltanás, Alan Bush, Alicia Couto, Lucía Durrieu, Stefan Hohmann, and Alejandro Colman-Lerner. Pheromone-induced morphogenesis improves osmoadaptation capacity by activating the HOG MAPK pathway. *Science signaling*, 6(272):ra26, may 2013. [2.1](#)
- [6] L Bardwell. Mechanisms of MAPK signalling specificity. *Biochemical Society transactions*, 34(Pt 5):837–841, nov 2006. [1](#), [1](#), [1](#), [1](#), [1](#), [1](#)

Bibliography

- [7] Lee Bardwell. A walk-through of the yeast mating pheromone response pathway. *Peptides*, 25(9):1465–1476, 2004. [1](#), [2.1](#), [3.1](#), [3.1](#), [3.2.6](#)
- [8] Naama Barkai, Mark D. Rose, and Ned S. Wingreen. Protease helps yeast find mating partners. *Nature*, 396(6710):422–423, 1998. [3.2.2](#), [3.2.3](#)
- [9] James M. Bean, Eric D. Siggia, and Frederick R. Cross. Coherence and timing of cell cycle start examined at single-cell resolution. *Molecular Cell*, 21(1):3–14, 2006. [2.2.3](#), [3.2.1](#), [3.2.1](#)
- [10] Clara Bermejo, Estefanía Rodríguez, Raúl García, Jose M Rodríguez-Peña, María L Rodríguez de la Concepción, Carmen Rivas, Patricia Arias, César Nombela, Francesc Posas, and Javier Arroyo. The sequential activation of the yeast HOG and SLT2 pathways is required for cell survival to cell wall stress. *Molecular biology of the cell*, 19:1113–1124, 2008. [2.1](#), [2.2.5](#)
- [11] Cosetta Bertoli, Jan M Skotheim, and Robertus A M de Bruin. Control of cell cycle transcription during G1 and S phases. *Nature reviews. Molecular cell biology*, 14(8):518–28, 2013. [3.1](#)
- [12] Edouard Bertrand, Pascal Chartrand, Matthias Schaefer, Shailesh M. Shenoy, Robert H. Singer, and Roy M. Long. Localization of ASH1 mRNA Particles in Living Yeast. *Molecular Cell*, 2(4):437–445, 1998. [4](#)
- [13] Samyabrata Bhaduri and Peter M. Pryciak. Cyclin-specific docking motifs promote phosphorylation of yeast signaling proteins by G1/S Cdk complexes. *Current Biology*, 21(19):1615–1623, 2011. [3.2.6](#), [3.2.6](#), [3.2.6](#)
- [14] Samyabrata Bhaduri, Ervin Valk, Matthew J. Winters, Brian Gruessner, Mart Loog, and Peter M. Pryciak. A docking interface in the cyclin Cln2 promotes multi-site phosphorylation of substrates and timely cell-cycle entry. *Current Biology*, 25(3):316–325, 2015. [3.2.6](#)

- [15] Anthony C Bishop, Jeffrey a Ubersax, Dejah T Petsch, Dina P Matheos, Nathanael S Gray, Justin Blethrow, Eiji Shimizu, Joe Z Tsien, Peter G Schultz, Mark D Rose, John L Wood, David O Morgan, and Kevan M Shokat. A chemical switch for inhibitor-sensitive alleles of any protein kinase. *Nature*, 407(6802):395–401, 2000. [2.2.1](#)
- [16] Ashton Breitkreutz and Mike Tyers. MAPK signaling specificity: It takes two to tango. *Trends in Cell Biology*, 12(6):254–257, jun 2002. [1](#), [1](#), [1](#), [1](#)
- [17] J Chenevert, K Corrado, A Bender, J Pringle, and I Herskowitz. A yeast gene (BEM1) necessary for cell polarization whose product contains two SH3 domains. *Nature*, 356(6364):77–79, 1992. [3.3](#)
- [18] Josep Clotet, Joan Vendrell, and Xavier Escoté. Control of the cell cycle progression by the MAPK Hog1. *MAP Kinase*, 2(e3):10–15, 2013. [1](#)
- [19] Patrick Conlon, Rita Gelin-Licht, Ambhighainath Ganesan, Jin Zhang, and Andre Levchenko. Single-cell dynamics and variability of MAPK activity in a yeast differentiation pathway. *Proceedings of the National Academy of Sciences of the United States of America*, 113(40):E5896–E5905, oct 2016. [1](#), [1](#), [3.1](#), [3.2.2](#), [3.2.6](#), [3.3](#)
- [20] J G Cook, L Bardwell, and J Thorner. Inhibitory and activating functions for MAPK Kss1 in the *S. cerevisiae* filamentous-growth signalling pathway. *Nature*, 390(6655):85–88, nov 1997. [1](#)
- [21] Michael Costanzo, Joy L. Nishikawa, Xiaojing Tang, Jonathan S. Millman, Oliver Schub, Kevin Breitkreuz, Danielle Dewar, Ivan Rupes, Brenda Andrews, and Mike Tyers. CDK activity antagonizes Whi5, an inhibitor of G1/S transcription in yeast. *Cell*, 117(7):899–913, 2004. [1](#), [3.2.1](#)
- [22] Frederick R Cross. The Role of Cdc42 in Signal Transduction and Mating *Saccharomyces cerevisiae* *. *The Journal of biological chemistry*, 1:8556–8559, 1998. [3.2.6](#), [3.3](#)

Bibliography

- [23] Robertus A M De Bruin, W. Hayes McDonald, Tatyana I. Kalashnikova, John Yates, and Curt Wittenberg. Cln3 activates G1-specific transcription via phosphorylation of the SBF bound repressor Whi5. *Cell*, 117(7):887–898, 2004. [3.2.1](#)
- [24] a S Dhillon, S Hagan, O Rath, and W Kolch. MAP kinase signalling pathways in cancer. *Oncogene*, 26:3279–3290, 2007. [1](#)
- [25] Stefano Di Talia, Jan M. Skotheim, James M. Bean, Eric D. Siggia, and Frederick R. Cross. The effects of molecular noise and size control on variability in the budding yeast cell cycle. *Nature*, 450(7173):1272–1272, 2007. [3.1](#), [3.2.1](#), [3.2.1](#), [3.3](#)
- [26] Stefano Di Talia, Hongyin Wang, Jan M. Skotheim, Adam P. Rosebrock, Bruce Futcher, and Frederick R. Cross. Daughter-specific transcription factors regulate cell size control in budding yeast. *PLoS Biology*, 7(10):1–19, 2009. [3.1](#), [3.3](#)
- [27] Christian Diener, Gabriele Schreiber, Wolfgang Giese, Gabriel del Rio, Andreas Schröder, and Edda Klipp. Yeast Mating and Image-Based Quantification of Spatial Pattern Formation. *PLoS Computational Biology*, 10(6):1–14, 2014. [3.1](#), [3.2.2](#), [3.2.3](#)
- [28] Andreas Doncic, Oguzhan Atay, Ervin Valk, Alicia Grande, Alan Bush, Gustavo Vasen, Alejandro Colman-Lerner, Mart Loog, and Jan M. M Skotheim. Compartmentalization of a bistable switch enables memory to cross a feedback-driven transition. *Cell*, 160(6):1182–95, mar 2015. [1](#), [3.1](#)
- [29] Andreas Doncic and Jan M. Skotheim. Feedforward Regulation Ensures Stability and Rapid Reversibility of a Cellular State. *Molecular Cell*, 50(6):856–868, 2013. [1](#), [3.1](#)
- [30] Eric Durandau, Delphine Aymoz, and Serge Pelet. Dynamic single cell measurements of kinase activity by synthetic kinase activity relocation sensors. *BMC Biology*, 13(1):55, 2015. [1](#), [1](#), [3.2.1](#), [3.2.1](#)

- [31] Erich Durchschlag, Julia Wolf, Elizabeth L. Brown, Gustav Ammerer, Helmut Ruis, Christoph Schu, Wolfram Görner, Erich Durchschlag, Julia Wolf, Elizabeth L. Brown, Gustav Ammerer, Helmut Ruis, and Christoph Schüller. Acute glucose starvation activates the nuclear localization signal of a stress-specific yeast transcription factor. *EMBO Journal*, 21:135–144, 2002. [2.3](#)
- [32] N P Edgington, M J Blacketer, T a Bierwagen, and a M Myers. Control of *Saccharomyces cerevisiae* filamentous growth by cyclin-dependent kinase Cdc28. *Molecular and cellular biology*, 19(2):1369–1380, 1999. [3.3](#)
- [33] M. B. Elowitz. Stochastic Gene Expression in a Single Cell. *Science*, 297(5584):1183–1186, 2002. [1](#)
- [34] J. G. English, J. P. Shellhammer, M. Malahe, P. C. McCarter, T. C. Elston, and H. G. Dohlman. MAPK feedback encodes a switch and timer for tunable stress adaptation in yeast. *Science Signaling*, 8(359):ra5–ra5, 2015. [2.2.2](#)
- [35] B Errede and Q Y Ge. Feedback regulation of map kinase signal pathways. *Philosophical transactions of the Royal Society of London. Series B, Biological sciences*, 351(1336):143–8; discussion 148–9, 1996. [3.2.6](#)
- [36] J. E. Ferrell Jr. The Biochemical Basis of an All-or-None Cell Fate Switch in *Xenopus* Oocytes. *Science*, 280(5365):895–898, 1998. [1](#), [1](#), [2.1](#)
- [37] Paul Ferrigno, Francesc Posas, Deanna Koepp, Haruo Saito, and Pamela A. Silver. Regulated nucleo-cytoplasmic exchange of HOG1 MAPK requires the importin β homologs NMD5 and XPO1. *EMBO Journal*, 17(19):5606–5614, 1998. [1](#), [1](#)
- [38] Matthew Fosbrink, Nwe-Nwe Aye-Han, Raymond Cheong, Andre Levchenko, and Jin Zhang. Visualization of JNK activity dynamics with a genetically encoded fluorescent biosensor. *Proceedings of the National Academy of Sciences of the United States of America*, 107(12):5459–5464, mar 2010. [1](#), [2.3](#)

Bibliography

- [39] Rafael D Fritz, Michel Letzelter, Andreas Reimann, Katrin Martin, Ludovico Fusco, Laila Ritsma, Bas Ponsioen, Erika Fluri, Stefan Schulte-Merker, Jacco van Rheenen, and Olivier Pertz. A versatile toolkit to produce sensitive FRET biosensors to visualize signaling in time and space. *Science signaling*, 6(285):rs12, jul 2013. [1](#), [2.3](#)
- [40] Alan L. Goldstein and John H. McCusker. Three new dominant drug resistance cassettes for gene disruption in *Saccharomyces cerevisiae* - Goldstein - 1999 - *Yeast* - Wiley Online Library. *Yeast (Chichester, England)*, 15(14):1541–1553, 1999. [5](#)
- [41] Mercè Gomar-Alba, Paula Alepuz, and Marcellí Del Olmo. Dissection of the elements of osmotic stress response transcription factor Hot1 involved in the interaction with MAPK Hog1 and in the activation of transcription. *Biochimica et Biophysica Acta - Gene Regulatory Mechanisms*, 1829(10):1111–1125, 2013. [1](#)
- [42] Alberto González-Novo, Javier Jiménez, Josep Clotet, Mariona Nadal-Ribelles, Santiago Cavero, Eulàlia de Nadal, and Francesc Posas. Hog1 Targets Whi5 and Msa1 Transcription Factors To Downregulate Cyclin Expression upon Stress. *Molecular and Cellular Biology*, 35(9):1606–1618, may 2015. [1](#)
- [43] Matthew Good, Grace Tang, Julie Singleton, Attila Reményi, and Wendell a. Lim. The Ste5 Scaffold Directs Mating Signaling by Catalytically Unlocking the Fus3 MAP Kinase for Activation. *Cell*, 136(6):1085–1097, 2009. [1](#), [3.2.2](#)
- [44] M C Gustin, J Albertyn, M Alexander, and K Davenport. MAP kinase pathways in the yeast *Saccharomyces cerevisiae*. *Microbiology and molecular biology reviews : MMBR*, 62(4):1264–1300, nov 1998. [1](#), [3.1](#)
- [45] J P Hall, V Cherkasova, E Elion, M C Gustin, and E Winter. The osmoregulatory pathway represses mating pathway activity in *Saccharomyces cerevisiae*: isolation of a FUS3 mutant that is insensitive to the repression mechanism. *Molecular and cellular biology*, 16(12):6715–6723, 1996. [1](#)

- [46] Nan Hao, Sujata Nayak, Marcelo Behar, Ryan H. Shanks, Michal J. Nagiec, Beverly Errede, Jeffrey Hasty, Timothy C. Elston, and Henrik G. Dohlman. Regulation of Cell Signaling Dynamics by the Protein Kinase-Scaffold Ste5. *Molecular Cell*, 30(5):649–656, jun 2008. [3.2.3](#)
- [47] Nan Hao, Necmettin Yildirim, Michal J. Nagiec, Stephen C. Parnell, Beverly Errede, Henrik G. Dohlman, and Timothy C. Elston. Combined computational and experimental analysis reveals mitogen-activated protein kinase-mediated feedback phosphorylation as a mechanism for signaling specificity. *Molecular Biology of the Cell*, 23(19):3899–910, oct 2012. [2.2.4](#)
- [48] Nan Hao, Necmettin Yildirim, Yuqi Wang, Timothy C. Elston, and Henrik G. Dohlman. Regulators of G protein signaling and transient activation of signaling: Experimental and computational analysis reveals negative and positive feedback controls on G protein activity. *Journal of Biological Chemistry*, 278(47):46506–46515, 2003. [3.2.3](#)
- [49] Michelle T. Harreman, Trisha M. Kline, Heidi G. Milford, M. Beth Harben, Alec E. Hodel, and Anita H. Corbett. Regulation of nuclear import by phosphorylation adjacent to nuclear localization signals. *Journal of Biological Chemistry*, 279(20):20613–20621, may 2004. [2.2.1](#)
- [50] L H Hartwell. *Saccharomyces cerevisiae* cell cycle. *Bacteriological reviews*, 38(2):164–198, 1974. [3.2.2](#), [3.2.3](#), [3.3](#)
- [51] Christopher D Harvey, Anka G Ehrhardt, Cristina Cellurale, Haining Zhong, Ryohei Yasuda, Roger J Davis, and Karel Svoboda. A genetically encoded fluorescent sensor of ERK activity. *Proceedings of the National Academy of Sciences of the United States of America*, 105(49):19264–19269, 2008. [1](#)
- [52] Stacy L Harvey, Germán Enciso, Noah Dephoure, Steven P Gygi, Jeremy Gunawardena, and Douglas R Kellogg. A phosphatase threshold sets the level of Cdk1 activity in early mitosis in budding yeast. *Molecular biology of the cell*, 22(19):3595–3608, 2011. [3.3](#)

Bibliography

- [53] Sandra Henchoz, Yong Chi, Barbara Catarin, Ira Herskowitz, Raymond J. Deshaies, and Matthias Peter. Phosphorylation- and ubiquitin-dependent degradation of the cyclin-dependent kinase inhibitor Far1p in budding yeast. *Genes and Development*, 11(22):3046–3060, 1997. [1](#), [3.1](#), [3.2.2](#), [3.3](#)
- [54] Jillian H Hurst and Henrik G Dohlman. Dynamic ubiquitination of the mitogen-activated protein kinase kinase (MAPKK) Ste7 determines mitogen-activated protein kinase (MAPK) specificity. *The Journal of biological chemistry*, 288(26):18660–71, jun 2013. [1](#), [3.2.2](#)
- [55] C. Inouye, N Dhillon, and J Thorner. Ste5 RING-H2 Domain: Role in Ste4-Promoted Oligomerization for Yeast Pheromone Signaling. *Science*, 278(5335):103–6, 1997. [3.1](#)
- [56] G. Jansen, F. Bühring, C. P. Hollenberg, and M. Ramezani Rad. Mutations in the SAM domain of STE50 differentially influence the MAPK-mediated pathways for mating, filamentous growth and osmotolerance in *Saccharomyces cerevisiae*. *Molecular genetics and genomics : MGG*, 265(1):102–117, mar 2001. [2.2.1](#), [3.3](#)
- [57] María Jiménez-Sánchez, Víctor J. Cid, and María Molina. Retrophosphorylation of Mkk1 and Mkk2 MAPKKs by the Slt2 MAPK in the yeast cell integrity pathway. *Journal of Biological Chemistry*, 282(43):31174–31185, oct 2007. [2.2.5](#)
- [58] Meng Jin, Beverly Errede, Marcelo Behar, Will Mather, Sujata Nayak, Jeff Hasty, Henrik G Dohlman, and Timothy C Elston. Yeast dynamically modify their environment to achieve better mating efficiency. *Science signaling*, 4(186):ra54, aug 2011. [3.2.3](#)
- [59] a Kaffman and E K O’Shea. Regulation of nuclear localization: a key to a door. *Annual review of cell and developmental biology*, 15:291–339, 1999. [2.3](#)
- [60] Yoshihiro Katsura, Hiroyuki Kubota, Katsuyuki Kunida, Akira Kanno, Shinya Kuroda, and Takeaki Ozawa. An optogenetic system for interrogating the temporal dynamics of Akt. *Scientific Reports*, 5:14589, 2015. [4](#)

- [61] C M Koehler and A M Myers. Serine-threonine protein kinase activity of Elm1p, a regulator of morphologic differentiation in *Saccharomyces cerevisiae*. *FEBS letters*, 408(1):109–114, 1997. [3.3](#)
- [62] N. Komatsu, K. Aoki, M. Yamada, H. Yukinaga, Y. Fujita, Y. Kamioka, and M. Matsuda. Development of an optimized backbone of FRET biosensors for kinases and GTPases. *Molecular Biology of the Cell*, 22(23):4647–4656, dec 2011. [1](#), [1](#), [2.3](#)
- [63] Alexei Kurakin. Stochastic Cell. *IUBMB Life (International Union of Biochemistry and Molecular Biology: Life)*, 57(2):59–63, 2005. [1](#)
- [64] R. E. Lamson, M. J. Winters, and P. M. Pryciak. Cdc42 Regulation of Kinase Activity and Signaling by the Yeast p21-Activated Kinase Ste20. *Molecular and Cellular Biology*, 22(9):2939–2951, may 2002. [3.2.6](#)
- [65] Daniel R. Larson, Daniel Zenklusen, Bin Wu, Jeffrey A. Chao, and Robert H. Singer. Real-time observation of transcription initiation and elongation on an endogenous yeast gene. *Science*, 332(6028):475–478, 2011. [4](#)
- [66] Ekkehard Leberer, Cunle Wu, Thomas Leeuw, Anne Fourest-Lieuvin, Jeffrey E. Segall, and David Y. Thomas. Functional characterization of the Cdc42p binding domain of yeast Ste20p protein kinase. *EMBO Journal*, 16(1):83–97, jan 1997. [3.2.6](#)
- [67] Thomas Leeuw, Cunle Wu, Joseph D Schrag, Malcolm Whiteway, and David Y Thomas. Interaction of a G-protein beta-subunit with a conserved sequence in Ste20/PAK family protein kinases. *Nature*, 4:191–195, 1998. [3.1](#)
- [68] David E Levin. Cell Wall Integrity Signaling in *Saccharomyces cerevisiae* Cell Wall Integrity Signaling in *Saccharomyces cerevisiae*. *Microbiol Mol Biol Rev*, 69(2):262–291, 2005. [2.1](#)
- [69] Daniel J. Lew and Steven I. Reed. Cell cycle control of morphogenesis in budding yeast. *Current Opinion in Genetics and Development*, 5(1):17–23, 1995. [3.3](#)

Bibliography

- [70] Mark S. Longtine, Amos McKenzie, Douglas J. Demarini, Nirav G. Shah, Achim Wach, Arndt Brachat, Peter Philippsen, and John R. Pringle. Additional modules for versatile and economical PCR-based gene deletion and modification in *Saccharomyces cerevisiae*. *Yeast*, 14(10):953–961, 1998. [5](#)
- [71] Javier Macia, Sergi Regot, Tom Peeters, Núria Conde, Ricard Solé, and Francesc Posas. Dynamic signaling in the Hog1 MAPK pathway relies on high basal signal transduction. *Science signaling*, 2(63):ra13, jan 2009. [2.2.2](#), [2.2.3](#), [A.2](#)
- [72] J. D. McKinney, F. Chang, N. Heintz, and F. Cross. Negative regulation of FAR1 at the start of the yeast cell cycle. *Genes and Development*, 7(5):833–843, may 1993. [1](#), [3.1](#), [3.1](#), [3.2.1](#), [3.2.2](#), [3.3](#)
- [73] Laura Merlini, Omayya Dudin, and Sophie G Martin. Mate and fuse: how yeast cells do it. *Open biology*, 3(3):130008, 2013. [3.1](#)
- [74] Jerome T Mettetal, Dale Muzzey, Carlos Gómez-Uribe, and Alexander van Oudenaarden. The frequency dependence of osmo-adaptation in *Saccharomyces cerevisiae*. *Science (New York, N.Y.)*, 319(5862):482–484, 2008. [1](#), [1](#)
- [75] Dale Muzzey, Carlos a. Gómez-Uribe, Jerome T. Mettetal, and Alexander van Oudenaarden. A Systems-Level Analysis of Perfect Adaptation in Yeast Osmoregulation. *Cell*, 138(1):160–171, jul 2009. [1](#), [1](#)
- [76] Michal J. Nagiec and Henrik G. Dohlman. Checkpoints in a yeast differentiation pathway coordinate signaling during hyperosmotic stress. *PLoS Genetics*, 8(1):e1002437, jan 2012. [3.3](#)
- [77] Michal J Nagiec, Patrick C McCarter, Joshua B Kelley, Gauri Dixit, Timothy C Elston, and Henrik G Dohlman. Signal inhibition by a dynamically regulated pool of monophosphorylated MAPK. *Molecular biology of the cell*, 26(18):3359–71, 2015. [1](#), [3.2.2](#), [3.2.3](#), [3.2.3](#)

- [78] John R. S. Newman, Sina Ghaemmaghami, Jan Ihmels, David K. Breslow, Matthew Noble, Joseph L. DeRisi, and Jonathan S. Weissman. Single-cell proteomic analysis of *S. cerevisiae* reveals the architecture of biological noise. *Nature*, 441(7095):840–846, 2006. [1](#)
- [79] Qiang Ni, Denis V. Titov, and Jin Zhang. Analyzing protein kinase dynamics in living cells with FRET reporters. *Methods*, 40(3):279–286, 2006. [2.3](#)
- [80] L J Oehlen, J D McKinney, and F R Cross. Ste12 and Mcm1 regulate cell cycle-dependent transcription of FAR1. *Molecular and cellular biology*, 16(6):2830–2837, 1996. [1](#), [1](#), [3.2.1](#), [3.3](#)
- [81] Lambertus J W M Oehlen and Frederick R. Cross. G1 cyclins CLN1 and CLN2 repress the mating factor response pathway at start in the yeast cell cycle. *Genes and Development*, 8(9):1058–1070, 1994. [1](#), [1](#), [1](#), [2.2.3](#), [3.2.2](#), [3.2.2](#), [3.2.2](#), [3.2.3](#), [3.2.4](#), [3.3](#)
- [82] Sean M. O’Rourke and Ira Herskowitz. The Hog1 MAPK prevents cross talk between the HOG and pheromone response MAPK pathways in *Saccharomyces cerevisiae*. *Genes and Development*, 12:2874–2886, 1998. [1](#)
- [83] Saurabh Paliwal, Pablo A. Iglesias, Kyle Campbell, Zoe Hilioti, Alex Groisman, and Andre Levchenko. MAPK-mediated bimodal gene expression and adaptive gradient sensing in yeast. *Nature*, 446(7131):46–51, mar 2007. [1](#), [1](#), [2.1](#)
- [84] Jesse C Patterson, Evguenia S Klimenko, and Jeremy Thorner. Single-cell analysis reveals that insulation maintains signaling specificity between two yeast MAPK pathways with common components. *Science signaling*, 3(144):ra75, jan 2010. [1](#)
- [85] Serge Pelet, Reinhard Dechant, Sung Sik Lee, Frank van Drogen, and Matthias Peter. An integrated image analysis platform to quantify signal transduction in single cells. *Integrative Biology*, 4(10):1274, oct 2012. [1](#), [2.2.1](#), [3.3](#), [3.2.1](#), [5](#)

Bibliography

- [86] Serge Pelet, Fabian Rudolf, Mariona Nadal-Ribelles, Eulàlia de Nadal, Francesc Posas, and Matthias Peter. Transient activation of the HOG MAPK pathway regulates bimodal gene expression. *Science (New York, N.Y.)*, 332(6030):732–735, may 2011. [1](#), [1](#), [1](#), [2.2.1](#), [3.2.1](#), [A.2](#)
- [87] M Peter and I Herskowitz. Direct inhibition of the yeast cyclin-dependent kinase Cdc28-Cln by Far1. *Science (New York, N.Y.)*, 265(5176):1228–1231, aug 1994. [1](#), [3.1](#), [3.1](#), [3.2.2](#)
- [88] Matthias Peter, Anton Gartner, Joe Horecka, Gustav Ammerer, and Ira Herskowitz. FAR1 links the signal transduction pathway to the cell cycle machinery in yeast. *Cell*, 73(4):747–760, 1993. [3.1](#), [3.2.4](#)
- [89] Alexander Plotnikov, Eldar Zehorai, Shiri Procaccia, and Rony Seger. The MAPK cascades: signaling components, nuclear roles and mechanisms of nuclear translocation. *Biochimica et biophysica acta*, 1813(9):1619–33, sep 2011. [1](#), [1](#), [3.1](#)
- [90] P. A. Pope and P. M. Pryciak. Functional overlap among distinct G1/S inhibitory pathways allows robust G1 arrest by yeast mating pheromones. *Molecular Biology of the Cell*, 24(23):3675–3688, dec 2013. [3.2.6](#)
- [91] Patricia A. Pope, Samyabrata Bhaduri, and Peter M. Pryciak. Regulation of cyclin-substrate docking by a G1 arrest signaling pathway and the Cdk inhibitor far1. *Current Biology*, 24(12):1390–1396, 2014. [1](#), [3.1](#), [3.2.2](#), [3.2.4](#), [3.22](#), [3.2.6](#)
- [92] Tata Pramila, Shawna Miles, Debraj Guhathakurta, Dave Jemiolo, and Linda L Breeden. Conserved homeodomain proteins interact with MADS box protein Mcm1 to restrict ECB-dependent transcription to the M / G1 phase of the cell cycle. *Genes & development*, 16:3034–3045, 2002. [2.2.3](#)
- [93] Peter M. Pryciak and Frederick A. Huntress. Membrane recruitment of the kinase cascade scaffold protein Ste5 by the $G\beta\gamma$ complex underlies activation of the yeast pheromone response pathway. *Genes and Development*, 12(17):2684–2697, 1998. [1](#), [3.1](#), [3.2.6](#), [3.3](#)

- [94] J. E. Purvis, K. W. Karhohs, C. Mock, E. Batchelor, A. Loewer, and G. Lahav. p53 Dynamics Control Cell Fate. *Science*, 336(6087):1440–1444, 2012. [2.1](#)
- [95] Jeremy E. Purvis and Galit Lahav. Encoding and decoding cellular information through signaling dynamics. *Cell*, 152(5):945–956, feb 2013. [1](#), [1](#)
- [96] Maosong Qi and Elaine a Elion. MAP kinase pathways. *Journal of cell science*, 118(Pt 16):3569–3572, aug 2005. [1](#), [2.1](#), [3.1](#)
- [97] Ethel Queralt and Frank Uhlmann. Cdk-counteracting phosphatases unlock mitotic exit. *Current Opinion in Cell Biology*, 20(6):661–668, 2008. [3.3](#)
- [98] J. M. Raser. Control of Stochasticity in Eukaryotic Gene Expression. *Science*, 304(5678):1811–1814, 2004. [1](#)
- [99] Sergi Regot, Jacob J. Hughey, Bryce T. Bajar, Silvia Carrasco, and Markus W. Covert. High-sensitivity measurements of multiple kinase activities in live single cells. *Cell*, 157(7):1724–1734, jun 2014. [2.3](#), [4](#), [4](#)
- [100] Brian J. Reid and Leland H. Hartwell. Regulation of mating in the cell cycle of *Saccharomyces Cerevisiae*. *Journal of Cell Biology*, 75(2):355–365, 1977. [3.2.4](#)
- [101] Attila Reményi, Matthew C. Good, Roby P. Bhattacharyya, and Wendell a. Lim. The role of docking interactions in mediating signaling input, output, and discrimination in the yeast MAPK network. *Molecular Cell*, 20(6):951–962, dec 2005. [1](#), [2.2.1](#), [2.2.1](#), [2.2.4](#), [3.2.4](#)
- [102] Marketa Ricicova, Mani Hamidi, Adam Quiring, A. Niemisto, Eldon Emberly, and Carl L Hansen. Dissecting genealogy and cell cycle as sources of cell-to-cell variability in MAPK signaling using high-throughput lineage tracking. *Proceedings of the National Academy of Sciences*, 110(28):11403–11408, jul 2013. [1](#), [3.3](#)
- [103] C J Roberts, B Nelson, M J Marton, R Stoughton, M R Meyer, H a Bennett, Y D He, H Dai, W L Walker, T R Hughes, M Tyers, C Boone, and S H Friend. Signaling and circuitry of

Bibliography

- multiple MAPK pathways revealed by a matrix of global gene expression profiles. *Science (New York, N.Y.)*, 287(5454):873–880, feb 2000. [1](#), [1](#), [3.1](#)
- [104] Jose Manuel Rodríguez-Peña, Raúl García, César Nombela, and Javier Arroyo. The high-osmolarity glycerol (HOG) and cell wall integrity (CWI) signalling pathways interplay: a yeast dialogue between MAPK routes. *Yeast (Chichester, England)*, 27(8):495–502, aug 2010. [1](#)
- [105] Hyunryul Ryu, Minhwan Chung, Maciej Dobrzyński, Dirk Fey, Yannick Blum, Sung Sik Lee, Matthias Peter, Boris N Kholodenko, Noo Li Jeon, and Olivier Pertz. Frequency modulation of ERK activation dynamics rewires cell fate. *Molecular systems biology*, 11(11):838, 2015. [1](#)
- [106] Walid Sabbagh, Laura J. Flatauer, A. Jane Bardwell, and Lee Bardwell. Specificity of MAP kinase signaling in yeast differentiation involves transient versus sustained MAPK activation. *Molecular Cell*, 8(3):683–691, 2001. [3.1](#)
- [107] Rupam Sahoo, Amjad Husain, and Elaine A. Elion. MAP kinase in yeast. In *Handbook of Cell Signaling*, 2/e, volume 2, chapter 163, pages 1303–1314. Elsevier Inc., 2010. [1](#), [1](#), [1](#), [1](#), [1](#), [2.1](#), [3.1](#), [3.1](#)
- [108] Haruo Saito. Regulation of cross-talk in yeast MAPK signaling pathways. *Current Opinion in Microbiology*, 13(6):677–683, dec 2010. [1](#), [1](#), [1](#), [1](#), [1](#), [1](#), [1](#), [2.1](#)
- [109] Monica A. Schwartz and Hiten D. Madhani. Principles of MAP Kinase Signaling Specificity in *Saccharomyces cerevisiae*. *Annual Review of Genetics*, 38(1):725–748, 2004. [1](#), [1](#), [1](#), [1](#)
- [110] Nathan C Shaner, Paul a Steinbach, and Roger Y Tsien. A guide to choosing fluorescent proteins. *Nature methods*, 2(12):905–909, 2005. [2.3](#)
- [111] Mark A Sheff and Kurt S Thorn. Optimized cassettes for fluorescent protein tagging in *Saccharomyces cerevisiae*. *Yeast (Chichester, England)*, 21(8):661–70, jun 2004. [5](#)

- [112] Teresa R. Shock, James Thompson, John R. Yates, and Hiten D. Madhani. Hog1 mitogen-activated protein kinase (MAPK) interrupts signal transduction between the Kss1 MAPK and the Tec1 transcription factor to maintain pathway specificity. *Eukaryotic Cell*, 8(4):606–616, apr 2009. [1](#)
- [113] R. S. Sikorski and P. Hieter. A system of shuttle vectors and yeast host strains designed for efficient manipulation of DNA in *Saccharomyces cerevisiae*. *Genetics*, 122(1 979):19–27, apr 1989. [5](#)
- [114] Berend Snijder and Lucas Pelkmans. Origins of regulated cell-to-cell variability. *Nature Reviews Molecular Cell Biology*, 12(2):119–125, 2011. [1](#), [1](#)
- [115] Sabrina L. Spencer, Steven D. Cappell, Feng Chiao Tsai, K. Wesley Overton, Clifford L. Wang, and Tobias Meyer. XThe proliferation-quiescence decision is controlled by a bifurcation in CDK2 activity at mitotic exit. *Cell*, 155(2):369–383, 2013. [2.3](#)
- [116] Shelly C. Strickfaden, Matthew J. Winters, Giora Ben-Ari, Rachel E. Lamson, Mike Tyers, and Peter M Pryciak. A Mechanism for Cell-Cycle Regulation of MAP Kinase Signaling in a Yeast Differentiation Pathway. *Cell*, 128(3):519–531, feb 2007. [1](#), [1](#), [2.2.3](#), [2.4](#), [3.1](#), [3.1](#), [3.2.4](#), [3.2.6](#), [3.2.6](#), [3.2.6](#), [3.3](#), [4](#)
- [117] Nico Stuurman, Arthur D Edelstein, Nenad Amodaj, Karl H Hoover, and D Ronald. Computer Control of Microscopes using μ Manager. pages 1–22, 2011. [5](#)
- [118] Xiao-xiao Sun and Qiang Yu. Intra-tumor heterogeneity of cancer cells and its implications for cancer treatment. *Acta Pharmacologica Sinica*, 36(10):1219–1227, 2015. [1](#), [1](#)
- [119] Satoe Takahashi and Peter M. Pryciak. Membrane Localization of Scaffold Proteins Promotes Graded Signaling in the Yeast MAP Kinase Cascade. *Current Biology*, 18(16):1184–91, aug 2008. [3.2.6](#), [3.3](#)

Bibliography

- [120] T Tanoue, M Adachi, T Moriguchi, and E Nishida. A conserved docking motif in MAP kinases common to substrates, activators and regulators. *Nature cell biology*, 2(2):110–116, 2000. [2.2.1](#)
- [121] Takuji Tanoue and Eisuke Nishida. Molecular recognitions in the MAP kinase cascades. *Cellular Signalling*, 15(5):455–462, may 2003. [2.2.1](#)
- [122] Kenneth Evan Thompson, Caleb J. Bashor, Wendell a. Lim, and Amy E. Keating. Synzip protein interaction toolbox: In vitro and in vivo specifications of heterospecific coiled-coil interaction domains. *ACS Synthetic Biology*, 1(4):118–129, apr 2012. [4](#)
- [123] Benjamin L. Timney, Jaclyn Tetenbaum-Novatt, Diana S. Agate, Rosemary Williams, Wenzhu Zhang, Brian T. Chait, and Michael P. Rout. Simple kinetic relationships and nonspecific competition govern nuclear import rates in vivo. *Journal of Cell Biology*, 175(4):579–593, 2006. [B](#)
- [124] T. Tomida, M. Takekawa, P. O’Grady, and H. Saito. Stimulus-Specific Distinctions in Spatial and Temporal Dynamics of Stress-Activated Protein Kinase Kinase Kinases Revealed by a Fluorescence Resonance Energy Transfer Biosensor. *Molecular and Cellular Biology*, 29(22):6117–6127, 2009. [1](#), [1](#), [2.1](#), [2.3](#)
- [125] Matthew P. Torres, Sarah T. Clement, Steven D. Cappell, and Henrik G. Dohlman. Cell cycle-dependent phosphorylation and ubiquitination of a G protein α subunit. *Journal of Biological Chemistry*, 286(23):20208–20216, 2011. [3.3](#)
- [126] Q Wang, J Niemi, C Tan, L You, and M West. Image segmentation and dynamic lineage analysis in single cell fluorescence microscopy. *Cytometry A*, 77a(1):101–110, 2010. [3.3](#)
- [127] Yuqi Wang and Henrik G Dohlman. Pheromone-dependent ubiquitination of the mitogen-activated protein kinase kinase Ste7. *The Journal of biological chemistry*, 277(18):15766–72, may 2002. [3.2.3](#), [3.2.6](#)

- [128] Yuqi Wang and Henrik G Dohlman. Pheromone signaling mechanisms in yeast: a prototypical sex machine. *Science (New York, N.Y.)*, 306(November):1508–1509, 2004. [3.1](#), [3.1](#)
- [129] Katja Wassmann and Gustav Ammerer. Overexpression of the G1-cyclin gene CLN2 represses the mating pathway in *Saccharomyces cerevisiae* at the level of the MEKK Ste11. *Journal of Biological Chemistry*, 272(20):13180–13188, may 1997. [1](#), [1](#), [1](#), [3.1](#), [3.2.2](#), [3.2.2](#), [3.2.4](#), [3.2.6](#)
- [130] Christian Widmann, Spencer Gibson, Matthew B Jarpe, and Gary L Johnson. Mitogen-Activated Protein Kinase: Conservation of a Three-Kinase Module From Yeast to Human. *Physiol Rev*, 79(1):143–180, 1999. [1](#), [1](#)
- [131] Matthew J. Winters, Rachel E. Lamson, Hideki Nakanishi, Aaron M. Neiman, and Peter M. Pryciak. A membrane binding domain in the Ste5 scaffold synergizes with G β γ binding to control localization and signaling in pheromone response. *Molecular Cell*, 20(1):21–32, 2005. [3.1](#), [3.2.6](#), [3.2.6](#)
- [132] Victoria Wosika, Eric Durandau, Clémence Varidel, Delphine Aymoz, Marta Schmitt, and Serge Pelet. New families of single integration vectors and gene tagging plasmids for genetic manipulations in budding yeast. *Molecular Genetics and Genomics*, 291(6):2231–2240, 2016. [5](#), [5](#), [A](#)
- [133] Victoria Wosika and Serge Pelet. Relocation sensors to quantify signaling dynamics in live single cells. [1](#)
- [134] Katsuyoshi Yamamoto, Kazuo Tatebayashi, Keiichiro Tanaka, and Haruo Saito. Dynamic control of yeast MAP kinase network by induced association and dissociation between the ste50 scaffold and the Opy2 membrane anchor. *Molecular Cell*, 40(1):87–98, oct 2010. [3.3](#)
- [135] S H Yang, a Galanis, and a D Sharrocks. Targeting of p38 mitogen-activated protein kinases to MEF2 transcription factors. *Mol Cell Biol*, 19(6):4028–4038, 1999. [2.2.1](#)

Bibliography

- [136] Richard C Yu, C Gustavo Pesce, Alejandro Colman-Lerner, Larry Lok, David Pincus, Eduard Serra, Mark Holl, Kirsten Benjamin, Andrew Gordon, and Roger Brent. Negative feedback that improves information transmission in yeast signalling. *Nature*, 456(7223):755–761, dec 2008. [1](#), [3.2.2](#), [3.2.3](#), [3.2.3](#)
- [137] P Zarzov, C Mazzoni, and C Mann. The SLT2(MPK1) MAP kinase is activated during periods of polarized cell growth in yeast. *The EMBO journal*, 15(1):83–91, jan 1996. [2.2.5](#), [2.2.6](#)
- [138] Xin X. Zhou, Linlin Z. Fan, Pengpeng Li, Kang Shen, and Michael Z. Lin. Optical control of cell signaling by single-chain photoswitchable kinases. *Science*, 355(6327):836–842, 2017. [4](#), [4](#)

A. Strains and plasmids

A. Strains and plasmids

Table A.1.: Table of strains

Name	Genotype	Figure
ySP2	<i>W303: MATa leu2-3, 112 trp1-1 can1-100 ura3-1 ade2-1 HIS3-11,15</i>	
yED42	<i>HTA2-CFP ura3:pED45</i>	
yED54	<i>HTA2-CFP ura3:pED45 ste11Δ::NAT</i>	
yED53	<i>HTA2-CFP ura3:pED55</i>	
yED51	<i>HTA2-CFP ura3:pED53</i>	
yED52	<i>HTA2-CFP ura3:pED54</i>	
ySP456	<i>HTA2-CFP ura3:pED45 leu2:pED198 kss1Δ::KAN fus3Δ::NAT</i>	
ySP603	<i>HTA2-CFP ura3:pED45 WHI5-mCitrine:HIS3</i>	
ySP568	<i>HTA2-CFP ura3:pED45 trp1:pED73</i>	
ySP591	<i>HTA2-CFP ura3:pED45 YOX1-mCitrine:HIS3</i>	
ySP570	<i>HTA2-CFP ura3:pSP303 trp1:pED73 fus3Δ::NAT</i>	
ySP571	<i>HTA2-CFP ura3:pSP303 trp1:pED73 kss1Δ::NAT</i>	
ySP572	<i>HTA2-CFP ura3:pSP303 trp1:pED73 kss1Δ::KAN fus3Δ::NAT</i>	
ySP569	<i>HTA2-CFP ura3:pSP303 trp1:pED73</i>	
ySP560	<i>HTA2-CFP ura3:pSP323</i>	
yED92	<i>HTA2-CFP ura3:pSP323 ste11Δ::NAT</i>	

yED87	<i>HTA2-CFP ura3:pSP323 bck1Δ::NAT</i>
ySP37	<i>HTA2-CFP</i>
yED55	<i>HTA2-CFP ura3:pED45 leu2:P_{FIG1}-qVenus</i>
yED56	<i>HTA2-CFP ura3:pED55 leu2:P_{FIG1}-qVenus</i>
yED57	<i>HTA2-CFP leu2:P_{FIG1}-qVenus</i>
yED91	<i>HTA2-CFP ura3:pED55 trp1:pED73</i>
ySP492	<i>HTA2-CFP ura3:pSP306</i>
yED67	<i>HTA2-CFP ura3:pSP306 bck1Δ::NAT</i>
ySP558	<i>HTA2-CFP ura3:pSP321</i>
ySP559	<i>HTA2-CFP ura3:pSP322</i>
ySP556	<i>HTA2-CFP ura3:pSP319</i>
ySP596	<i>HTA2-CFP ura3:pSP323 WHI5-mCitrine:HIS3</i>
ySP594	<i>HTA2-CFP ura3:pSP323 YOX1-mCitrine:HIS3</i>
ySP300	<i>cdc28_{as}</i>
yED136	<i>HTA2-iRFP-HIS</i>
yED152	<i>HTA2-iRFP-HIS ura3:pED92</i>
yED164	<i>HTA2-iRFP-HIS ura3:pED92 leu2:pED94</i>
yED195	<i>cdc28_{as} HTA2-iRFP-HIS</i>
yED238	<i>HTA2-iRFP-HIS ura3:pED92 leu2:pED94</i> <i>WHI5-mCitrine:TRP</i>

A. Strains and plasmids

yED253	<i>HTA2-iRFP-KAN ura3:pED92 leu2:pED94</i> <i>WHI5-mCitrine:TRP ste5Δ::pED137</i>
yED254	<i>HTA2-iRFP-KAN ura3:pED92 leu2:pED94</i> <i>WHI5-mCitrine:TRP ste5Δ::pED138</i>
yED255	<i>HTA2-iRFP-HIS ura3:pED92 leu2:pED94</i> <i>WHI5-mCitrine:TRP bar1Δ::NAT</i>
yED258	<i>HTA2-iRFP-KAN ura3:pED92 leu2:pED94</i> <i>WHI5-mCitrine:TRP</i>
yED264	<i>HTA2-iRFP-KAN ura3:pED92 leu2:pED94</i> <i>WHI5-mCitrine:TRP ste5Δ::NAT</i>
yED275	<i>cdc28_{as} HTA2-iRFP-HIS WHI5-mCitrine:TRP</i>
yED281	<i>cdc28_{as} HTA2-iRFP-HIS ura3:pED141</i> <i>WHI5-mCitrine:TRP</i>
yED284	<i>HTA2-iRFP-KAN ura3:pED92 leu2:pED94</i> <i>WHI5-mCitrine:TRP ste5Δ::pED137 bar1Δ::NAT</i>
yED285	<i>HTA2-iRFP-KAN ura3:pED92 leu2:pED94</i> <i>WHI5-mCitrine:TRP ste5Δ::pED138 bar1Δ::NAT</i>
yED288	<i>cdc28_{as} HTA2-iRFP-HIS ura3:pED141</i> <i>WHI5-mCitrine:TRP bar1Δ::NAT</i>
yED289	<i>HTA2-iRFP-KAN ura3:pED92 leu2:pED94</i> <i>WHI5-mCitrine:TRP ste5Δ::pED147</i>
yED299	<i>HTA2-iRFP-HIS ura3:pED92 leu2:pED94</i> <i>WHI5-mCitrine:TRP bar1Δ::NAT far1Δ::KAN</i>

yED300	<i>HTA2-iRFP-KAN ura3:pED92 leu2:pED94</i> <i>WHI5-mCitrine:TRP ste5Δ::pED147 bar1Δ::NAT</i>
yED306	<i>HTA2-iRFP-KAN ura3:pED92 leu2:pED94</i> <i>WHI5-mCitrine:TRP ste5Δ::pED147 ste20Δ::NAT</i>
yED307	<i>HTA2-iRFP-KAN ura3:pED92 leu2:pED94</i> <i>WHI5-mCitrine:TRP ste5Δ::pED147 ste7Δ::NAT</i>
yED310	<i>HTA2-iRFP-KAN ura3:pED92 leu2:pED94</i> <i>WHI5-mCitrine:TRP ste5Δ::pED147</i> <i>ste20Δ::pED159</i>
yED311	<i>HTA2-iRFP-KAN ura3:pED92 leu2:pED94</i> <i>WHI5-mCitrine:TRP ste5Δ::pED147</i> <i>ste20Δ::pED160</i>
yED312	<i>HTA2-iRFP-KAN ura3:pED92 leu2:pED94</i> <i>WHI5-mCitrine:TRP ste5Δ::pED147</i> <i>ste20Δ::pED161</i>
yED313	<i>HTA2-iRFP-KAN ura3:pED92 leu2:pED94</i> <i>WHI5-mCitrine:TRP ste5Δ::pED147</i> <i>ste7Δ::pED162</i>
yED314	<i>HTA2-iRFP-KAN ura3:pED92 leu2:pED94</i> <i>WHI5-mCitrine:TRP ste5Δ::pED147</i> <i>ste7Δ::pED163</i>
yED316	<i>cdc28_{as} HTA2-iRFP-HIS ura3:pED141</i> <i>WHI5-mCitrine:TRP ste5Δ::NAT</i>

A. Strains and plasmids

yED321	<i>cdc28_{as} HTA2-iRFP-HIS ura3::pED141</i> <i>WHI5-mCitrine:TRP ste5Δ::pED164</i>
yED324	<i>cdc28_{as} HTA2-iRFP-HIS ura3::pED141</i> <i>WHI5-mCitrine:TRP ste5Δ::pED164 bar1Δ::NAT</i>

Table A.2.: Table of plasmids.

Plasmid	Insert	Backbone
pED45	$P_{RPS2}\text{-}STE7_{1-33}\text{-}NLS\text{-}NLS\text{-}mCherry$	pRS306
pED53	$P_{RPS2}\text{-}STE7_{1-33}\text{-}NLS_{(S14A,S22A)}\text{-}NLS_{(S14A,S22A)}\text{-}mCherry$	pRS306
pED54	$P_{RPS2}\text{-}STE7_{1-33}\text{-}NLS_{(S14E,S22E)}\text{-}NLS_{(S14E,S22E)}\text{-}mCherry$	pRS306
pED55	$P_{RPS2}\text{-}STE7_{ND}\text{-}NLS\text{-}NLS\text{-}mCherry$	pRS306
pED73	$P_{RPS2}\text{-}STE7_{1-33}\text{-}NLS\text{-}NLS\text{-}mCitrine_{A206K,L221K}$	pRS304
pSP31	$P_{FIG1}\text{-}quadrupleVenus$ [86]	pRS305
pSP198	$P_{Fus3}\text{-}FUS3_{as}$ [71]	pRS406
pSP303	$P_{RPS2}\text{-}FAR1_{DS}\text{-}NLS\text{-}NLS\text{-}mCherry$	pRS306
pSP306	$P_{RPS2}\text{-}MKK2_{1-33}\text{-}NLS\text{-}NLS\text{-}mCherry$	pRS306
pSP319	$P_{RPS2}\text{-}MKK2_{1-27}\text{-}NLS\text{-}NLS\text{-}mCherry$	pRS306
pSP321	$P_{RPS2}\text{-}MKK2_{1-60}\text{-}NLS\text{-}NLS\text{-}mCherry$	pRS306
pSP322	$P_{RPS2}\text{-}MKK2_{1-80}\text{-}NLS\text{-}NLS\text{-}mCherry$	pRS306
pSP323	$P_{RPS2}\text{-}MKK2_{1-100}\text{-}NLS\text{-}NLS\text{-}mCherry$	pRS306
pED92	$P_{RPS6B}\text{-}STE7_{1-33}\text{-}NLS\text{-}NLS\text{-}Cherry$	pSIV _{URA}
pED94	$P_{RPS6B}\text{-}STE7_{ND}\text{-}NLS\text{-}NLS\text{-}CFP$	pSIV _{LEU}
pED137	$STE5:HIS$	pGT _{HIS}
pED138	$STE5_{8A}:HIS$	pGT _{HIS}
pED141	$P_{RPS6B}\text{-}STE7_{1-33}\text{-}NLS\text{-}NLS\text{-}mCherry$ $P_{RPS6B}\text{-}STE7_{ND}\text{-}NLS\text{-}NLS\text{-}CFP$	

A. Strains and plasmids

pED147	<i>STE5_{ND}:HIS</i>	pGT _{HIS}
pED159	<i>STE20_{ND}:ADE</i>	pGT _{ADE}
pED160	<i>STE20_{11A}:ADE</i>	pGT _{ADE}
pED161	<i>STE20_{CRIBΔ}:ADE</i>	pGT _{ADE}
pED162	<i>STE7_{ND}:ADE</i>	pGT _{ADE}
pED163	<i>STE7_{6A}:ADE</i>	pGT _{ADE}
pED164	<i>STE5_{ND}:ADE</i>	pGT _{ADE}

- NLS represents the peptidic sequence : QQMGRGSEFEELGSPLKKLKISPDTASGLV
- *STE7₁₋₃₃* represents the peptidic sequence: MFQRKTLQRRNLKGLNLNLHPDVG-NGQLQEKT
- *STE7_{ND}* represent the peptidic sequence: MFQRKTLQAANLKGANANLHPDVGNNGQLQEKT
- Far1_{DS} represents the peptidic sequence: MFQRKTLQKRGNIPKPLNLSLHPDVGNNGQLQEKT
- pSIV and pGT backbone from [132]

B. Mathematical Model

B. Mathematical Model

Modelling of MAPK activity from biosensor measurements. The table B.1 lists the reactions

Reaction	Kinetic constant
$SKARS_{Cyto} \rightarrow SKARS_{Cyto-P}$	V_{MAPK}, K_{MAPK}
$SKARS_{Nucl} \rightarrow SKARS_{Nucl-P}$	V_{MAPK}, K_{MAPK}
$SKARS_{Cyto-P} \rightarrow SKARS_{Cyto}$	V_{PPase}, K_{PPase}
$SKARS_{Nucl-P} \rightarrow SKARS_{Nucl}$	V_{PPase}, K_{PPase}
$SKARS_{Cyto} \rightarrow SKARS_{Nucl}$	k_{Imp}
$SKARS_{Nucl} \rightarrow SKARS_{Cyto}$	k_{Diff}
$SKARS_{Cyto-P} \rightarrow SKARS_{Nucl-P}$	k_{Diff}
$SKARS_{Nucl-P} \rightarrow SKARS_{Cyto-P}$	k_{Diff}

Table B.1.: Reactions implemented in the model.

implemented in the model. The sensors in the nucleus and in the cytoplasm are phosphorylated by the MAPK. We assume simple Michaelis-Menten kinetics for this reaction. The dephosphorylation is also modelled by a Michaelis-Menten law. We assume that these enzymes are processive and that the four phosphorylation events do not lead to ultra-sensitivity of the response. We think this is a fair assumption since during the development of the sensor we tested constructs with a variable number of phosphorylation sites and the general response of the sensor increased almost linearly with this number. We consider the amount of phosphatase and their linked activity to be constitutive. On the opposite, the MAPK activity changes with time. To account for this, V_{MAPK} is calculated as $k_{Cat} * MAPK * MAPK_{Activity}$. MAPK represents the total concentration of the kinase estimated to $0.7 \mu M$ (Fus3+Kss1 $\sim 14'000$ molecules/cell, volume of yeast cell ~ 35 fl). The parameter $MAPK_{Activity}$ varies between 0 and 1 and represents the fraction of MAPK that is activated in the cell and thus can contribute to the phosphorylation of the sensor.

The sensor diffusion in and out of the nucleus has been estimated based on the formula: $k_{Diff} = NPC/Na/Vn * p$ [123]. This determines the diffusion rate between nucleus and cytoplasm. Using the nuclear accumulation of the non-functional sensor, we can estimate that the active import of the sensor is 3.3 times larger than passive diffusion. The concentration of sensors was

estimated to be relatively similar to the one of the MAPK (0.6 μM). For the starting condition, it is enriched almost three folds in the nucleus. Kinetic parameters and starting concentrations are listed in table B.2. For forward simulation of the model, the $\text{MAPK}_{Activity}$ evolves with time according to the formula:

$$\text{MAPK}_{Activity} = \frac{A}{1 + \exp(-R(t - T_0))} + O$$

A: Amplitude of the response, which varies from 0 to 1 in the different traces presented in figure 2.10.A.

R: Rate of activation of the MAPK, set to 0.04

t: time axis

T₀: Start time, set to 950s

O: Offset value, set to 0

The model is simulated for 1800s. Time 900 is set to 0 in the graphs from figure 2.10. A-B. The first 500s (-900 to -400) allow an equilibration of the SKARS between cytoplasm and nucleus. To extract the $\text{MAPK}_{Activity}$ based on experimental data, Matlab optimises the set of variables defining the variation of the $\text{MAPK}_{Activity}$ with time (A, R, T_0, O). For the dose-response calculation (figure 2.11.A), we used the same equation as above. The nuclear to cytoplasmic ratio to be fitted consists on five time-points before 0 set to the value of the active import and eight time-points from 8 to 15 set to the nuclear to cytoplasmic ratio measured for one concentration of the dose response. The final value of the $\text{MAPK}_{Activity}$ after simulation is used as the steady-state MAPK ratio plotted in the dose response graph (figure 2.11.A).

To extract the $\text{MAPK}_{Activity}$ from the experimental data from Figure 2B a more complex equation was used to account for the rise and decay in $\text{MAPK}_{Activity}$:

$$\text{MAPK}_{Activity} = \frac{A_1}{1 + \exp(-R(t - T_0))} + \frac{A_2}{1 + \exp(-R(t - T_0))} + O - 1$$

B. Mathematical Model

A1 and A2: Amplitude of the response

R and D: Rate of activation (deactivation) of the MAPK

t: time axis

T0 and TD: Start time and Decay time

O: Offset value

The time axis and median value of nuclear to cytoplasmic ratio to the simulation. From an initial starting set of parameters, the program optimises them to fit the experimental trace. The outcome of the fit is presented in figure 2.10.C. The starting and final parameters are given in table B.3.

Modelling of CDK-dependent MAPK activity From the NAPPI dose response experiment presented in 3.2.5 we extract the MAPK activity and the CDK activity either prior ($MAPK_{Pre\alpha}$, $CDK_{Pre\alpha}$) or after stimulation ($MAPK_{Post\alpha}$, $CDK_{Post\alpha}$) with α -factor for each individual cell. The median of these parameters were calculated for each experiment including all replicates. We plotted the data using a scatter plot showing the MAPK parameters against the CDK parameters. We then used the *fit* function of matlab to fit our data. For the scatter plot of $MAPK_{Post\alpha}$ against $CDK_{Post\alpha}$ we obtained the best fit using a polynome 2 equation (figure 3.20.C). For the scatter plot of $MAPK_{Post\alpha}$ against $CDK_{Post\alpha}$ we obtained the best fit using a linear equation.

These two equations are then used to estimate the MAPK activity from the dynamic CDK activity data. We use values of single cells from a completely independent experiment. The estimated MAPK activity prior pheromone addition is defined as:

$$MAPK'_{t \leq 0, CDK} = A_1 CDK_{t \leq 0} + B_1$$

Under stimulating condition:

$$MAPK'_{t>0,CDK} = A_2CDK_{t>0}^2 + B_2CDK_{t>0} + C_2$$

Dynaminc single cell MAPK and MAPK' values are then plotted against the time relative to pheromone addition for comparaison (figure [3.21.A](#)).

B. Mathematical Model

Parameter	Value	Unit
V_{MAPK}	$k_{Cat} \times MAPK \times MAPK_{Activity}$	$\mu\text{M/s}$
K_{MAPK}	0.5	μM
k_{Cat}	0.18	1/s
V_{ppase}	0.1	$\mu\text{M/s}$
K_{ppase}	0.5	μM
k_{Diff}	$NPC/N_A/VN^*p \sim 0.05$	1/s
NPC: number of nuclear pores	~ 160	
N_A : Avogadro's Number	6.022 1023	1/mol
V_N Volume of the Nucleus	3.5	fl
p: permissiveness of nuclear pores	~ 0.06	1/ $\mu\text{M/s}$
k_{Imp}	$k_{Diff} \times \text{RatioActiveImport}$	1/s
RatioActiveImport	3.3	-
MAPK	0.7	μM
MAPK _{Activity}	0	-
SKARSC _{yto}	0.43	μM
SKARSC _{yto}	0.166	μM

Table B.2.: Kinetic parameters and starting concentrations

Parameter	Initial guess	Final value
$A1$	0.9	0.608
$A2$	1	0.772
R	0.01	0.041
D	0.2	0.0087
T_0	850	856
T_D	1500	1511
O	0.05	0.377

Table B.3.: Parameters describing the MAPK activity dynamics.

Parameter	Value
A_1	-0.973
A_2	-2.763
B_1	1.579
B_2	2.073
C_2	1.217

Table B.4.: Equation parameters.

C. Clustering and synchronisation

C. Clustering and synchronisation

On the histogram of the $\text{Whi5}_{N/C}$ values we easily identify two populations: one with a low $\text{Whi5}_{N/C}$ and one with a high $\text{Whi5}_{N/C}$ figure [C.1](#)

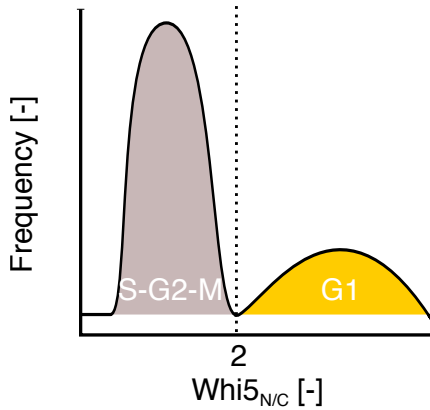


Figure C.1.: Schematic representation of a histogram of the whole $\text{Whi5}_{N/C}$. The histogram includes all values from all cells independently of the time. The threshold value presented on the scheme was indeed used to sort cells.

Cells having only zeros are considered as starting in S-G2-M. The same strategy was used to identify G1-locked cells and the S-G2-M cells except that we consider all time points. G1-locked and S-G2-M cells are extracted from dataset.

We recover Bin_{thre} to identify the cell entering in G1 or in S-phase and passing through G1. Two vectors ($V_1=[0 \ 0 \ 1 \ 1]$, $V_2=[1 \ 1 \ 0 \ 0]$) are created and are used to scan Bin_{thre} along the time axes. In a zeros matrix of the same size as Bin_{thre} , further referred as Mat_{Pos} , a value of 1 is assigned at the position where V_1 is matching Bin_{thre} (or -1 for the vector V_2). Column containing 1 is considered as cell entering in G1 (in S if -1). If one column contains a -1 and 1 the cell is considered as passing-through G1. For the cases where a column contains more

In order to identify growth stages of cells and to synchronise them, we set an arbitrary threshold between the two groups of cells (threshold=2). After YeastQuant analysis, the $\text{Ratio}_{N/C}$ of the Whi5 channel is organised as a matrix of values where each column corresponds to one cell and each row correspond to one time point. We first transform the matrix in a matrix of binaries where 1 is above the threshold and 0 is below this threshold. We named this matrix Bin_{thre} . We focus on Bin_{thre} values spanning from the first time-point until the time-point of pheromone addition. Cells which have only ones are considered as starting the time lapse in G1. Cells

than 2 values different from 0 the cell is totally rejected from the analysis. Depending on, the experiment, our criteria can reject until a maximum of 5% of the total population.

The position of the -1 and 1 into the matrix Bin_{thre} indicate when the cell transit from one stage to another. The vector time of each cell entering in G1 is recovered and and time 0 changed based on the position of the -1, 1 into the Bin_{thre} matrix.